KfK 3845
März 1985

Extrapolation of Data from Simulant-Material Experiments to the Work Potential of Fuel Penetrating Through Upper Core Structures in Core Disruptive Accidents

L. Meyer, D. Wilhelm
Institut für Neutronenphysik und Reaktortechnik
Projekt Schneller Brüter

Kernforschungszentrum Karlsruhe

Kernforschungszentrum Karlsruhe

Institut für Neutronenphysik und Reaktortechnik
Projekt Schneller Brüter

KfK 3845

Extrapolation of Data from Simulant-Material Experiments to the Work Potential of Fuel Penetrating Through Upper Core Structures in Core Disruptive Accidents

L. Meyer, D. Wilhelm

Kernforschungszentrum Karlsruhe GmbH, Karlsruhe

Kernforschungszentrum Karlsruhe GmbH
ISSN 0303-4003

ABSTRACT

This report addresses questions that arose after having completed a detailed study of a simulant-material experimental investigation of flow dynamics in the Upper Core Structures during a Core Disruptive Accident of a Liquid-Metal Fast Breeder Reactor. The main findings of the experiments were about the reduction of work potential of the expanding fuel by the presence of the Upper Core Structures. This report describes how the experimental data can be extrapolated to prototypic conditions, which phenomena modelled in code predictions by SIMMER-II are different for simulant and prototypic transients, and how the experimental results compare to effects of prototypic phenomena which could not be modelled in the experiment.

ZUSAMMENFASSUNG

Extrapolation von Daten aus Experimenten mit Simulationsmaterial auf das Arbeitspotential von Brennstoff, der in Kernzerlegungsunfällen durch die oberen Kernstrukturen dringt

Dieser Bericht behandelt Fragen, die nach Beendigung einer detaillierten Studie über Simulationsmaterial-Experimente der Fluiddynamik in den oberen Kernstrukturen während eines Kernzerlegungsunfalles in einem Natriumgekühlten Schnellen Brutreaktor auftraten. Die Hauptergebnisse der Experimente lagen im Bereich der Reduktion des Arbeitspotentials von expandierendem Brennstoff durch die oberen Kernstrukturen. Dieser Bericht beschreibt, wie die experimentellen Daten auf die prototypischen Bedingungen extrapoliert werden können, welche in numerischen Berechnungen des Rechenprogramms SIMMER-II modellierten Phänomene sich für simulierte und prototypische Transienten unterscheiden, und wie die experimentellen Ergebnisse in Beziehung stehen zu Wirkungen prototypischer Phänomene, die nicht im Experiment modelliert werden konnten.

CONTENTS

I. INTRODUCTION

A simulant-material experimental investigation of flow dynamics in the Upper Core Structure (UCS) during a Hypothetical Core Disruptive Accident (HCDA) of a Liquid-Metal Fast Breeder Reactor (LMFBR) was performed with the Upper Structure Dynamics (USD) experiment in the past /1,2/. The experiment had been designed to verify some of the thermal-hydraulics models in SIMMER-II /3/. Four different liquids had been used to simulate the flashing UO_2 and numerous parameter variations had been made, regarding the initial pressures and temperatures.

One important result from the experiment was the data on the the kinetic energy of a movable piston and thus the work potential of the fuel simulation on its exit from the UCS. The ratio of the kinetic energy, directly measured by tracking the rigid piston, and the maximum kinetic energy, calculated with SIMMER at the same conditions, but with zero friction and heat transfer in UCS, could be shown to be a function of the initial pressure and the temperature difference between core and UCS.

Two questions immediately arose. First, can we expect the same reduction factors for the prototypic case by simply transforming the pressure and temperature via the scaling factors? The length scale of the test section and the simulant fluids had been chosen according to a scaling analysis /4,1/. The scaling factors for pressure and temperature had been found to be 25:1 and 10:1, respectively.

And second, how would these reduction factors be changed, if all the prototypic phenomena were added which were not modelled in the experiment, such as steel in the core, melting of structures, freezing of liquid, liquid sodium in the UCS and a cosine power distribution.

These two questions will be addressed in this report. Since no experiments with prototypic materials are available, calculations with SIMMER-II, using input parameters which were found to apply to the USD experiment, were performed. The analysis is strictly limited to the thermohydraulics of the flow below the rigid piston which represents a model boundary condition.

II. THE EXPERIMENTAL CASE

1. Results from the USD-experiment

Fig.1 shows a model of the USD experiment showing details as described in Ref. /2/. On top of the UCS, the initial position of a rigid movable piston is indicated.

The velocity of the movable piston at the end of its flight path was taken as a measure for the conversion of thermal energy into mechanical energy.

The kinetic energy of the piston (E) of various experiments at different initial core pressures and temperatures and different UCS temperatures was related to the maximum kinetic energy (E_o) which was calculated with SIMMER at the same conditions, but with zero friction and heat transfer in the UCS. The ratio (E/E_o) was a function of the initial pressure and the temperature difference between core and UCS ($T_{core} - T_{UCS}$) /2/.

Because of nonequilibrium effects the calculated kinetic energy (E_o) is not the same as that of an isentropic expansion. The work potential due to an isentropic expansion (E_{is}) was calculated by a different code, K-EX, /5/.

The isentropic work potential E_{is} turned out to be larger than the kinetic energy E_o by a factor of approximatly two. In order to study the accuracy with which the total kinetic energy is calculated by SIMMER-II, calculations with a piston weight increased by factors of 10 and 50 were performed, thereby slowing down the expansion process and reducing the non-equilibrium effects.

The resulting kinetic energy E_o of the piston was 90% of the isentropic work potential E_{is} in the case of 10 piston masses and 100% in the case of 50 piston masses. This is a proof for the accuracy of SIMMER-II. A similar study with SIMMER-I /6/ had found similar agreement.

Fig. 2 shows the experimental results related to the isentropic work potential (E/E_{is}) versus the initial core pressure. Also shown is the calculated ratio (E_o/E_{is}).

2. Calculations with UO_2

The scaling factors of the USD-experiment for length, temperature and pressure had been found to be 2.5:1, 10:1 and 25:1, respectively /1,4/. The USD experiments were performed with core pressures, between 0.35 and 1.25 MPa and core temperatures between 410 K and 537 K. Accordingly, SIMMER-calculations were performed with the following initial fuel temperatures and pressures in the core:

p_{core} (MPa)	2.5	5.0	10.0	15.0	25.0
T_{core} (K)	4495	4736	5004	5175	5409

The temperature of the UCS was varied keeping the temperature difference (ΔT) between core and UCS at constant values in order to obtain a set of curves with constant T (Fig. 3) similar to that from the experiment.

The T which leads to prototypic UCS-temperatures is T=4000 K. For T=2000 K the UCS-temperatures lie above the melting temperature of the structure, but for a comparison with the experimental curves calculations for this T were performed, nevertheless. Since in the USD experiments no melting occurred, the melting temperatures of steel and fuel in the UCS were set to 5000 K.

Hence, the working fluid UO_2 in the core region had to be simulated by sodium and the sodium vapor was simulated by the fission gas.

The dimensions were that of a prototypic subassembly, which means the dimensions of the experiment were scaled up by a factor of 2.5 (Fig. 1). The piston weight was 26.6 kg, which is the weight of a sodium column of 3 m height and a piston cross section area of 0.01262 m^2. The scaling of

the lengths results in a smaller surface area to volume ratio, compared to the experiment, by the factor of 2.5 which is important for all heat transfer processes.

One parameter which needs to be changed going from experiment to prototype, but which cannot simply be scaled, is the structure side heat transfer coefficient. SIMMER defines a single temperature for each structure material in each mesh cell. A structure side heat transfer coefficient is defined by dividing the thermal conductivity by the half-thickness of a wall. This assumed "thin wall behaviour" is only correct for very thin walls or slow transients. For rapid transients in which the thermal penetration distance into the wall is less than the thickness of the wall this method underestimates the heat flux. In the calculations of the USD-experiments this parameter was tuned to obtain agreement with experimental results. This was necessary because the pins ("cladding") and the can wall were too thick for a "thin wall behaviour" in rapid transients. On the other hand, the prototypic cladding is thin enough for the heat transfer model in SIMMER-II to be applicable. The subassembly can wall is not quite thin enough in fast transients. However, the surface area of the can wall is only 1/10 of the cladding surface area, which reduces its effect on the transient correspondingly. Additionally, the can wall has reached its melting temperature typically after one third of the transient. Hence both structure side heat transfer coefficients were determined from the half-thickness and thermal conductivity of the structure.

Another parameter, which prevents a simple scaling between USD experiment and prototypic calculation is the melting temperature of UO_2 of 3047 K. With the initial UCS-temperatures much lower, freezing of UO_2 during the early phase of the transient is possible. This was not the case with the simulant fluids in the USD experiment. Sample calculations with an artificial melting temperature set to 1200 K yielded approximately 20% higher kinetic energies than with T_{melt}=3047 K.

An important parameter in the calculation of the USD experiments had been the droplet size respectively its upper and lower bound. The minimum droplet size in the core had to be set to $2*10^{-4}$ m in order to obtain agreement for the pressure histories. With prototypic materials a change of the minimum droplet size from 10^{-7} m to 10^{3} m did not change the results substantially.

The following table shows all the parameters which have to be considered when the results regarding the kinetic energy reduction in the USD-experiment and the prototypic calculations are compared.

fluid	Propanol - Helium Methanol - Helium Ethylene Glycol Helium	UO_2 - Sodium
length	1	2.5
surface area/ volume ratio	1	/2.5
H-T-can	125000 (aluminium)	18000 (steel)
H-T-clad	41600 (steel)	132000 (steel)
piston mass	0.36 kg	26.6 kg
displacement	1.20 m	3.00 m
fluid melt temp.	below UCS-temperature	above UCS-temperature
min. drop size	strong effect	no effect

Table I and Fig.3 show the results of the SIMMER-calculations. The cases denoted with '0' are the results for the isentropic expansion, calculated with K-EX /5/. The curves in Figs. 2 and 3 show a similar trend. The fuel conditions in the core seem to be scaled correctly by the chosen pressures and temperatures.

The scaling factor for the temperature difference, fuel-UCS, however, is rather 25:1 than 10:1. There is no simple explanation for this discrepancy. The scaling analysis did not, - and can not, incorporate all effects of variable physical properties and their impact on heat transfer and pressure reduction. In Appendix B the scaling analysis is reviewed.

The conclusion is, that in scaling such a complex thermohydraulic experiment the uncertainty will be in this order of magnitude. However, physical effects which will be discussed in the following chapters, increase the uncertainty about the kinetic energy by a much larger number.

III. THE PROTOTYPIC CASE

1. The reason for prototypic calculations

The extensive data base obtained by the USD experiment was made possible by using simulant materials at modest pressures and temperatures. By concentrating on the dynamics of the fuel simulant, effects that might impose similar gauge readings were excluded. The possibility of misleading interpretations was thus reduced.

The goal of the USD experiment was, however, to spread some light on the complex discharge of core material through the UCS during a post-disassembly expansion. We acknowledge the difficult task of giving a reasonable mechanistic description of the expansion, and do not want to contribute to this by the following chapter. The USD data however, extrapolated to the real material conditions, as presented in chapter II.2 should be put into relation to those calculations that include phenomena not observed by the experiments.

2. The model used in prototypic calculations

We therefore used the one-dimensional USD model of SIMMER-II, scaled up to SNR-type dimension, starting with the base case used to calculate table I (Case D-4). Modelling a fuel expansion against a rigid movable piston eases the evaluation of the system kinetic energy. However, major effects of the three-dimensional pool movement, decelerated by internal structures, are neglected. The scaling of the piston has been mentioned in chapter I.2. Fig.1 shows the USD model in conjunction with noding used for the present analysis. Particularly in the core region and at the core-UCS interface, the noding of the experimental recalculations had to be slightly modified to incorporate only prototypic features.

3. The conditions used in prototypic calculations

A matrix of SIMMER calculations is given in table II.

Six different columns contribute to the matrix. Although the order indicates that step by step additional prototypic features have been added, some of the cases are only artificial. That means that these combinations are exclusively used to gather information about the influence of single parameters. In case No.1 to 6 for example, the steel inventory has been omitted. This is unrealistic with respect to prototypic conditions because there is indeed steel cladding and can wall present in the core. We denote these cases as theoretical combinations. We have tried to analyse each case separately to learn about effects that could not be modelled in the USD experiment. The descriptions of the separate cases show that the most prototypic one is not just a linear combination of separate effects. We have not taken into account in-core sodium and mechanically failing structures, for example, because these cases cannot be addressed in the present simplified one-dimensional model.

In all cases, UO_2 was the working fluid as given by the initial conditions. Original SIMMER component assignments were used. The initial conditions are characterized by a constant fuel temperature of 5175 K throughout the core region, a constant UCS temperature of 1175 K, a totally voided UCS region at a sodium vapor pressure of 10^5 Pa, and a piston lower interface located at the upper end of the assembly structure. The piston was tracked up to a maximum displacement of 3 m (see Fig. 1), the transient was then terminated. The actual displacement of the sodium pool might be smaller depending on the form of the discharge bubble injected into it. If the displacement is smaller the kinetic energy can be smaller as well. If the piston velocity stays constant there is no increase in kinetic energy.

Melting steel structures were made possible by using a steel melting temperature of 1700 K and a latent heat of fusion of 0.26 MJ/K. If melting was to be inhibited, the melting temperature was increased up to 5300 K. By adding steel in the core, the mass of cladding and can wall of the undisrupted core region was contributed to the initial liquid field of the cores at 1701 K. Consequently, the fuel is added to the liquid field as there is no intact clad geometry left. When liquid sodium is added in the UCS region, a total of 32 g liquid sodium is present in the UCS and mixing head. The initial droplet radius is about $2*10^{-5}$ m depending on the result of the SIMMER droplet model. This leads to a specific droplet surface of 1060 m^2/m^3, related to the total volume of a SIMMER node. If the sodium would form a uniform film on all available structure surfaces, only 350 m^2/m^3 would be available. The film would have a thickness of about 0.02 mm in the pin bundle, and 0.1 mm in the mixing head. Due to the large exchange area presently used, the sodium vapor generation upon impact of hot core material will be near the upper bound.

Additional to the uniform initial core temperatures, a cosine profile was used to model the fuel temperature distribution after a nuclear excursion. The form factor is given by $T_{average}/T_{max} = 0.93$.

In two cases, a one-dimensional sodium pool was modelled to provide a further link to whole core prototypic SIMMER calculations. The cover gas height was fixed at 1.6 m.

4. The SIMMER version and parameters used in prototypic calculations

The URANUS-10 version of SIMMER-II, dating June 1983, was used in conjunction with a slightly modified plug model, as described in Ref. /2/. If not mentioned explicitely, the parameters for phase exchange and structure breakup were held constant for all cases. The fraction of the heat of fusion at structure failure was 0.5, the fraction of the

failed structure that is liquid was 0.51, and the URANUS-10 model allowing for an instant transfer of the pellets to the liquid field upon failure was used. Consequently, we have chosen the maximum packing fraction, which represents the volume fraction at which the fluid drag becomes infinite, to be 0.99 to prevent an early blockage of the UCS and a reduction of the piston kinetic energy to zero. Additionally, the particle viscosity multiplier was 0.01 in order not to overemphasize the influence of the particles on the discharge through the UCS. The heat transfer and friction multipliers of the above-core structure were set according to the experimental data. They are 2.0, 1.6, and 3.0 for the UCS entrance section, the UCS, and the mixing head, respectively. In the mixing head, a non-flow volume fraction of 6% represented an angular gap which is added to the free flow area upon can wall failure. All other parameters were taken according to the runs recalculating the experimental blowdown, as referred to in Ref. /2/. Appendix A shows the input data set for the base case No.1.

5. The kinetic energy of the prototypic calculations

Table II shows additional information about the piston impact time, the piston velocity, the piston kinetic energy and its fraction compared to the energy of an isentropic fuel expansion to the volume related to the 3m-flight distance of the piston. An evaluation of the results will be given in chapter 6.

Each of the cases is described in the following chapter, reference to the kinetic energy is made if necessary.

6. Description of the prototypic calculations

We now comment on the 12 different cases of table II. Case 0 is the isentropic expansion, D-0 in table I.

6.1 Case 1

Case 1 is analogous to case D-4 representing the blowdown of the USD experiment. Fig. 4 shows a selection of different output variables plotted versus time. Six representative nodes have been selected according to the scheme in Fig. 1. The figure shows on the left hand side the noding for the prototypic calculations and the length starting with zero at the lower core boundary. Hence, in the plots, node 6 and 10 stand for the core center and periphery, respectively, node 11,15 and 18 stand for the upper axial blanket, and node 26 for the top of the subassembly at the end of the upper space.

The pressure history of Fig.4a shows how the pressure in the core is reduced during the blowdown, whereas the pressures near the piston increase as hot fuel penetrates through the UCS, and drive the piston. Successively more volume is opened during the movement of the piston. The initial liquid volume fraction is 0.28 in the core, according to input fuel mass and the equation of state of fuel at the given input temperature of 5175 K, see Fig. 4b. 19.2 kg are liquid fuel 0.6 kg are fuel vapor. During the blowdown, the fluid of the core periphery first penetrates into the UCS, see Node 18, Fig. 4b. The fuel below (Node 26) follows with a time lag. Inside the UCS, at a given structure volume fraction of 0.55, the liquid fills up to three quarters of the free volume (Node 26,22 ms).

The liquid fuel temperature of the core region, plotted in Fig. 4c, decreases slightly during the blowdown. The exponential variation of vapor pressure with temperature leads to a substantial pressure drop as can be seen in the pressure plot, Fig. 4a. Inside the UCS, there is no

liquid fuel initially. SIMMER reads a zero temperature. As the fuel penetrates into the cold structures, the liquid fraction is cooled down to near-clad temperatures, see Node 18 and 20, Fig. 4c. The vapor temperatures are closely linked to the liquid temperatures, see Fig. 4d.

The plot of the fuel droplet size (Fig. 4g) shows a vigorous change between upper and lower droplet size bounds during the first 40 ms. The axial blanket droplets (Node 18) are always small, not greater than 0.2 mm, resulting in a large heat transfer area. The core droplet size (Node 6 and 10) starts at the maximum value and decreases rapidly because of the flashing breakup and fluid dynamic breakup criterion.

The clad and can wall temperatures (Fig. 4e,f) show a fast heating up of the structures. The present case does not allow for structure melting. The clad temperatures quickly reach fuel temperature levels whereas the can wall temperature increase is delayed by a smaller surface to mass ratio.

Additional information for Case 1 (table II) is given in Fig.5. Pressures, temperatures, and liquid volume fractions are plotted versus length in time intervals of 10 ms. Reference to the length, given in millimeters, can be made to the nodal system by Fig. 1. There, the core region extends from 0 to 950 mm, the axial blanket from 950 to 1379 mm, and the above blanket structures from 1379 to 1932 mm. The piston is tracked until its lower interface reaches 4932 mm. The pressures above the piston interface are 0.1 MPa, the corresponding liquid volume fraction is zero. Fig.5 a-d shows the subsequent pressure equilibration during the blowdown, which has not been terminated when the piston reaches its final displacement. Deviations from a steady decrease of pressures with length can be observed mainly because of fuel vapor pressures, (see Fig. 5b).

Fig.5 e-h show the liquid volume fraction over the axial length. The plots show the discharge of core material as well as the concentration of

liquid fuel just upstream of the piston interface, e.g. in Fig. 5f. On its way through the UCS, fuel vapor condensates. The flow transports a substantial amount of liquid fuel downstream where it accumulates in regions of large decelerations. The plots show the perception of a density wave travelling with the piston interface.

Additional information is listed in the long prints of the SIMMER-II output file. The total amount of liquid fuel in the system decreases slightly during the first 40 ms due to an excess of evaporation over the condensation on cold surfaces. The evaporation is a result of the pressure decrease. From 40 to 107 ms, more and more condensation compensates the loss of liquid mass until it terminates in the final value to be equal to the inital one. The energy balance of the whole system shows on the other hand, that there is a continuous flow of energy to the structures, which gain 60% of its initial energy, whereas the fuel looses 20% of its initial energy.

Fig.5 i-m show fuel temperature profiles, the temperature being zero in nodes without fuel mass. Temperatures are close to the saturation temperature. For example at 110 ms, Fig. 5m, the fuel temperatures increase slightly from 1700 mm to 4800 mm and so does the pressure in Fig. 5d because of equilibrium between the two fuel phases.

6.2 Case 2

In Case 2, liquid sodium is added in all above-core structures. This leads to a substantial pressure build-up due to sodium evaporation in the UCS, see Fig.6. Additionally, Fig.7 shows the pressure and liquid volume fraction over the length for different times up to 50 ms. At time=0, liquid fuel fills a fraction of 0.29 of the core region (Fig. 7d, up to 950 mm). The above-core structures (Fig. 7d, up to 1930 mm) are filled with a liquid sodium volume fraction of 0.007. As liquid fuel penetrates into the mixing head and upper space (Fig. 7d,e), pressure is being built up by vigorous sodium evaporation (Fig.7a,b). If all sodium would be

heated up instantaneously to the liquid fuel temperature in the UCS and mixing head of 4000 K, pressures of 15 MPa would be generated. Fig.7b, 30 ms, shows maximum pressures of 6 MPa because of finite heat transfer rates to sodium and pressure relief to adjacent volumes.

The piston is driven mainly by sodium vapor pressures. The axial pressure profile is not steady-state like, which is very much different to the USD experiment. The comparison of Fig.7 a-e and Fig.5 a-d shows the impact of sodium vapor generation. In Fig.5b, the pressure profiles in the above-core structures show a steady decrease. With sodium added, an early build-up of sodium vapor pressures (Fig. 7b) dominates the piston kinetics.

6.3 Case 3

In Case 3, the only change to Case 1 is that steel is allowed to melt. The steel melting temperature is 1700 K. Fig.8 shows selected variables plotted over the time. The clad and can wall temperatures of Fig.8c and d increase up to the melting temperature of 1700 K. After that they stay constant until 50% of the heat of fusion is used up. No subsequent temperatures are recorded because the structure has failed. The UCS clad melts within the first 20 ms (Fig. 8d), the UCS can wall melts within 70 ms (Fig. 8d). As the clad melts, the pellets are broken up into particles of 3 mm radius, and added to the liquid field. Comparing, for instance, the liquid volume fractions of Node 18 (end of UCS) in Fig.4b and Fig.8b, the early melt-down of upstream-UCS structures adds liquid during the first 20 ms. Then, the structure of Node 18 melts and the liquid volume fraction is increased by a factor of two. The can wall structure occupies about 10% of the volume. The bulk of the liquid mass moves downstream. By this movement, it opens up the upstream flow area for the final discharge of core material.

After 60 ms all pressures of Fig. 8a are closely tied to each other. They decrease as the zone of high liquid volume fraction moves downstream

together with the piston interface (Node 18 and 26 in Fig. 8b). As the vapor temperature in the opened-up section becomes very high, steel vapor pressures contribute substantially to the kinetics of the system. The impact on the piston energy is reduced by the fact that in addition to the piston mass the slug of high liquid volume fraction has to be accelerated, too.

6.4 Case 4

For Case 4 (Fig.9) a cosine temperature distribution in the core region has been used as initial condition. The initial pressure profile is now very much different with a peak core pressure of 34.5 MPa, and a minimum pressure of 2.3 MPa (Node 10 in Fig. 9a). Fig. 9a cuts off plot values above 15 MPa. Node 6 starts at 34.5 MPa and reaches pressure values below 15 MPa only after 25 ms. The high pressure drives the relatively cold fuel of the core periphery into the UCS. There, the steel walls melt instantaneously (Fig. 9 e-f). A liquid slug with only a few percent void fraction is being built up (Fig. 9b). Part of the slug evaporates during its travel downstream. An early vigouros pressure increase at the exit of the above-core structures leads to an early piston acceleration but the slug kinetics and consecutive pressure equilibration upstream add only a little amount to the kinetic energy of the piston, in comparison to case No.3. Fig. 9c and d show the liquid fuel and vapor temperature. In the above-core structures (Node 18,26), before the void fraction is drastically reduced, the vapor temperature is lower than the liquid temperature. After 30 ms, the plots of Fig. 9c and d are very similar, both temperature are closely related.

6.5 Case 5

Case 5 describes the combination of melting steel structures and left-over liquid sodium mass in all above-core nodes. The initial pressure and liquid volume fraction profiles in Fig.10a and b are similar to those of case 3 in Fig.8a and b. After 20 ms, substantial

pressure generation due to sodium evaporation drives the piston faster than before. The peak pressure of node 26 at 40 ms shows that the pressure near the piston partially exceeds the pressure in the core.

6.6 Case 6

Case 6 is a recalculation of case 5 using cosine temperature profiles in the core. Fig. 11b shows an early liquid slug formation similar to case 4 (Fig.9b). While the slug dynamics is comparable to case 4, the pressure build-up near the piston is much earlier and much more vigorous (Fig.11a). This early downstream pressurization due to sodium vapor generation, backed-up by following steel vapor pressure generation, leads to the most energetic theoretical blowdown of 43% isentropic energy. The value for the isentropic energy is based on the energy potential of fuel only. We refer to page 7 for the arguments of defining such artificial, though unrealistic parameter combinations. Here, the three predominant energy intensifiers are:

a) the cosine temperature and pressure profiles in the core resulting in an early injection of liquid fuel into the UCS,

b) the presence of melting steel with subsequent build-up of steel pressures,

c) the sodium vapor generation due to the presence of left-over liquid sodium after voiding.

The effects of these energy intensifiers must be related to the effects of the energy mitigators, presented in chapter 6.11. Any consideration of the energy intensifiers separated from other inherent effects is not admissable.

6.7 Case 7

Case 7 is the first with steel inventory in the core. The steel properties under these conditions have to be prototypic, so that melting

steel structures are mandatory. Steel vapor pressure correlations used in SIMMER were checked against data recently published /12/. They lie within the standard deviation of the experimental data. The rest of the parameters has successively been changed in case No.7 to 10.

Fig.12 shows time dependent plots for case 7. The data should be compared to case 3 (Fig.8), since the presence of steel in the core is the only difference between these cases. There is substantially more liquid mass in the core now. The liquid volume fraction is increasd from 0.28 to 0.51 (Fig. 12b), the added mass is relatively cold, at 1701 K.

Consequently, a large amount of energy is flowing from the fuel to the steel, depending on how much exchange area is available. The initial liquid droplet radius is equivalent to the maximum value which is set to be 10 mm. This is to avoid an overemphasis of instantaneous fuel quenching. However, during the transient, the droplets break up very fast and reach levels below 1 mm within 5 ms. This causes the fuel vapor pressure to decrease rapidly. After 20 ms, the core region exhibits a fuel vapor pressure of about 7 MPa. Some of the steel has been evaporated. There is not enough time and exchange area to evaporate all the steel. The steel vapor is overheated adding about 3 MPa partial pressure (Fig. 12a).

The liquid mass is injected into the UCS where more liquid is added by ablation of the steel wall (Node 18 of Fig. 12b before 35 ms). As can be seen from the clad temperature plot (Fig. 12d), the pin structure disintegrates near 35 ms. The pellets break up into particles of 3 mm radius. They contribute to the liquid volume fraction (Node 18 of Fig. 12b) which is drastically increased. Different to the cases before, the plugging of the UCS with more than 90% liquid volume fraction with respect to the flow area remains for almost the whole transient. After 60 ms, the bulk of liquid has reached the outlet of the upper space (Node 26 of Fig. 12b), about 40% of the flow area is still void. The pressure history for times greater than 40 ms (Fig. 12a) shows that pressures equilibrate upstream of the blockage, but an early increase of pressures near the piston is inhibited.

Fig. 13 shows pressures and liquid volume fractions plotted over the axial distance. The build-up of the liquid slug between 1000 and 1500 mm can clearly be seen (Fig.13c-h). After 70 ms, a region with high liquid volume fractions is formed near the piston where injected fluid is decelerated and hence mass is collected (Fig. 13g,h). The pressure plot shows a single-phase peak near 20 ms (Fig. 13a). After 50 ms, two pressure regions are formed, a high pressure region near the core and a low pressure region near the piston, divided by a peak at the blockage due to the heat-up of steel vapor (Fig. 13c,d). The pressures near the piston are always rather low. The kinetic energy of the piston is small, too. The impact time exceeds the time limit for the plots, 120 ms. The piston needs 206 ms to travel the 3m distance.

6.8 Case 8

In case 8, (Fig.14) a cosine input temperature profile was used in the core in conjuction with the parameters of case 7. Equivalent to case 4, the high pressure of the core center (Fig. 14a) drives the liquid mass of the core periphery (Fig. 14b) into the UCS resulting in an early melt-down of the UCS structures. The liquid can catch up momentum and is driven out of the mixing head already after 25 ms. This opens up more flow area for the vapor to escape towards the piston. After 35 ms, both vapor temperature and pressure of node 26 increase indicating that hot vapor reaches the piston interface (Fig. 14c,d). Not much more kinetic energy is generated with the cosine power distribution, but the impact is earlier. Comparing these results to those of case 4 (Fig.9c,d), one notices the higher temperature level of liquid fuel and vapor for all nodes of case 4. It is the quenching of the fuel that leads to a decrease in the temperature level near the core of case 8. Consequently, temperatures at the exit of the above-core structures cannot be higher. However, the vapor pressures of downstream material do not contribute much to the near-piston pressures in both cases. The pressure near the piston governs the kinetics. Compared to case 4, a reduction of core pressures by more than a factor of two can be noticed for the case with in-core steel.

6.9 Case 9

In Case 9 (Fig. 15), liquid sodium has been added to the above-core structure. Core liquid volume histories (Fig. 15b), and core pressure histories (Fig. 15a) are similar to case 7 (Fig. 12a,b). For case 9 however, the sodium vapor generation increases the pressure in the above-core structures and in the piston track (Fig. 15a). This is most obvious for times greater than 40 ms. Fig. 16 a-h show pressure and liquid volume fraction profiles. The comparison with Fig. 13 a-h shows similar blockage formations but higher pressures downstream of the blockage for case 9.

6.10 Case 10

Case 10 (Fig. 17) has the same parameter set as case 9, except that an initial cosine temperature profile is used in the core. Comparing both cases, the high pressure at the center of the core of case 10 (Fig. 17a) leads to a generally faster transient. The plugging characteristics of both cases (see the liquid volume fractions of node 18 and 26 in Fig. 17b and Fig. 15b) is very similar, but case 10 is faster. The flow area of case 10 (Node 26 in Fig. 17b), however, is more open for a longer period. This leads to a more effective pressure equilibration between core and piston track pressures. The combination of early pressure build-up near the piston because of sodium vapor generation and the later pressure equilibration on core pressure levels lead to a kinetic energy of the piston very close to that of case 9. Only the impact time is smaller now.

6.11 Solid steel inventory in the core

The low kinetic energy of the in-core steel cases gave rise to evaluate cases where the steel inventory was initially distributed as solid particles at 1175 K over the core region. In order not to overemphasize the heat exchange area we have chosen a particle radius of 1 mm which results in surface areas similar to those which are formed when the

cladding of 0.45 mm thickness is disrupted into reasonably large parts. Calculations using the same parameter set as in case 9 resulted in a substantially smaller kinetic energy. The blockage formation was much smaller, but a substantial amount of fuel energy was used to melt the steel particles at 1700 K. In this case, the energy flows were of the same magnitude as those which would be expected by radiation between fuel droplets and steel particles. Only a reduction of the exchange coefficients by nearly a factor of 10 would increase the kinetic energy to the value observed for case 9. The time intervals during which most of the fuel-steel energy exchange takes place are the very first 15 to 25 ms. These time scales have also been reported in Ref. /11/.

Comparing the results of the different forms of the initial steel inventory, one with intially liquid and the other with solid steel, a substantial difference in the phenomena that lead to a reduction of the kinetic energy can be found.

In the case with solid steel, the steel particles are heated up from 1175 K to 1700 K. At this point, the temperatures are locked until the fusion energy is compensated by the energy flow from the fuel. In addition, the liquid steel heat capacity is about 50% higher than of liquid fuel. Steel under these conditions represents a formidable heat sink even if the exchange area is being kept low.

In the cases with liquid steel, the droplets which are initially at 1701 K, are broken up into smaller droplets very early in the transient. They are injected into the UCS forming a high liquid density area together with the molten steel of the structures. It is mainly the hydraulic separation of the core volume from the volume just upstream the piston interface that leads to the specific energy release observed in the cases presented here.

The steel does not contribute much to the vapor pressure because the temperature range in which it is liquid is rather broad. Fuel and steel melt at 3047 K and 1700 K, respectively. The vapor temperature of fuel at 0.1 MPa is close to the melting temperature, i.e. 3635 K. However, the steel vapor temperature is 3073 K, and steel is initially at a much lower temperature.

With respect to the Cases 7 to 10, the main energy mitigators are:

a) the presence of steel as a direct heat sink in the core next to the fuel,

b) the formation of a zone of high liquid volume fraction inside the UCS which partly separates the core volume from the piston.

As can be seen from the present analysis, the effects of the main energy intensifiers (see chapter 6.6) are strongly reduced by the effects of the main energy mitigators. An artificial separation of these effects leads to unrealistic results.

7. Calculations with a sodium pool model

Case 11 and 12 have only been added to demonstrate that the movement of the rigid piston, as modelled by SIMMER-II, version 10, is similar to the movement of a one-dimensional pool consisting of liquid sodium. The sodium pool is 3.2 m deep, the cover gas volume above the pool has a length of 1.6 m. The expansion of the pool leads to an early slug impact which is not consistent with the piston flight distance of 3 m. However, this flight distance was chosen according to arguments given in Ref.2. Both results, of the piston and of the pool displacement, can therefore be compared for only the first 1.6 m.

7.1 Case 11

Case 11 is shown in Fig. 18. This case is equivalent to case 9, except for using the pool model. The histories past 80 ms are post-slug impact and do not contribute to the analysis (Fig. 19d). There is an important difference between the two cases, 9 (Fig.15) and 11 (Fig.18). Using the sodium pool model, steep transients come earlier, especially for nodes near the lower pool interface (Node 18 and 26 of Fig. 18b). Fig. 19 a-d show the liquid volume fraction plotted over the length. Because of the numerical solution of the code, the pool interfaces start to be smeared.

An effective pool movement can first be watched at the upper pool interface (Fig. 19b). At the lower interface, however, volume displacement occurs into both the upstream and downstream direction, with a net balance into the downstream direction. The volume that is now occupied by the smeared sodium interface is not available to the discharge. Additionally, pressure is building up very early at the sodium interface because of sodium vaporization. The blockage of discharge and the additional sodium vapor generation are compensating effects. The net result, with respect to the kinetic energy of the system, is very similar in both cases, 9 and 11.

Fig. 20 shows the displacement plotted over the time for case 9 and 11. It shows a good agreement between the displacement of the piston and the pool. The piston, by definition, has only one interface. The pool model has not been added to demonstrate any effect of pool sodium vaporization. First, it is well known that the numerical diffusion of sharp interfaces is a problem in any finite difference code. Second, there is no model available to calculate the physical processes at the pool interface. A comprehensive study is given in Ref. /13A/. SIMMER related work is published in Ref. /14/, where a two-dimensional pool has been studied.

In the accident analysis of a prototypic expansion phase, all these effects play a major role. It was the intention of this study, however, to evaluate the impact of SIMMER modeling on processes inside the UCS and adjacent volumes. The rigid interface of the piston which is unable to diffuse represents a much better boundary condition for this study.

7.2 Case 12

Case 12, has initial conditions like case 10. The high pressure in the core center (Fig. 21a) as a result of the cosine temperature profile drives an early discharge (Fig.21b). Times past 80 ms are not representative because the sodium pool has already impacted on the vessel head. Fig. 22 shows the history of the interface displacement for case 10 and 12. There is a substantial difference between the plots for the lower sodium interface and the lower piston interface.

The comparison between the piston interface displacement of case 9 and 10, (Fig. 20 and 22) again shows that the acceleration of the piston of case 10 starts 17 ms earlier. Both displacement curves, however, are almost congruent once the piston has started moving. This is another indication of similar energetics in both cases.

8. Summary of the prototypic transient analysis

Fuel which is initially in equilibrium with its vapor is ejected from the high pressure region of the core into the low pressure region above the core. Near the entrance to the UCS where flow area and hydraulic diameter decrease the mass flow is reduced, liquid mass accumulates. Consequently, the liquid volume fraction is slightly increased.

In case with in-core steel, the fuel temperatures are drastically reduced already in the core region due to the presence of cold liquid steel droplets. The fuel-steel mixture forms a front of high liquid volume fraction while penetrating into the UCS.

Inside the UCS a substantial amount of fluid thermal energy is flowing into the cold structures. During this process, liquid fuel and vapor are close to equilibrium. In cases where steel ablation is inhibited, the pressures in the UCS decrease with the fuel vapor pressures. In cases with steel ablation, regions of high liquid volume fractions are formed which represent more or less effective blockages to the main flow. Pressures in cases of steel ablation are partly increased by the evaporation of steel droplets. In cases with left-over sodium films, sodium evaporates and increases the pressures vigorously. Consequently, with dense droplet areas as blockages, pressures near the core can be lower than near the piston.

The pressures driving the piston are governed a) by fuel vapor pressures, for the cases without steel melting and without sodium, b) by fuel vapor pressure plus low partial pressures of steel vapor, for cases with steel melting and without sodium, and c) by fuel vapor pressure increased by high partial pressures of sodium vapor, for cases with both steel melting and sodium.

Near the piston interface, a cloud of liquid droplets is formed as the mass flow ejected from the UCS is decelerated.

9. The impact of disregarding ablation and core temperature distribution in the experiment

The analysis of the calculational matrix (Table II) shows, that even if we had modelled ablating walls in the USD experiment, which was once under consideration, we would have neglected the predominant influence of the steel inventory in the core. Because the ablation could not have been quantified directly, a mere energetic discussion would have been inconclusive. Adding a steel simulant in the USD experiment was unfeasible.

The prototypic cosine temperature distribution in the core could not be modelled in the experiment. We have tried, however, to model the liquid distribution shortly after the start of the transient for an initial cosine temperature distribution in the core. The USD experimental set-up was changed to have an initial vapor cushion below the working fluid in the core region (see /2/). No substantial change in the piston kinetic energy was noticed by adding this feature. But impact times were smaller which is consistent with the data given in Table II.

10. Comments on the energy balance

In order to give an overview over the absolute energies involved, Fig.23 to 25 list energy summations over the whole model on a linear scale. The figures show the black bars in units defined on the right hand ordinate. The light bars are used to visualize small energies by increasing the black bar length by a factor of ten, in units being defined on the left hand ordinate. All liquid and solid field energies are only plotted in right hand units. For each energy field, two bars are plotted, the first for the initial conditions at t=0, the second for the impact time when the piston has travelled 3 m. The piston initial energy which is zero has been omitted. Only the final energy is shown. Energies of the steel vapor, the liquid sodium, and the frozen fuel are not shown because they are always below 0.1 MJ. The amount of energy plotted is a summation over the whole SIMMER model for a specified mass. For each of these masses, called energy field, SIMMER-II solves a separate energy equation. There are two ways of energy transport to or from an energy field, one by energy convection or conduction, the other by mass transport. If, for example, the fuel pellets break up upon failure of the clad, the mass involved is added to the fuel particle field taking along its whole internal energy. The same procedure is valid for evaporation, condensation, melting, and solidification. Four different cases have been selected, the presentation of the others would not give any new perspective.

Fig. 23 shows the energy summations of Case 1. There is much more energy stored in liquid fuel in comparison with fuel vapor because the bulk of the fuel is liquid. During the blowdown, part of the fuel energy is flowing into the structures, as there are fuel pellets, clad, and can wall. As fuel particles are formed which are a part of the fluid field, energy is being transmitted to them. In this simple case where structure is inhibited to melt, all the energy released from fuel vapor and liquid fuel is added to the structures and the particles. Hence, 97% of the transmitted energy which is about 15 MJ flows via convection and

conduction. The piston kinetic energy which is finally 0.04 MJ, is only affected by the vapor field, the only contributor being here the fuel vapor. Only vapor performs displacement work. As long as the vapor energy is not changed, the work potential is not affected. The energy balance of Fig.23 shows that most of the transferred energy flows directly from liquid fuel to the structures. The small amount of energy that is first transferred to the vapor field and then to the structures cannot be shown in figure. As long as the vapor field is not affected by any of the ongoing energy flows, the magnitude of the flows is of no relevance to the piston energy. This implies, that errors being made on the basis of the large energies are not as relevant as their absolute value suggests. The discrepancy between the change in fuel vapor energy and piston energy indicates that a major amount of fuel vapor energy is transferred to the structures or liquid fuel.

By the simple energy balance of the figure we cannot understand the increase of the piston energy. The transient fluid dynamics as described in chapter 6.2 to 6.10, shows the complicated interaction between the working fluid and the piston. Fig.23 to 26 only show the magnitude of the energies involved. Further on, they show that it is not possible to estimate any mechanical energy by balancing the energies between two anticipated thermodynamic states.

Fig. 24 shows the energy summation of Case 5. The liquid steel and steel particles energy fields are added because structures are allowed to melt. There are substantial differences to Case 1. Now, fuel pellets and clad "loose" energy because of pellet failure and clad melting. This energy adds to the liquid steel and fuel particles which get additional energy from liquid fuel. Important for the mechanical energy is the presence of energy in a rather mobile form (liquid steel, fuel particles) and the generation of sodium vapor. As sodium vapor is close to the piston interface, the magnitude of its energy is related to the magnitude of the piston energy.

Fig. 26 shows the energy summations of Case 7. The predominant energy transfer is from liquid fuel to the in-core liquid steel. A subdivision into contributions from melting steel structures in the UCS is impossible. Another important process is the reduction of fuel vapor energy leaving hardly any driving potential for the piston energy. As for Case 5, all fuel pellets fail, and so do parts of the clad and can wall.

Fig. 26 shows the energy summations of Case 10. The figure is similar to that of Case 7 with respect to the liquid and solid fields. The initial fuel vapor energy is higher because of the cosine temperature profile. Not as much energy flows from liquid fuel to liquid steel, but is diverted to the fuel vapor. Like for Case 5, the sodium vapor generation affects the increase in piston energy. Again, the large decrease in fuel vapor energy does not contribute much to the piston energy. However, the fuel vapor energy is transferred to the structures and the liquid field.

11. Recommendations and future work

Although multicomponent flow through the UCS has not been modelled in the USD experiment, the capability of SIMMER to recalculate the single component two-phase flow reasonably well implies that, for this part of the transient, the code has been verified. Any uncertainty of UCS-connected energetics reduction is dominated by uncertainties in other parts of the transient. The present analysis explicitely states three effects which should be subject of future work. These are the influences of steel inventory in the core and of left-over liquid sodium in the UCS. Here, we recommend additional sensitivity analysis in two-dimensional whole core accident analysis. The third effect, the phenomenon at the sodium pool interface is subject of both theoretical and experimental work at KfK.

IV. Conclusions

Calculations with SIMMER-II modeling a single subassembly as in the USD experiment, but with prototypic materials and scale were performed.

The objective was to validate the kinetic energy reduction factors, as they were found in the USD experiment, with regard to their application to the prototypic case of an HCDA.

Since a simple replacement of experimental input data by prototypic data does not meet the requirements, a more thourough investigation of physical effects was necessary. The main findings of this investigation can be summarized as follows:

1. Some physical effects, which are not well modeled in SIMMER, did have less impact in the calculations for prototypic materials and scale than for USD-experimental conditions. These are, first, the transient heat conduction in the structure, because the cladding is thin enough to behave as a "thin wall".
   And second, the droplet size does not decrease to such an extent, that a lower bound has to be defined.

2. The kinetic energy of the piston in the USD-experiment and in SIMMER-calculations with UO_2 show a similar dependence on core pressure and temperature difference between working fluid and UCS-structure. The core pressure and temperature are scaled fairly well by factors in the order of 25:1 and 10:1, respectively.

   The temperature difference between fluid and UCS is not scaled correctly by a factor of 10. Similar reduction factors for the kinetic energy in simulant experiments and UO_2-calculations are obtained by scaling this temperature difference with a factor of approximatly 25.

3. Three major prototypic phenomena or conditions were not feasable to be modelled in the USD experiment. These are in-core steel inventory, melting steel structures, and left-over liquid sodium in the UCS. Effects of an initial cosine temperature profile in the core were modelled by a vapor cushion below the liquid. These phenomena and conditions change the characteristics of the transient to such an extent that their impact on the magnitude of the kinetic energy was different in each case.

   Sodium vapor was the predominant kinetic energy intensifier because it is generated near the downstream outlet of the above-core structures. Melting steel structures were adding partial pressures to the system but generally blocked the fuel discharge so that the kinetic energy was reduced. The effect of the cosine temperature distribution on the kinetic energy was small. The major kinetic energy mitigator was the presence of cold liquid steel droplets in the core, because the fuel vapor pressures are reduced by the energy transfer from fuel to steel.

4. The reduction factor between kinetic energy and the isentropic energy potential of the fuel is similar, within the one-dimensional model, for the most prototypic case and the case equivalent to the USD experiment.

   The reasons for the energy reduction, however, are different in both cases. An extrapolation of USD results to prototypic conditions can only be made if the effects of steel inventory in the core, melting steel structures, and left-over liquid sodium in the UCS are being considered carefully.

References:

1. D. Wilhelm, V.S. Starkovich and E.J. Chapyak,
A Simulant-Material Investigation of Flow Dynamics in the CRBR Upper Core Structure, NUREG/CR-2866, Los Alamos National Laboratory report LA-9478-MS (Sept. 1982).

2. L. Meyer,
Experimental Investigation of Flow Dynamics in the SNR-Upper Core Structure, to be published as Los Alamos National Laboratory report and KfK-Report (KfK-3709, (1984)).

3. L.L. Smith,
SIMMER-II, A Computer Programm for LMFBR Disrupted Core Analysis, NUREG/CR-0453, Los Alamos National Laboratory report LA-7515-M (October 1978).

4. E.J. Chapyak and V.S. Starkovich,
The Role of Similitude in the Design of LMFBR Safety-Related Simulation Experiments, Int. Meeting on Fast Reactor Safety and Technology, Seattle, Washington, 1979.

5. P. Schmuck,
K-EX: Ein Programm zur Berechnung der Brennstoffarbeit und der verdampften Brennstoffmengen bei einem hypothetischen Störfall, unpublished program description (1978,1984).

6. J.F. Jackson and M.G. Stevenson, Compilers,
Nuclear Reactor Safety Progress Report, 1978, Los Alamos National Laboratory report, LA-7195-PR (1978), pp. 97-105.

7. P. Royl et al.,
Untersuchungen zu Kühlmitteldurchsatzstörfällen im abgebrannten Mark 1A-Kern des Kernkraftwerks Kalkar, Kernforschungszentrum Karlsruhe report, KfK 2845, 1979, pp.112-117.

8. C.R. Bell, R.D. Burns, L.B. Luck,
Impact of SIMMER-II Model Uncertainties on Predicted Postdisassembly Dynamics, Los Alamos National Laboratory report, LA-8053-MS, NUREG/CR-1058, 1979.

9. J.R. Moszynski, T. Ginsberg,
Effect of Dispersed Particulate or Droplet Phase on the Rayleigh-Taylor Instability of a Gas-Liquid Interface, Brookhaven National Laboratory report, BNL-NUREG-51533, NUREG/CR-2688, 1982.

10. P. Schmuck,
The Postdisassembly Phase in LMFBRs: SIMMER Results and their Evaluation, Proceedings of the LMFBR Safety Topical Meeting, Lyon, 1982, pp. IV 79-88.

11. P.B. Abramson,
The Importance of Heat Transfer in Hypothetical Core Disruptive Accident Analysis, Nuclear Technology, Vol. 35, No.1, pp. 87-96.

12. M. Bober, J. Singer,
High Temperature Vapor Pressures of Stainless Steel Type 1.4970 and of Some Other Pure Metals From Laser Evaporation, Kernforschungszentrum Karlsruhe report, KfK 3772, 1984.

13. J.R. Moszynsky, T. Ginsberg,
Effect of Dispersed Particular or Droplet Phase on the Rayleigh - Taylor Instability of a Gas-Liquid Interface, Brookhaven National Laboratory repot NUREG/CR-2688, BNL-NUREG-51533, 1982.

14. P. Schmuck,
The Postdisasembly Phase in LMFBRs: SIMMER Results and Their Evaluation, Proceedings of the LMFBR Safety Topical Meeting, Lyon, 1982, pp. IV 79-88.

15. D. Wilhelm, L. Meyer, E.J. Chapyak,
Expansion of Flashing Fuel Simulants Into the Upper Core Structures Using CRBR and SNR Geometries, Proceedings of the LMFBR Safety Topical Meeting, Lyon, 1982, pp. IV 89-97.

Appendix A. SIMMER-II prototypic input file

```
    0  -105              SIMMER 2
   20     0     0     0     0     3     1     1  1000     0
          SNR REAL MATERIAL
XXXXXX    CASE NO.1
XXXXXX    BASE CASE EQUIVALENT TO USD EXPERIMENT
XXXXXX
XXXXXX    USD KONFIGURATION,    ONLY FLUID DYNAMICS
XXXXXX    VERSION: URANUSA4
XXXXXX    LAYOUT:  ONE DIMENSIONAL VERTICAL CHANNEL
XXXXXX    CHANNEL LENGTH = 4.932 M
XXXXXX
XXXXXX    FERTILE FUEL = FISSILE FUEL
XXXXXX    REDUCED LIQUID SODIUM IN UCS (ORIGINALLY 5 KG/M**3)
XXXXXX    T(CORE,FUEL) = KONSTANT
XXXXXX    INCREASED TMELT(STEEL) = 5300 K, DECREASED HFUSION
XXXXXX    NO STEEL INVENTORY IN CORE REGION
XXXXXX    PLUG-MODEL: FLIGHT DISTANCE=3.0 M, PISTON AREA=.0127 M**2
XXXXXX    UCS MULTIPLIERS 2.0 AND 1.6, MIXING HEAD MULTIPLIERS 3.0
XXXXXX
XXXXXX    DSNAME=INP.DATA(USD8)
XXXXXX    PLOT-FILE = DIRK.CP4.PLOT AUF UNIT=SDG01,VOL=INR002
XXXXXX
      0.200          1.0          0.9
    1    51
FLUID DYNAMICS INTEGER INPUT
    7    50     0     0     1     0     9     0     0
    0     0     0     0     0     0     0     0     0     0     0
   16     0     0     0     0     0     0     0     0     0     0     0
    1     1     1     4     1     7     1    10     1    11     1    13
    1    18     1    19     1    21     1    23     1    26     1    30
    1    51     1    57     1    62     1    63
    5  1000  1000   100    50     5     0    -1     0     0     0     1
PROBLEM DIMENSIONS AND OPERATIONAL CONTROLS
  0.0566900           1
  0.0950000          10   0.0375000          12   0.0590000          18
  0.0300000          19   0.0683000          22   0.0796000          26
  0.1280000          51
        0.5         0.0        -9.8      1.0-10
     0.0001       1.0-6      0.0001      1.0-06       1.0-8        0.05
      1.0-8       1.0-8       1.0-8       1.0-9        0.10      1.0-10
     0.0500        0.98        0.40       800.0      0.0001      0.0001
EDIT CONTROLS AND POSTPROCESSOR CONTROLS
        0.0
      0.005       0.005
        0.0
      0.050       2.000
        0.0
     0.0002
        0.0
      1.000
        0.0
1.0
0.0
4.0
0.0
0.0
```

SIMMER-II prototypic input file, cont.

```
0.0
0.0
0.0
0.0
0.0
0.0
THREE DIMENSIONAL PLOT PARAMETERS (VIEW FACTORS)
-3.0          -1.0          -4.0
TIME STEP CONTROLS
          0.0 1.00000E-05 1.00000E-12          0.3
       0.0005          0.25          10.0          1.0          1.0          1.0
       3.5E07          0.96          0.02         0.02          0.0          0.0
STRUCTURE AND SOLID FAILURE PARAMETERS
          0.5           0.5           0.5           0.5          0.5          0.5
          0.5
          .51           .51           .51           .51          .51          .51
         3.+6          1.+6          7.+5          8.+5         9.+5         2.+3
         3.+6          9.+5          2.+3
     0
 FUEL DATA     M=1
9890.         638.0         3047.         2.76000E+05 2.00
8767.4        504.0         0.45          2.50          4.30000E-03
2.07000E+12 6.12550E+04 0.0           2.62000E+06 6401.00       0.597
511.0         1.05          4.40          4.69537E+06 270.0         6468.
2763.         0.0           2763.         0.0
9.999943E+3 1.905027E-1-2.510704E-4 1.830919E-8
3.155782      4.658050E-1-1.071800
2212.339      0.3539176     400.
 STEEL DATA    M=2
7400.0        639.0         5300.0        2.60000E+00 25.00
6100.0        750.00        1.60          20.0          5.36000E-03
1.33800E+11 4.33700E+04 0.0           8.17000E+06 10500.0       0.360
492.0         1.26          1.64          0.0           56.0          7700.
3134.         0.0           3134.
8710.436    -0.8460045    4.323923E-5 6.34571E-10
1.938042      0.787118    -1.607633
 SODIUM DATA    M=3
0.            0.            0.            0.            0.
705.0         1300.         0.10          50.0          1.50000E-04
3.27600E+09 1.20230E+04 10.0          4.81600E+06 2509.         0.341
543.0         1.665         3.567         4.53500E+06 23.0          1375.
214.10        46.7          214.1         0.0
1.011630E+3-2.243262E-1-1.922490E-5 5.637876E-9
2.371000      3.146500E-1 1.521860
 CONTROL MATERIAL DATA    M=4
2520.0        1893.0        2623.0        2.50000E+05 83.74
2520.0        1890.0        1.            80.0          1.00000E-03
4.28600E+14 8.36800E+04 0.0           5.00000E+06 7107.0        0.350
500.          1.50          1.46          0.0           55.3          5472.
0.0
 FISSION GAS DATA    M=5
0.0           0.0           0.0           5.00000E+06
1.0
1.00000E+12 4.00000E+03 0.0           0.0           1.0           0.3
95.10         1.667         4.047         0.0           131.0         231.0
0.0           0.0
```

SIMMER-II prototypic input file, cont.

```
COMPONENT PROPERTIES
     9890.0      9890.0      9890.0      9890.0      7400.0      7400.0
     2520.0
     8580.0      8580.0      6100.0       705.0      2520.0      9890.0
     9890.0      7400.0
2.00000E 03 2.00000E+03 2.00000E+03 2.00000E+03 2.00000E+03 2.00000E+03
2.00000E+03 2.00000E+03 2.00000E+03
HEAT TRANSFER CORRELATION DATA
        1.0         1.0         1.0         1.0         1.0         1.0
        1.0         1.0         1.0         1.0         1.0         1.0
        1.0         1.0         1.0         1.0         1.0         1.0
      0.023         0.8         0.4         2.0
      0.025         0.8         0.8         5.0
      0.025         0.8         0.8         5.0
      0.023         0.8         0.4         2.0
      0.023         0.8         0.4        20.0
      0.370         0.6        0.33         2.0
DRAG CORRELATION DATA
    5.0E-01     1.5E 01     2.0E-04     9.2E-07     1.0E 00
    2.5E 00     1.0E 00        0.50        0.01        0.99     1.0E 10
      0.083       -0.25       0.008       0.083       -0.25       0.008
PARAMETER REGION 1, CORE
        1.0         0.0     1.0E+05    2.55E-03    3.00E-03    2.80E-03
       268.         0.0         0.0        .5108         0.0         0.0
    .005200     .007500      0.1100        2000.    132000.0     18000.
     1950.0        0.64     1.0E+05       2.3-5      1.0-17       0.001
      1.E-6    1.0 E+19     1.0E-06         1.0         1.0         1.0
PARAMETER REGION 2, PIN BUNDLE ENTRANCE SECTION
        1.0         0.0     1.0E+05    2.55E-03    3.00E-03    2.80E-03
       268.        316.         35.        .3406       .1581       .0963
    .005000     .007500      0.1100        2000.    132000.0     18000.
     1950.0        0.64     1.0E+05       2.3-5      1.0-17       0.001
      1.E-6    1.0 E+19     1.0E-06         1.0         2.0         2.0
PARAMETER REGION 3, PIN BUNDLE
        1.0         0.0     1.0E+05    2.55E-03    3.00E-03    2.80E-03
       268.        316.         35.        .3406       .1108       .0963
    .005200     .007500      0.1100        2000.    132000.0     18000.
     1950.0        0.64     1.0E+05       2.3-5      1.0-17       0.001
      1.E-6    1.0 E+19     1.0E-06         1.0         1.6         1.6
PARAMETER REGION 4, SPACE BEFORE MIXING HEAD
        1.0         0.0        1.0+5         0.0    1.0000-6      2.800-3
        0.0       1.0-3          35.         0.0    1.0000-4      0.09630
     0.1100      0.1100      0.1100         0.0        10.0       17860.
     1950.0        0.64        1.0+4       2.3-5      1.0-17     1.0E-03
      1.E-6    1.0 E+19     1.0E-06         1.0         1.0         1.0
PARAMETER REGION 5,  MIXING HEAD, HTCAN+CLAD INTERCHGD - SEE MESH SET
        1.0      0.0635        1.0+5         0.0    4.6000-2      2.800-3
        0.0        59.5        1.0-3         0.0        0.42     1.0E-04
   2.3000-2      0.1100      0.1100         0.0       18000.     132000.
     1950.0        0.64        1.0+5       2.3-5      1.0-17     1.0E-03
      1.E-6    1.0 E+19     1.0E-06         1.0         3.0         3.0
PARAMETER REGION 6,  UPPER SPACE
        5.0         0.0        1.0+5         0.0         0.0      2.800-3
        0.0       1.0-3         20.0         0.0    1.0000-4      0.14680
     0.1000      0.1000      0.1000         0.0      132000.       18000.
     1950.0        0.64        6.0+3       2.3-5      1.0-17     1.0E-03
```

SIMMER-II prototypic input file, cont.

```
      1.E-6    1.0 E+19     1.0E-06          1.0          1.2          1.2
PARAMETER REGION 7,  SODIUM POOL (NOT USED)
        5.0         0.0        1.0+5          0.0          0.0          0.0
        0.0         0.0         25.0          0.0          0.0          0.0
     0.1100      0.1100      0.1100          0.0     132000.       18000.
     1950.0        0.64        6.0+3       2.3-5      1.0-17     1.0E-03
      1.E-6    1.0 E+19     1.0E-06          1.0          1.0          1.0
PARAMETER REGION 8, COVER GAS (NOT USED)
        3.0         0.0     1.0E+05          0.0          0.0          0.0
        0.0         0.0         0.0          0.0          0.0          0.0
     0.1100      0.1100      0.1100        2000.    132000.0       18000.
     1950.0        0.64     1.0E+05       2.3-5      1.0-17        0.001
      1.E-6    1.0 E+19     1.0E-06          1.0          1.0          1.0
PARAMETER REGION 9, PISTON TRACK
        5.0      0.9998     1.0E+05          0.0          0.0    5.08E-02
        0.0         0.0         34.0          0.0          0.0      0.9998
     0.1100      0.1100      0.1100        2000.    132000.0       18000.
     1950.0        0.64     1.0E+05       2.3-5      1.0-17        0.001
      1.E-6    1.0 E+19     1.0E-06          1.0          1.0          1.0
PLUG MODEL
    1    27    63    23    27     1     1
    1     1     1     1     1     1
       26.6       150.0    100000.0          3.0       0.0127
INITIAL BOTTOM BOUNDARY VELOCITIES
        0.0
        0.0
MESH SET 1, ACTIVE CORE
    1    10     1     1     1    -1     0     1     1
   69
        0.0         0.0         0.0          0.0          0.0          0.0
        0.0         0.0         0.0
     1600.0         0.0      1000.0        1000.          0.0
     2056.0         0.0         0.0          0.0          0.0          0.0
        0.0         0.0
        0.0      1701.0         0.0          0.0          0.0          0.0
        0.0         0.0         0.0          0.0       1.0-4        1.0-3
POINTWISE LIQUID FERTILE FUEL TEMPERATURES
      5175.       5175.       5175.       5175.       5175.       5175.
      5175.       5175.       5175.       5175.
MESH SET 2, AXIAL BLANKET ENTRANCE SECTION
   11    12     1     1     3     1     0     0     2
     3369.0         0.0         0.0          0.0       1169.0       713.
        0.0         0.0         0.0
     1175.0         0.0      1175.0        1175.          0.0
        0.0         0.0         0.0         .001          0.0          0.0
        0.0         0.0
        0.0         0.0        1175.          0.0          0.0          0.0
        0.0         0.0         0.0       .23000          0.0          0.0
     1175.0
        0.0        0.0          0.0          0.0       1.0-4        1.0-3
MESH SET 3, AXIAL BLANKET
   13    18     1     1     3     1     0     0     3
     3369.0         0.0         0.0          0.0        820.0       713.
        0.0         0.0         0.0
     1175.0         0.0      1175.0        1175.          0.0
        0.0         0.0         0.0         .001          0.0          0.0
```

SIMMER-II prototypic input file, cont.

```
        0.0         0.0
        0.0         0.0       1175.         0.0         0.0         0.0
        0.0         0.0         0.0       .23000         0.0         0.0
     1175.0
        0.0       0.0           0.0         0.0       1.0-4       1.0-3
MESH SET 4, SPACE IN FRONT OF MIXING HEAD
   19    19     1     1     3     1     0     0     4
        0.0         0.0         0.0         0.0         0.0       713.
        0.0         0.0         0.0
        0.0         0.0      1175.0       1175.         0.0
        0.0         0.0         0.0        .001         0.0         0.0
        0.0         0.0
        0.0         0.0       1175.         0.0         0.0         0.0
        0.0         0.0         0.0       .23000         0.0         0.0
     1175.0
        0.0       0.0           0.0         0.0       1.0-4       1.0-3
MESH SET 5, MIXING HEAD, DENSITY CAN TO CLAD ,NONFLOW AREA PRESENT
   20    22     1     1     3     1     0     0     5
        0.0         0.0         0.0         0.0      3108.0         0.0
        0.0         0.0         0.0
        0.0         0.0       1175.       1175.         0.0
        0.0         0.0         0.0        .001         0.0         0.0
        0.0         0.0
        0.0         0.0       1175.         0.0         0.0         0.0
        0.0         0.0         0.0       .23000         0.0         0.0
     1175.0
        0.0       0.0           0.0         0.0       1.0-4       1.0-3
MESH SET 6, UPPER SPACE
   23    26     1     1     3     1     0     0     6
        0.0         0.0         0.0         0.0         0.0       1086.
        0.0         0.0         0.0
        0.0         0.0      1175.0       1175.0         0.0
        0.0         0.0         0.0        .001         0.0         0.0
        0.0         0.0
        0.0         0.0      1175.0         0.0         0.0         0.0
        0.0         0.0         0.0       .23000         0.0         0.0
     1175.0
        0.0       0.0           0.0         0.0       1.0-4       1.0-3
MESH SET 7, PISTON TRACK
   27    51     1     1     3     1     0     0     9
        0.0         0.0         0.0         0.0       0.001         0.0
        0.0
        0.0         0.0       900.0       900.0
        0.0         0.0         0.0        .001         0.0
        0.0
        0.0         0.0       900.0       900.0
        0.0         0.0         0.0       .23000
      900.0
        0.0         0.0         0.0         0.0       1.0-4       1.0-3
```

Appendix B

Review of the scaling analysis

The scaling analysis for the USD experiment was originally started to select a suitable simulant fluid /4/. The conditions for which it had to be selected were limited to the expansion phase of two-phase fuel with vapor pressure as the driving source. Propanol was found to be the best simulant fluid on the conditions described below.

The analysis presented in Ref. /1/ and /4/ used the three generic mass, momentum, and energy conservation equations to extract nondimensional groups after normalization of the homogeneous parts of the equations. The latent heat of vaporization was the main normalization parameter because the fuel vapor as the only working fluid is closely related to building up the work potential of the transient. The density as a normalization constant was taken from the liquid field inspite of the expected large vapor fraction of the fluid penetrating the UCS. However, vapor field density would have introduced a strong dependance upon the state of the vapor, so that the choice of the state would have dominated the result of the scaling. In the energy equation, the vapor specific heat was chosen because the energy change of the fluid after the evaporation is governed by this property. A change to the liquid specific heat has only a small effect on the scaling because the ratio of specific heats of propanol to fuel is 8.25 and 6.83 for vapor and liquid, respectively. The normalization of the conservation equations resulted in a set of scaling factors for the pressure, temperature and length.

The values found with propanol at room temperature were 0.04, 0.1 and 0.4 for pressure, temperature and length, respectively. The scaling analysis was supplemented by a comparison of additional nondimensional groups of the simulant and prototypic fluids.

It has been stated before /4/ that "it is impossible except in the most simple situations to design an experiment that rigorously fulfills the requirements of similitude. A more realistic goal is to insure that any imbalances that do occur in the relative magnitudes of terms in the appropriate equations are relatively small (i.e. much less than an order of magnitude discrepancy)."

In the present report, simulant and prototypic calculations have been presented to validate SIMMER-II predictions for the expansion phase transient. To be able to compare simulant and prototypic transients one has to analyse the validity of the scaling factors and its range.

Four questions should be discussed in this context.

1. The gravity term of the momentum equation was used to scale the length. However, the rapid expansion of the fuel simulant makes it improbable that gravity has a major effect during most of the transient. What then, is a proper length scaling parameter?

2. How will the scaling parameters change when the temperature of the propanol is changed from 300 K to 450 K?

3. Which properties should be used in each case, those of vapor or those of liquid?

4. Are there any other nondimensional parameters relevant to similitude?

To tackle the last question first, the checking for the completeness of nondimensional groups, a dimensional analysis was performed using a limited number of fluid properties which were,

- h, the latentheat of evaporation
- ρ, the density
- ν, the viscosity

- λ, the thermal conductivity
- c, the specific heat and
- σ, the surface tension

If we apply dimensional analysis in a complex system, we have to acknowledge the impossibility of a unique solution like in steady state hydrodynamics. Therefore, the input to the analysis, as well as any result obtained must be submitted to engineering judgement and is subject to a considerable band of uncertainty.

Table A shows three different sets of nondimensional groups with the length, the pressure, and the temperature as the additional variable. These are results of a dimensional analysis using different subsets of the properties above.

The length groups Nx offer solutions to question No.1 because the gravitational acceleration has not been used. Nx_1 stands for a modified Reynolds number, with the square root of the latent heat replacing the velocity. Nx_1 compares forces due to the potential energy of the fuel with the friction forces of a steady state flow. Only the vapor field adds a substantial amount to the momentum balance in conjunction with entrainment and de-entrainment forces. The phenomena are too complicated as to be able to justify the exclusive use of Nx_1. Nx_2 is a modified Weber number. By this, the droplet size is compared to the size of the flow channel. The droplet size governs the heat transfer between the liquid and vapor phase. The relevance of this group is reduced by the fact that the energy flow to the wall is governed by the phenomena at the wall, not in the main stream. Nx_3 is an extention of Nx_1 with the Prandtl number yielding a modified Peclet number. It governs the energy balance at a liquid film on which vapor condenses. Consequently, Nx_3 is important for the energy flows from the fluid to the wall. The main reduction of the kinetic energy of the system is governed by this phenomenon. The actual length scaling factor used in the USD experiments was 0.4 which offers a reasonable representation of the scales found in the present

analysis. Nx_4 and Nx_5 are groups combining all properties except the surface tension. They are extensions of the previous sets by the Prandtl number and do not relate to any physical phenomenon in the system. They, and any other additional extensions are not used in setting the length scale.

Before answering the remaining two questions, the pressure groups and temperature groups of Table A have to be discussed. The pressure group Np_1 has already been used in the first USD scaling analysis. The use of Np_2 and Np_3 seems not to be justified by a physical model. Additional groups using the surface tension would introduce limited scaling of local effects, like the dynamics of vapor bubbles. These play a role when the fluid flashes in the core region. However, the prototypic expansion is unlikely to be submitted to a similar phenomenon so that any similarity laws are questionable.

The physical significance of the temperature groups is similar to that of the pressure groups. NT_1 which has been used in the first USD scaling analysis relates the vapor temperature to the vapor pressure via Np_1. Additionally, NT_1 and Np_1 are results of forming dimensionless conservation equations. Expanding NT_1 with the Prandtl number results in NT_2. However, NT_2 does not relate to any single heat transfer model. NT_3 and NT_4 are expansions to the full set of parameters. Again, there exists no model by which to select them.

To calculate any scaling factors by the nondimensional groups selected, it has to be decided whether to use vapor or liquid properties. The latent heat and surface tension are not affected. The remaining properties will now be discussed. The density plays a substantial role in selecting the pressure by Np_1. If the vapor density would be used, it would depend strongly on the pressure. This interdependence inhibits the use of the vapor property. The specific heat which governs the scaling of the temperature does not differ much for vapor and liquid, as stated above. The thermal conductivity is only important with respect to the liquid phase.

In the gas phase, energy transport through conduction is dominated by the transport through convection. For the groups selected, the dynamic viscosity occurs only in Nx_1 which was not selected as a major group because of the complex entrainment and de-entrainment phenomena. Nx_1 is calculated for both vapor and liquid phase. The other scaling factors in Table A, if not explicitely stated, were determined with the liquid viscosity for consistency with the other properties.

The last question remaining is caused by the considerable variation of liquid properties with the temperature.

Between 370 K and 470 K, the density changes by 20%, the specific heat by 50%, the thermal conductivity by 70%, the surface tension by 100%, and the dynamic viscosity by 280%. The initial conditions of the experiment have been chosen as a first reference, although a single value only represents an average over different conditions.

Table A shows the scaling factors on the basis of the above discussion. The propanol temperature of 450 K has been used in conjunction with a fuel temperature of 4500 K. The ratio of 0.1 of propanol to fuel temperatures was chosen in reasonable agreement with the vapor pressure curves, see Ref. /15/. Because the mechanical energy released by the system through a movable piston was the main objective of the analysis, the vapor pressure as the main energy source was identified to be of predominant importance. The scaling factors related to Nx_3, Np_1, and NT_1 must be compared to the factors by which the USD experimental conditions were selected. These were taken on the basis of a propanol temperature of 300 K. The pressure and temperature factors resulted in 0.04 and 0.1, respectively. The length scale was set to 0.4.

The original scaling factors and their differences to those in Table A show that projecting simulant results onto prototypic conditions is only possible within the given uncertainty.

Variable to be Scaled	Nondimensional Group	Scaling Factor
Length x	$Nx_1 = x\rho h^{1/2}\eta^{-1}$ { liquid	0.74
	vapor	0.17
	$Nx_2 = x\rho h\sigma^{-1}$	0.94
	$Nx_3 = x\rho c h^{1/2}\lambda^{-1}$	0.12
	$Nx_4 = x\rho c^{1/2} h^{1/2}\lambda^{-1/2}\eta^{-1/2}$	0.29
	$Nx_5 = x\rho\lambda^{1/2} h^{1/2} c^{-1/2}\eta^{-3/2}$	1.82
Pressure p	$Np_1 = p\rho^{-1} h^{-1}$	0.025
	$Np_2 = p\lambda\rho^{-1} h^{-1} c^{-1}\eta^{-1}$	0.004
	$Np_3 = p\eta c\rho^{-1} h^{-1}\lambda^{-1}$	0.16
Temperature T	$NT_1 = Tch^{-1}$	0.04
	$NT_2 = T\lambda h^{-1}\eta^{-1}$	0.27
	$NT_3 = T\lambda^2 h^{-1} c^{-1}\eta^{-2}$	0.009
	$NT_4 = T\eta c^2 h^{-1}\lambda^{-1}$	1.7

c = specific heat (J kg^{-1} K^{-1})
h = latent heat of evaporation (J kg^{-1})
η = dynamic viscosity (kg m^{-1} s^{-1})
λ = thermal conductivity (J s^{-1} m^{-1} K^{-1})
ρ = density (kg m^{-3})
σ = surface tension (J m^{-2})

Table A. Nondimensional groups

Case No.	P-core (MPa)	T-core (K)	T-UCS (K)	t-imp (ms)	v-imp (m/s)	E-kin (kJ)	E/E-isen
A-0	2.5	4495	-	-	-	99.5	-
A-1	2.5	4495	-	86.0	65.8	57.5	0.577
A-2	2.5	4495	4495	95.6	63.2	53.1	0.532
A-3	2.5	4495	2495	258.9	22.7	6.9	0.069
B-0	5.0	4736	-	-	-	180.4	-
B-1	5.0	4736	-	63.3	88.6	104.4	0.579
B-2	5.0	4736	4736	71.8	83.6	92.9	0.515
B-3	5.0	4736	2736	160.3	40.8	22.1	0.123
B-4	5.0	4736	736	187.1	25.9	8.9	0.049
C-0	10.0	5004	-	-		315.5	-
C-1	10.0	5004	-	46.1	118.0	185.2	0.587
C-2	10.0	5004	5004	54.8	109.4	159.1	0.504
C-3	10.0	5004	3004	106.8	63.1	53.0	0.168
C-4	10.0	5004	1004	127.2	44.0	25.8	0.082
D-0	15.0	5175	-	-	-	429.9	-
D-1	15.0	5175	-	39.1	140.4	262.1	0.610
D-2	15.0	5175	5175	47.0	127.4	215.8	0.502
D-3	15.0	5175	3175	87.9	78.8	82.6	0.192
D-4	15.0	5175	1175	107.4	54.2	39.1	0.091
E-0	25.0	5409	-	-	-	625.5	-
E-1	25.0	5409	-	31.1	174.9	406.8	0.650
E-2	25.0	5409	5409	39.0	153.0	311.2	0.498
E-3	25.0	5409	3409	65.9	100.0	133.1	0.213
E-4	25.0	5409	1409	89.7	71.3	67.6	0.108

Table I. Calculations with UO_2 and simulated experimental conditions in the UCS. Results are time, velocity and kinetic energy at piston impact and the ratio of the kinetic energy of the piston and the isentropic work potential.

Case	Expanding Fuel	Melting Steel Structures	Steel in Core	Liquid Sodium in UCS	Pool Version	Cosine Temperature Profile	Impact Time (ms)	Piston Velocity (m/s)	Kinetic Energy (kJ)	Fraction of Isentropic Energy
0									430	1.00
1	B						107	55	41	0.10
2	O			O			64	103	142	0.33
3	O	O					98	62	52	0.12
4	O	O				O	94	67	60	0.14
5	O	O		O			73	109	159	0.37
6	O	O		O		O	58	118	186	0.43
7	X	X	X				206	23	7	0.02
8	X	X	X			X	168	26	9	0.02
9	X	X	X	X			104	72	69	0.16
10	X	X	X	X		X	84	72	70	0.16
11	X	X	X	X	X		-	-	40	0.09
12	X	X	X	X	X	X	-	-	30	0.07

B = base case equivalent to USD experiment

O = theoretical combinations

Table II. Matrix of prototypic calculations.

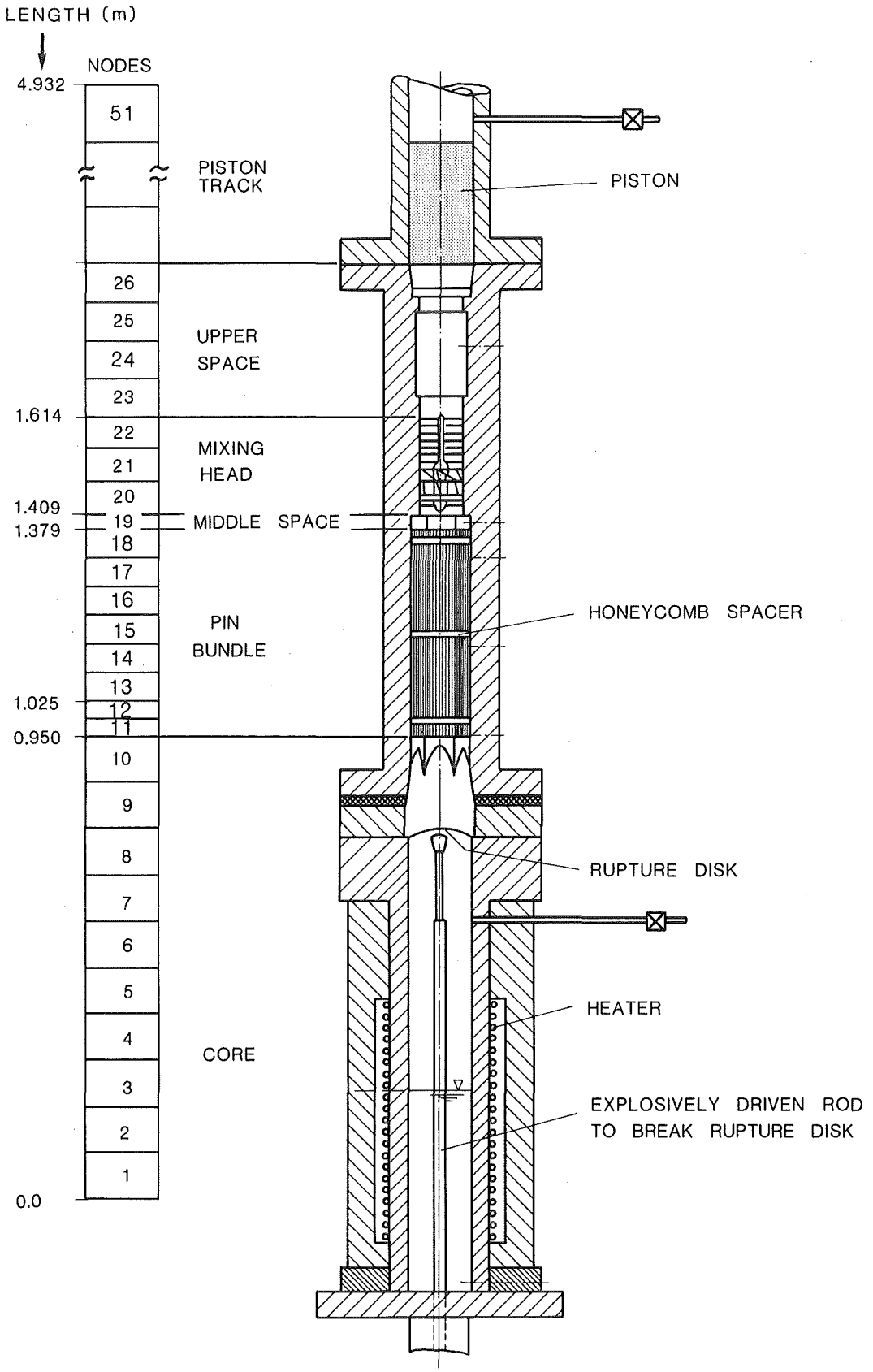

Fig.1. Model of the USD experiment with SIMMER-II noding.

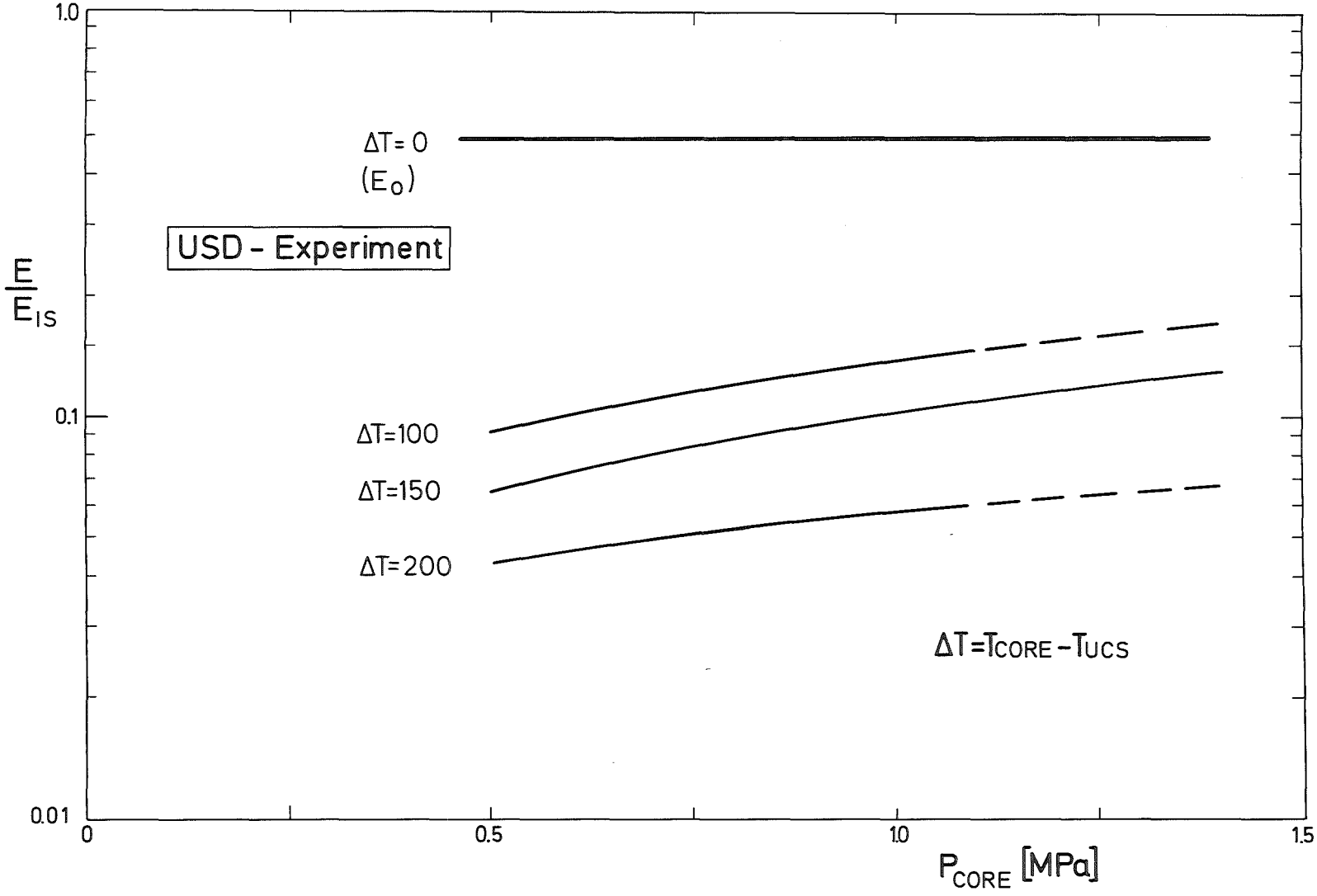

Fig.2. Kinetic energy of the piston related to the isentropic work potential of the fuel simulant in the USD-experiment.

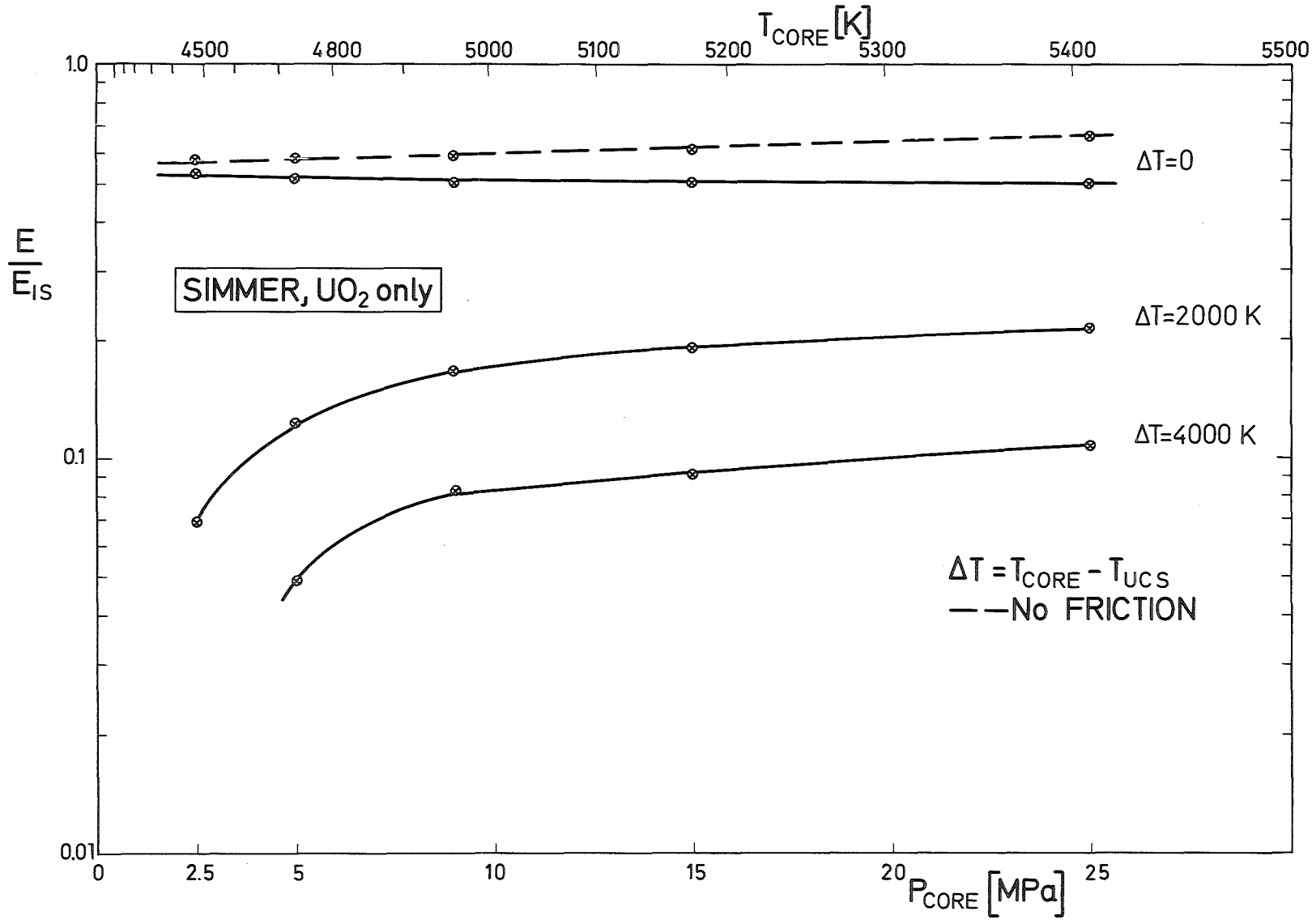

Fig.3. Kinetic energy of the piston related to the isentropic work potential of UO_2 calculated with SIMMER at simplified conditions (without prototypic phenomena).

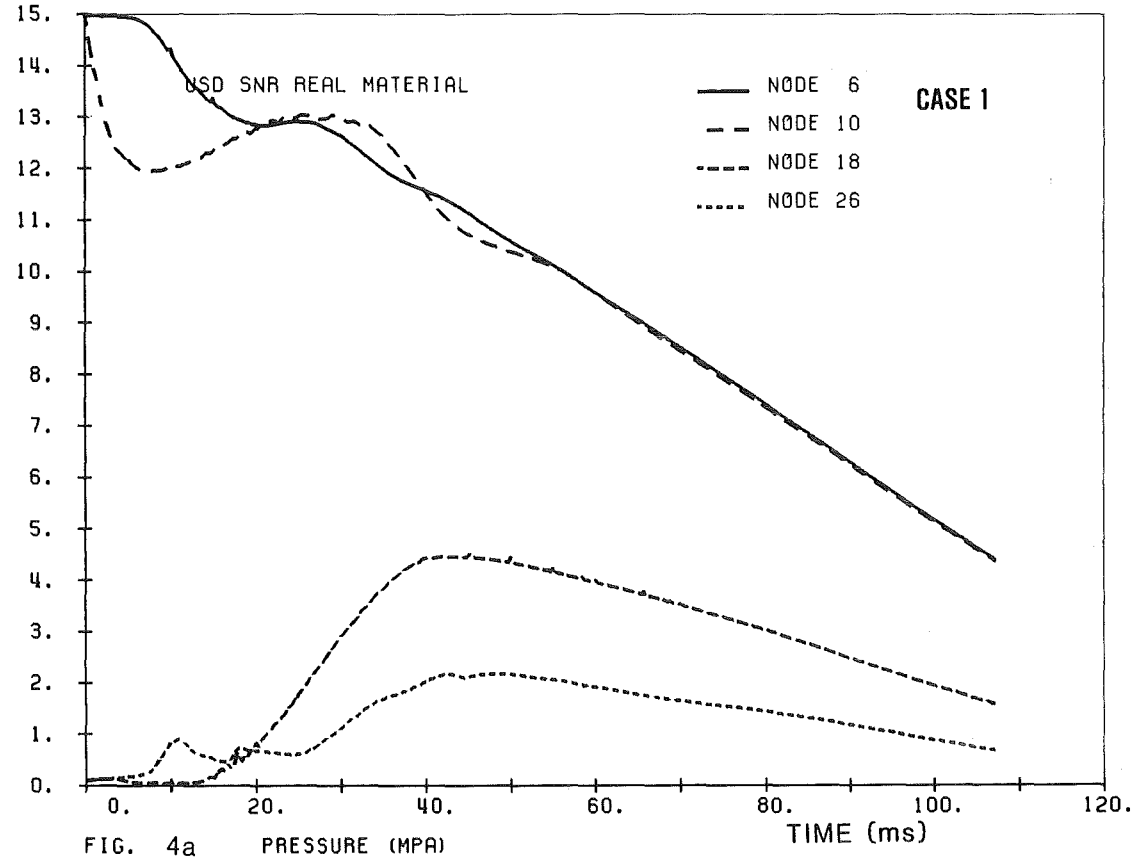

FIG. 4a PRESSURE (MPA)

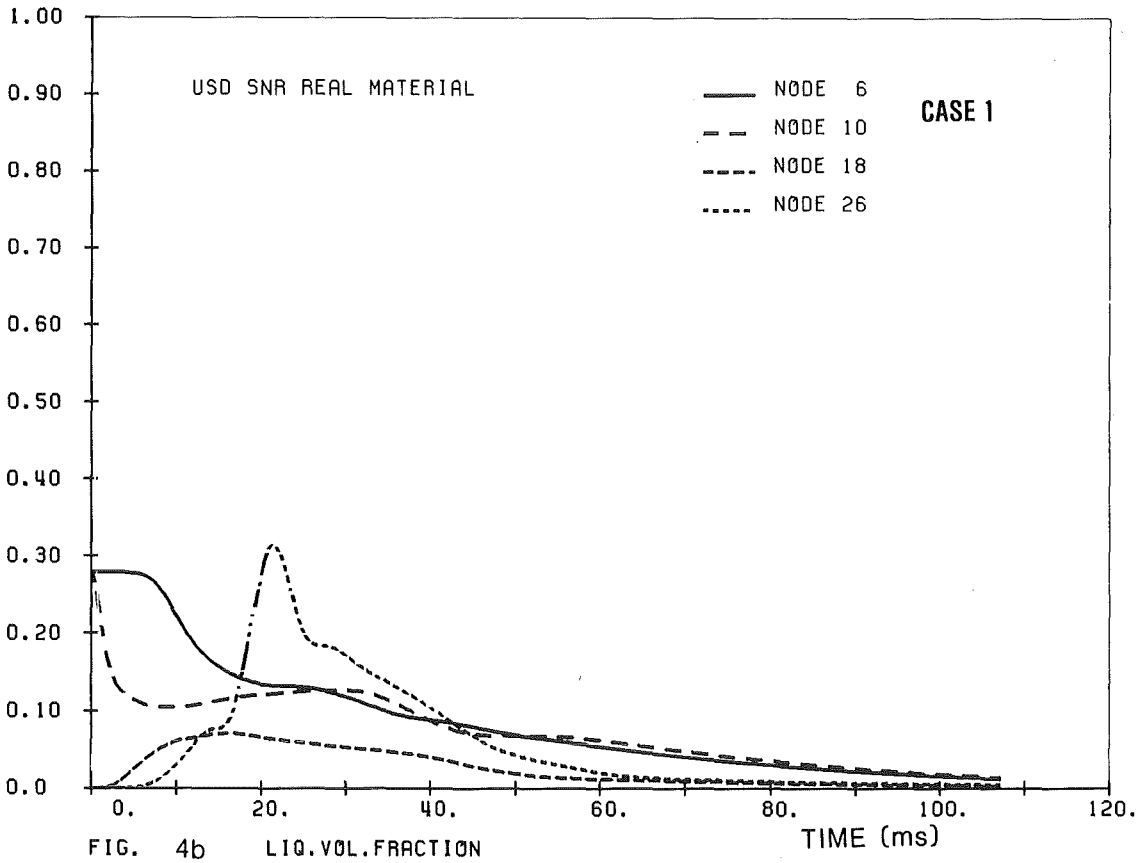

FIG. 4b LIQ.VOL.FRACTION

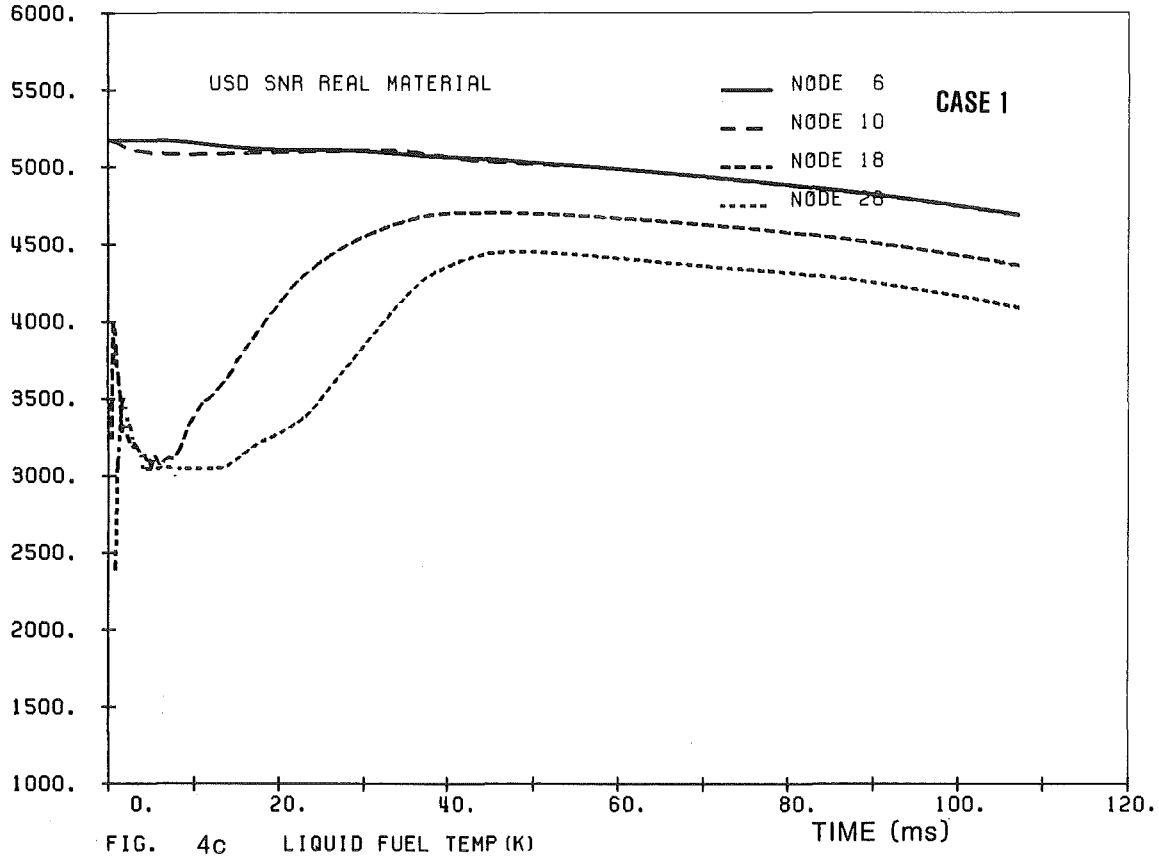

FIG. 4c LIQUID FUEL TEMP (K)

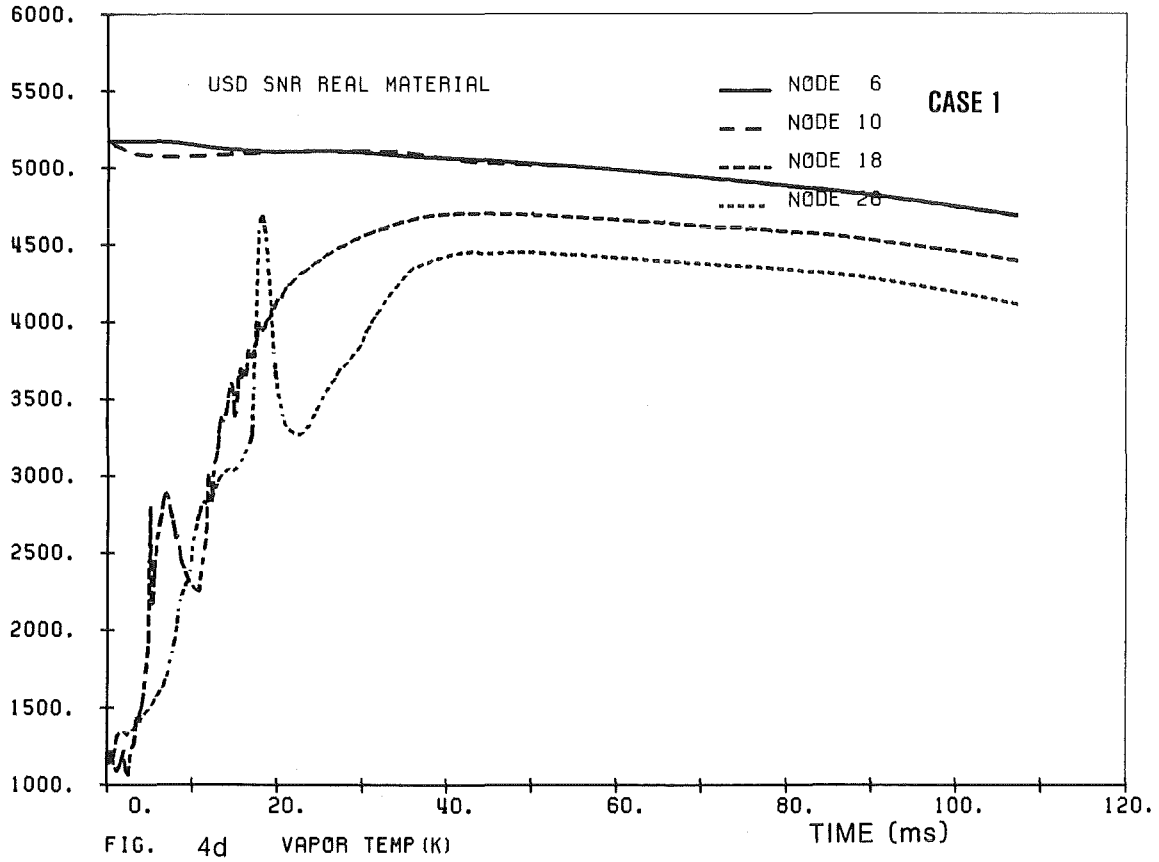

FIG. 4d VAPOR TEMP (K)

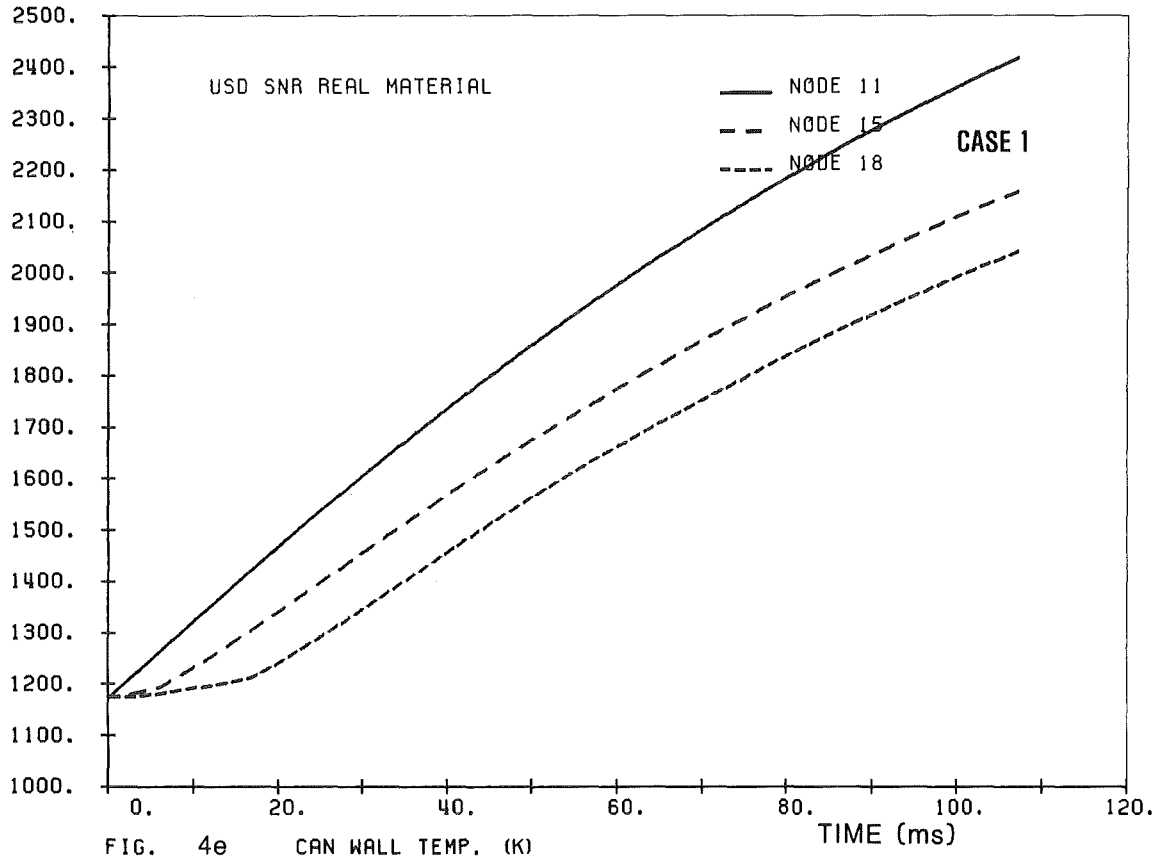

FIG. 4e CAN WALL TEMP. (K)

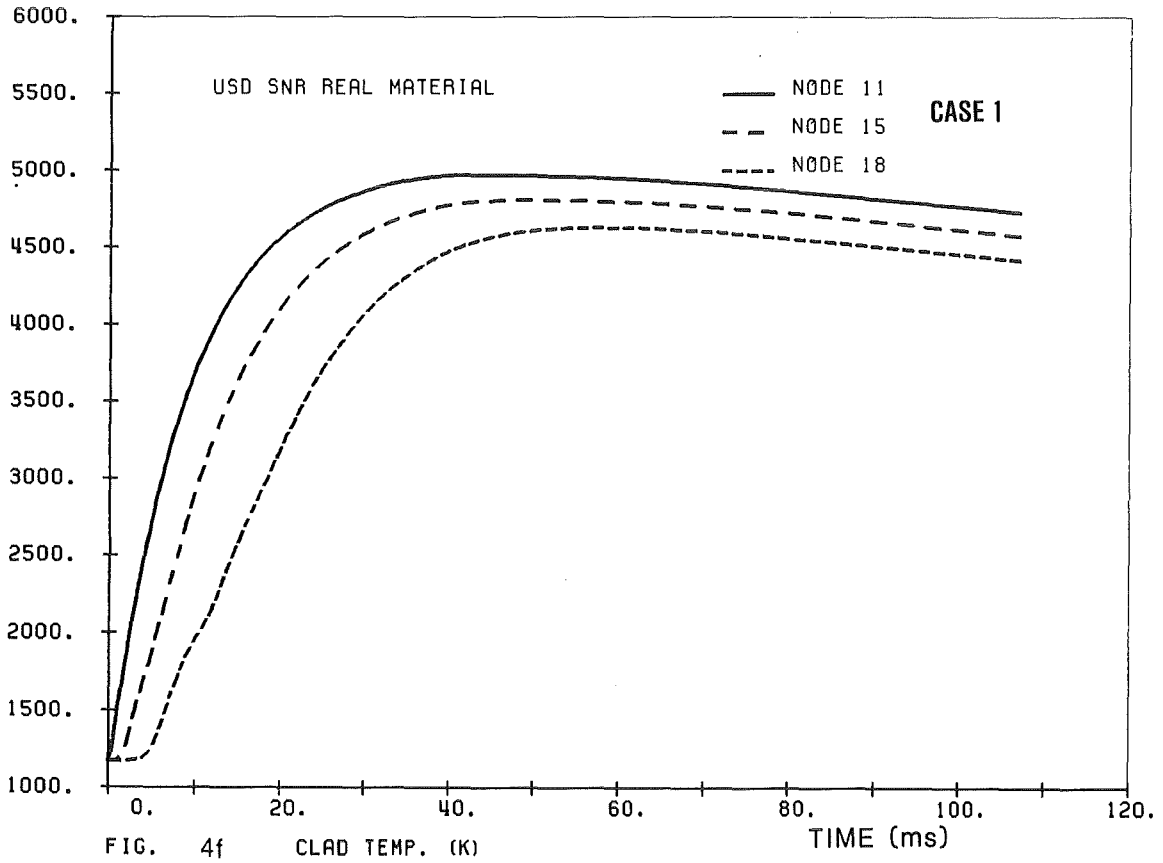

FIG. 4f CLAD TEMP. (K)

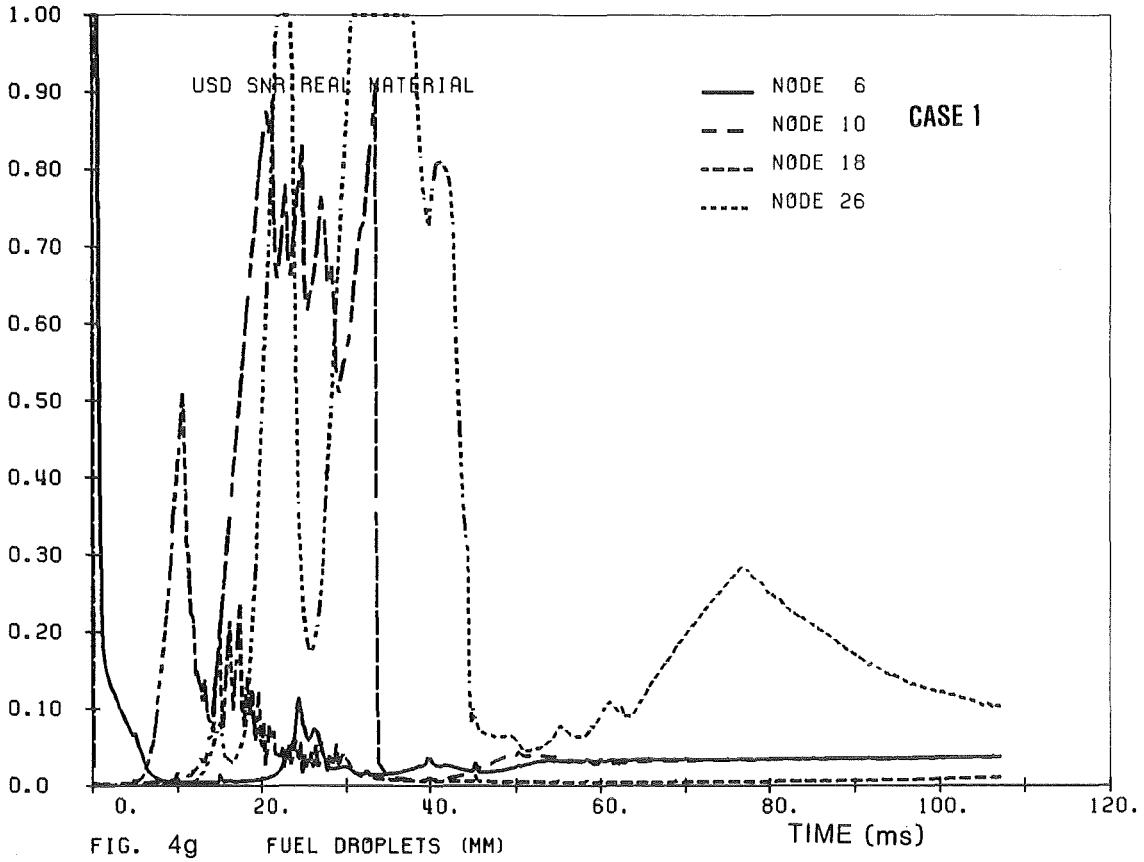

FIG. 4g FUEL DROPLETS (MM)

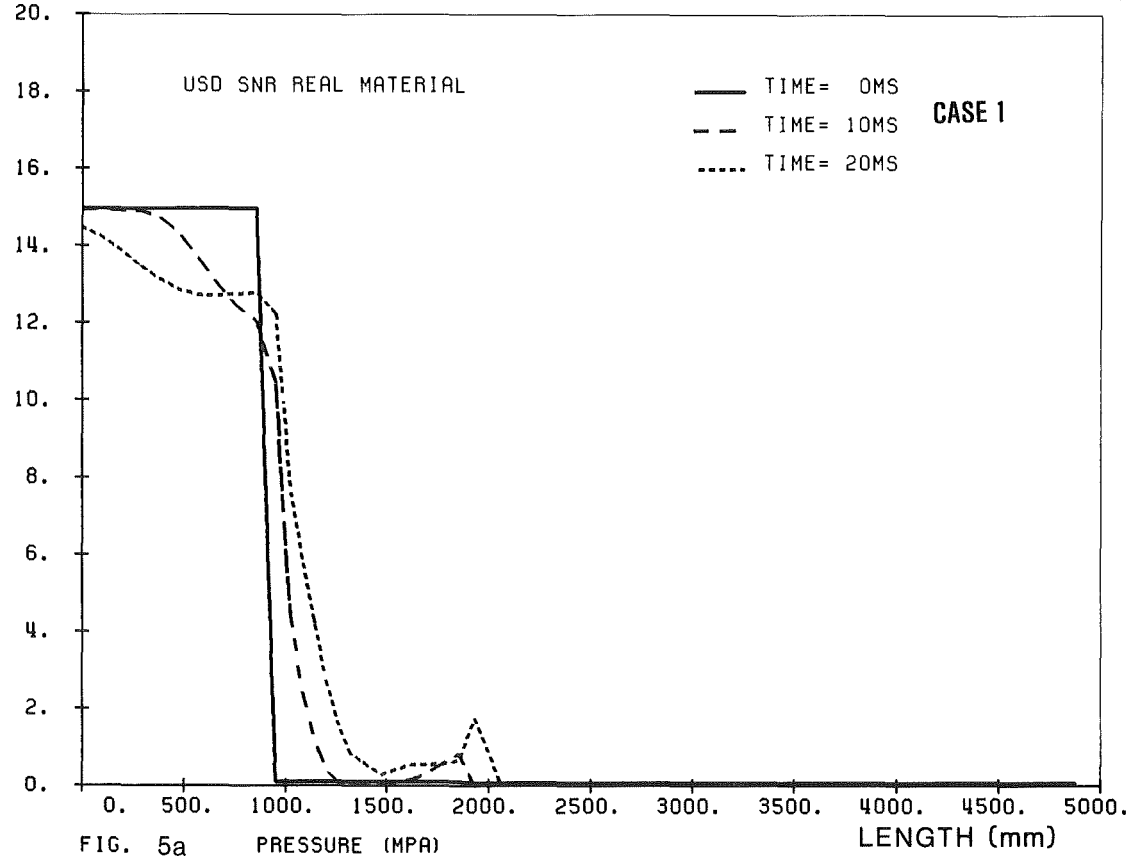
USD SNR REAL MATERIAL
TIME= 0MS
TIME= 10MS
TIME= 20MS
CASE 1
20.
18.
16.
14.
12.
10.
8.
6.
4.
2.
0.
0. 500. 1000. 1500. 2000. 2500. 3000. 3500. 4000. 4500. 5000.
PRESSURE (MPA)
LENGTH (mm)

FIG. 5a

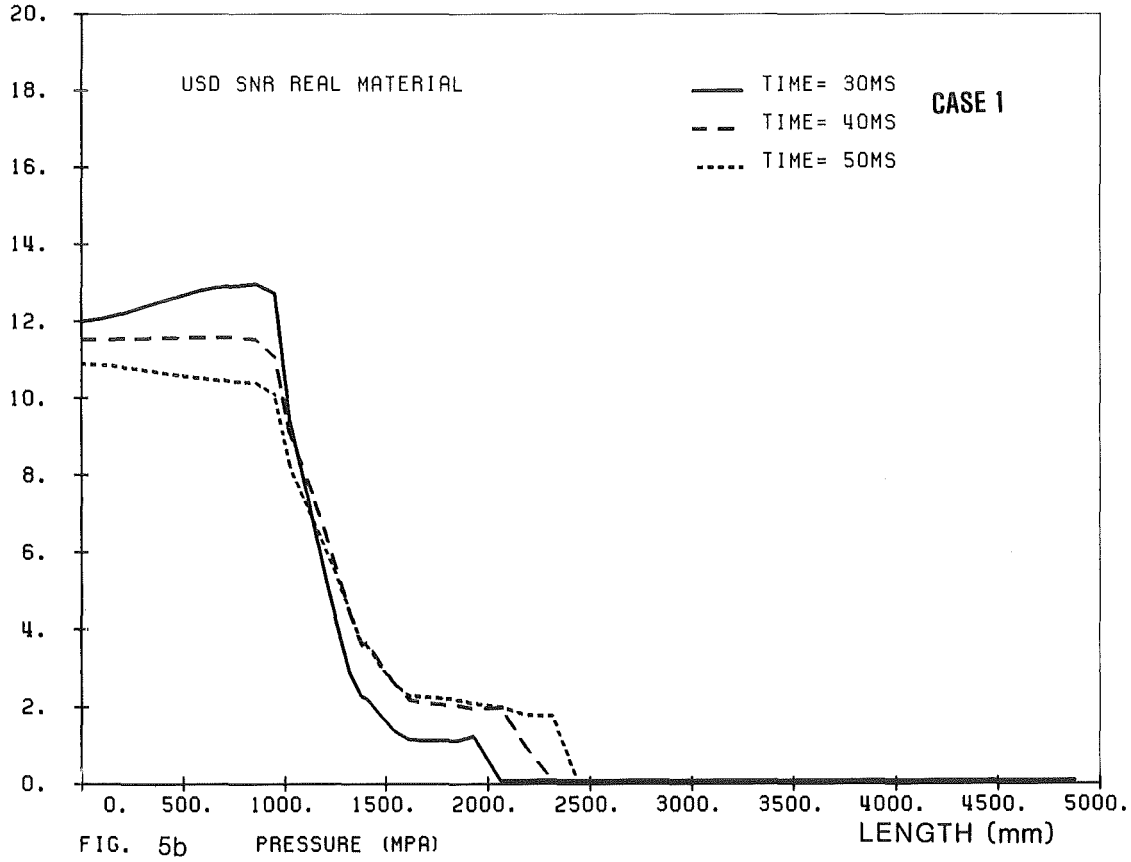
USD SNR REAL MATERIAL
TIME= 30MS
TIME= 40MS
TIME= 50MS
CASE 1
20.
18.
16.
14.
12.
10.
8.
6.
4.
2.
0.
0. 500. 1000. 1500. 2000. 2500. 3000. 3500. 4000. 4500. 5000.
PRESSURE (MPA)
LENGTH (mm)

FIG. 5b

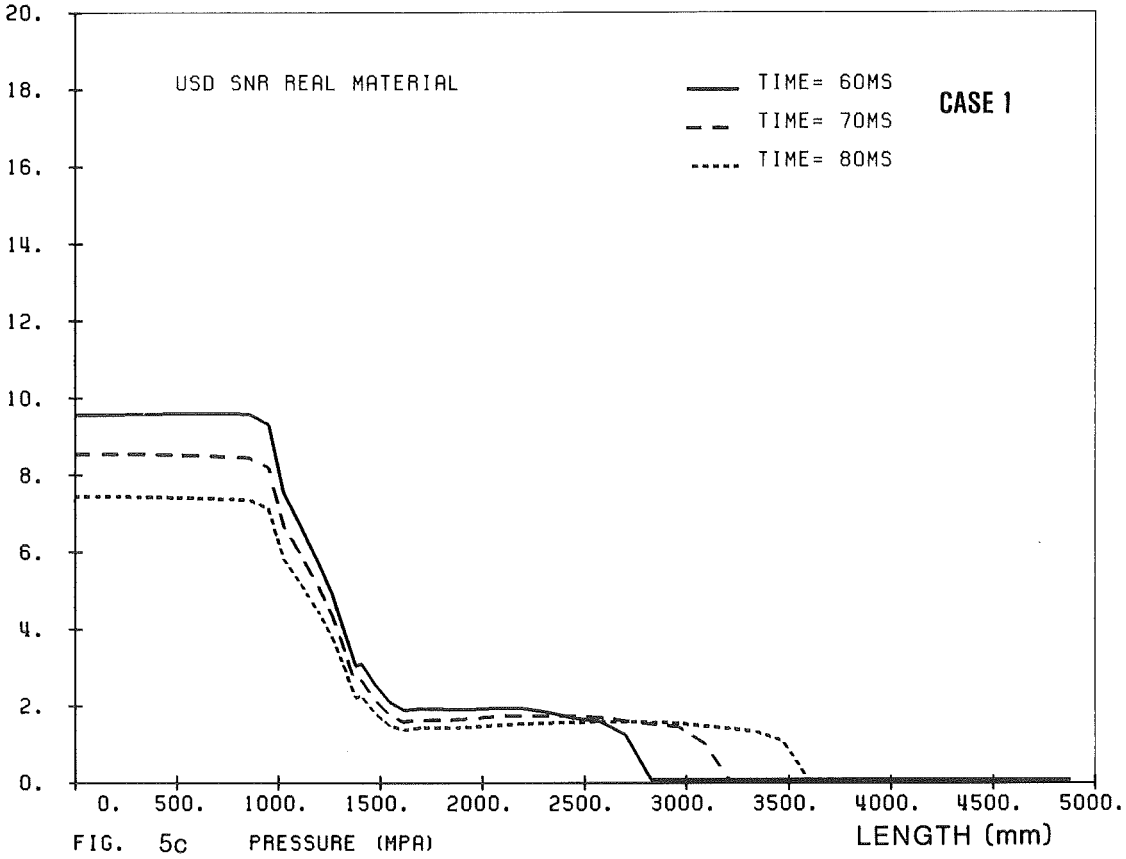
USD SNR REAL MATERIAL
TIME= 60MS
TIME= 70MS
TIME= 80MS
CASE 1
20.
18.
16.
14.
12.
10.
8.
6.
4.
2.
0.
0. 500. 1000. 1500. 2000. 2500. 3000. 3500. 4000. 4500. 5000.
PRESSURE (MPA)
LENGTH (mm)

FIG. 5c

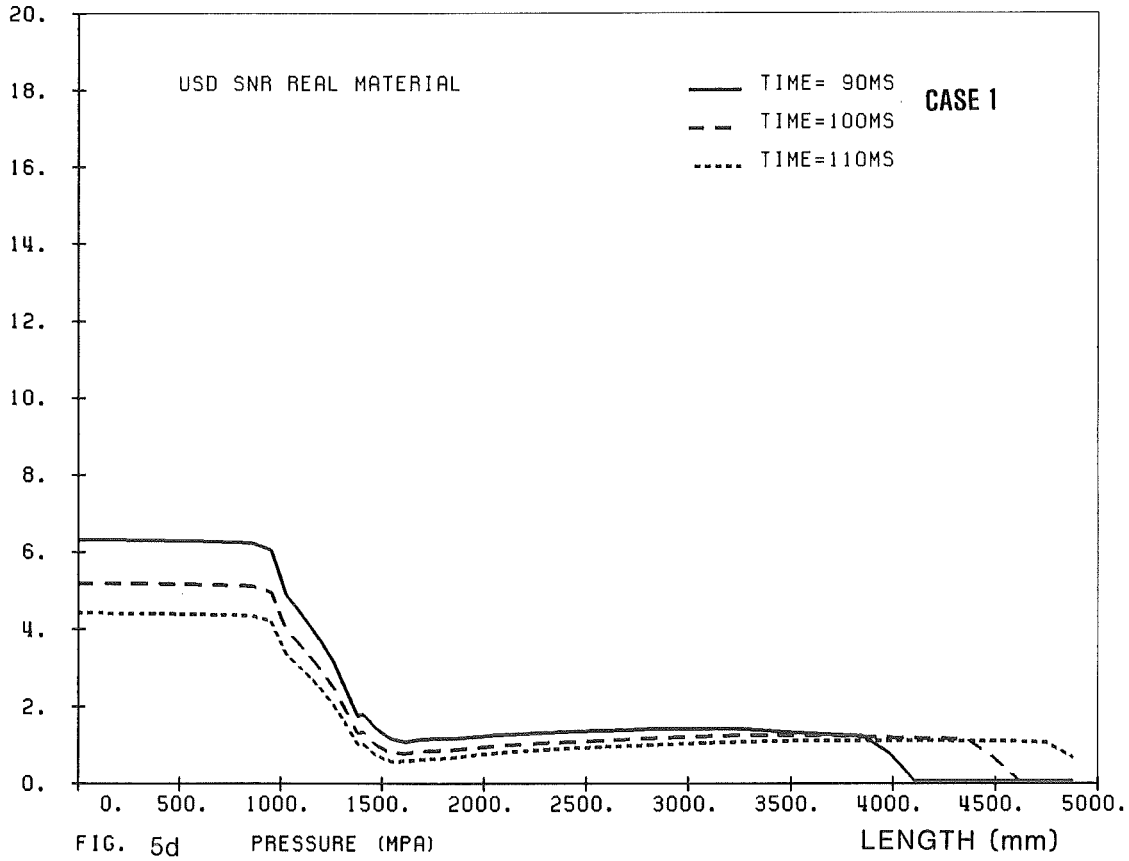
USD SNR REAL MATERIAL
TIME= 90MS
TIME=100MS
TIME=110MS
CASE 1
20.
18.
16.
14.
12.
10.
8.
6.
4.
2.
0.
0. 500. 1000. 1500. 2000. 2500. 3000. 3500. 4000. 4500. 5000.
PRESSURE (MPA)
LENGTH (mm)

FIG. 5d

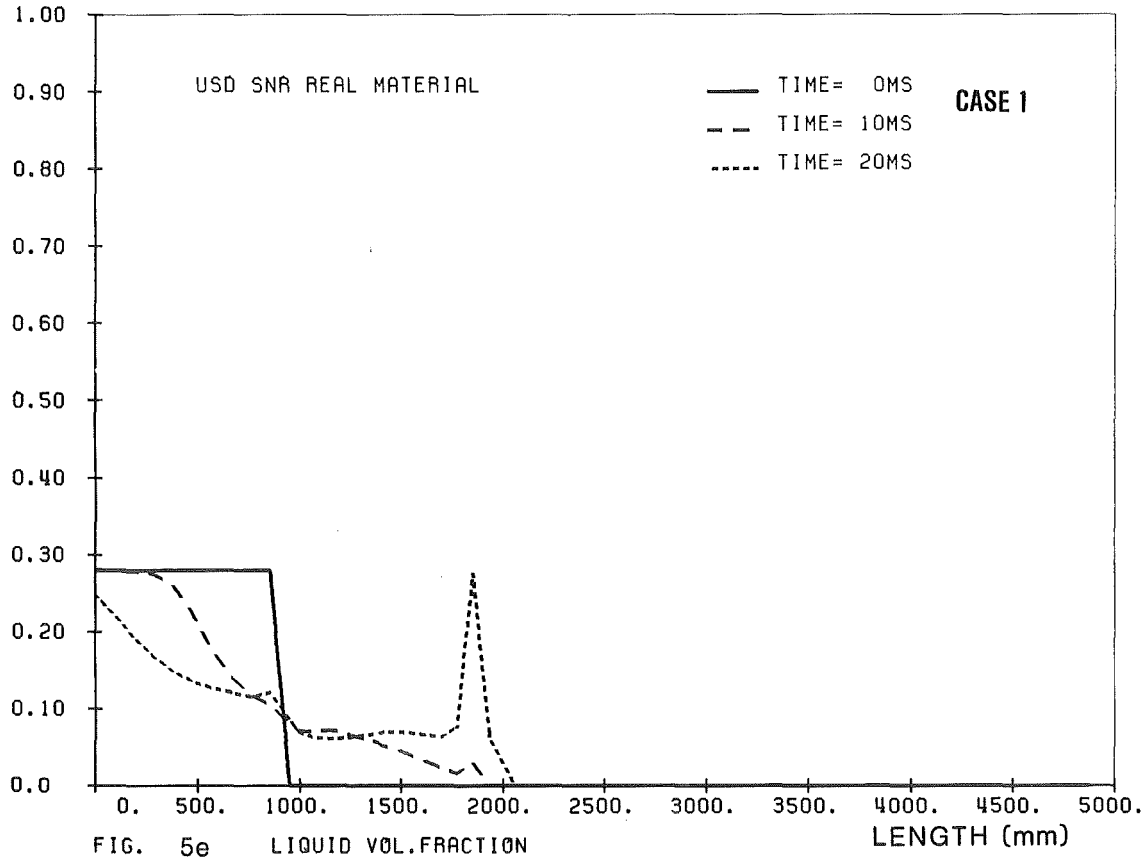

FIG. 5e LIQUID VOL.FRACTION

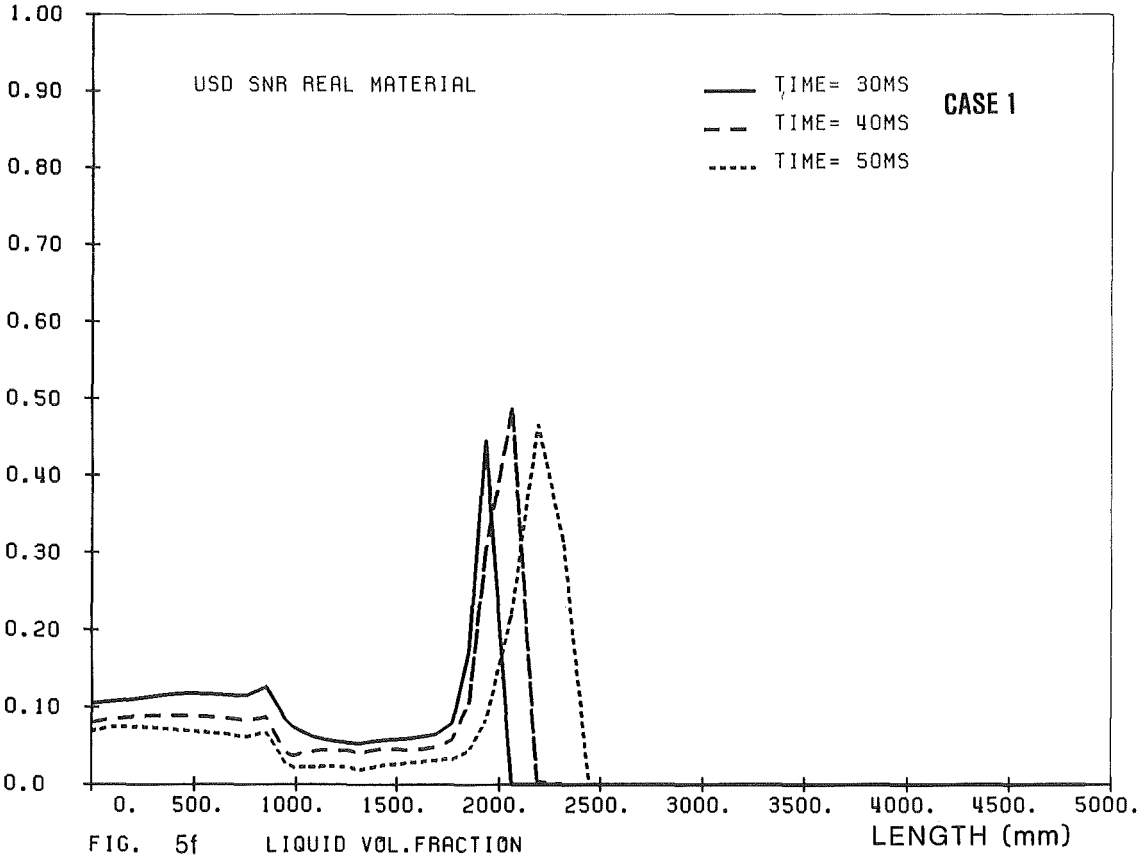

FIG. 5f LIQUID VOL.FRACTION

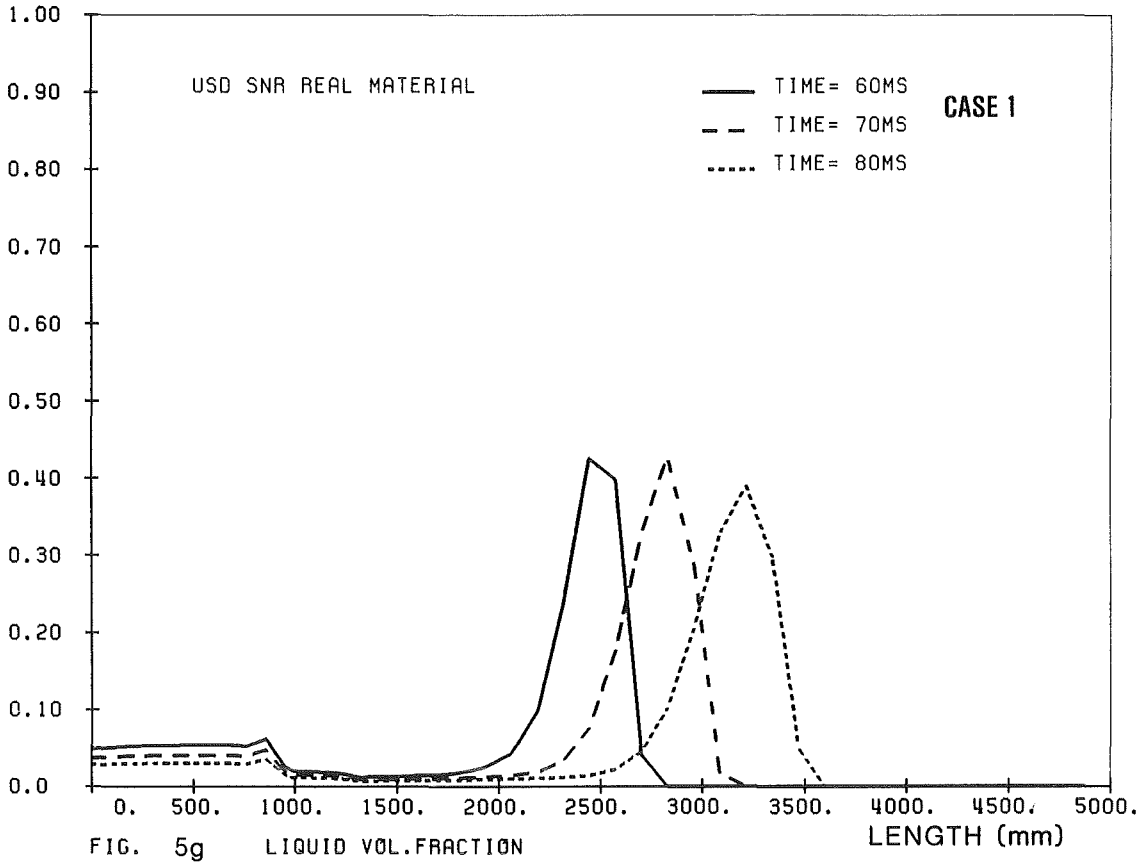

FIG. 5g LIQUID VOL.FRACTION

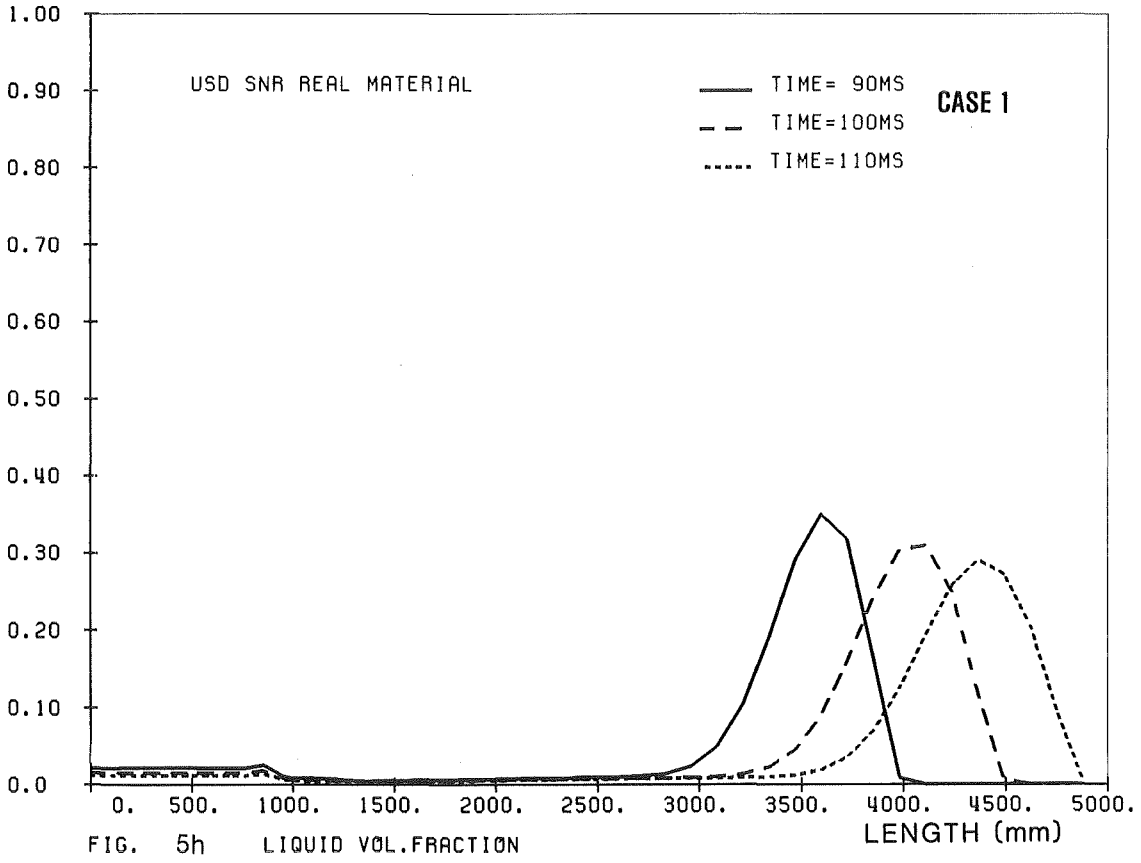

FIG. 5h LIQUID VOL.FRACTION

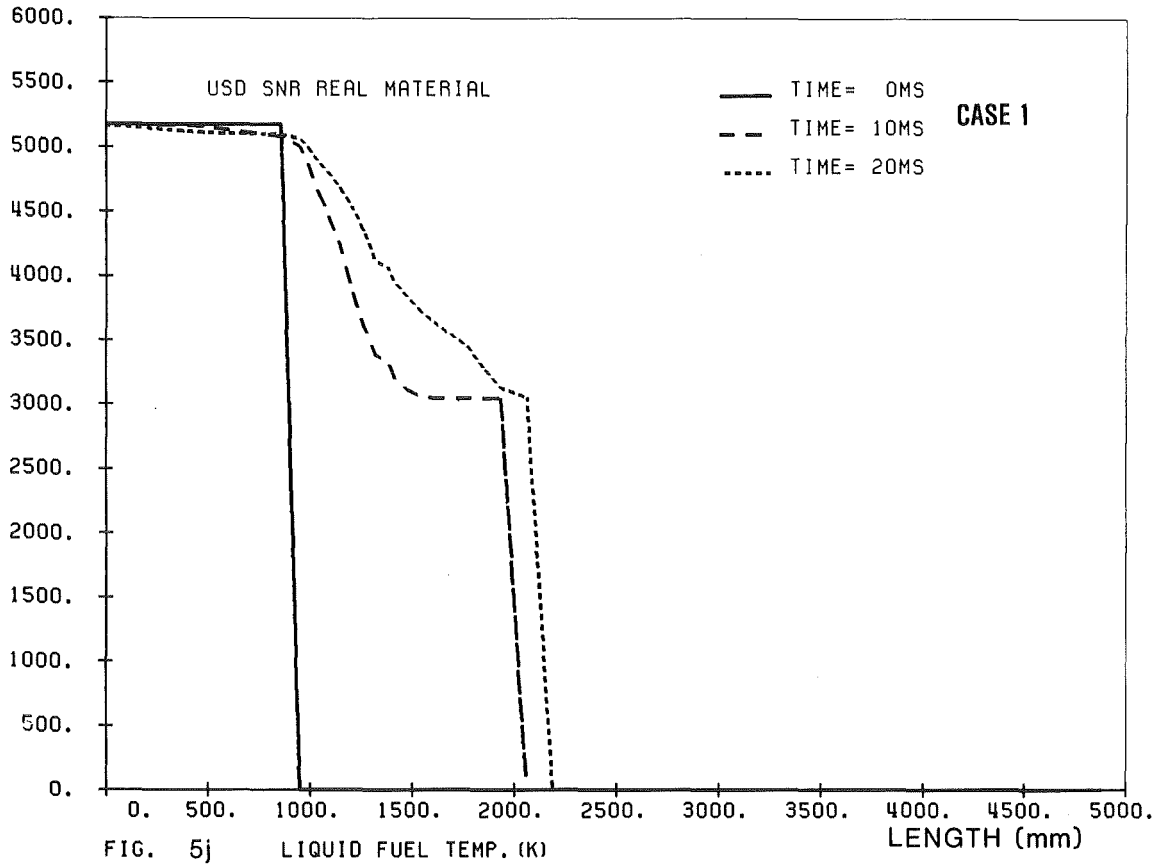

FIG. 5j LIQUID FUEL TEMP. (K)

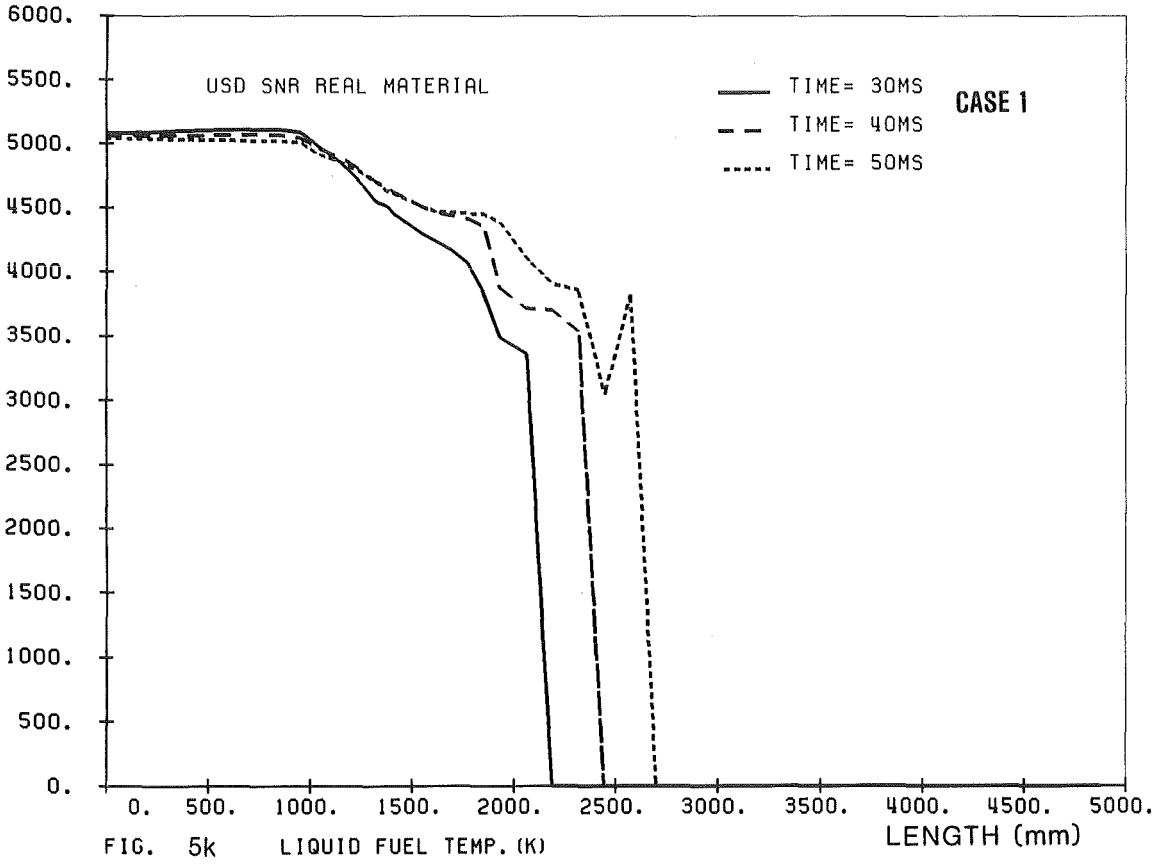

FIG. 5k LIQUID FUEL TEMP. (K)

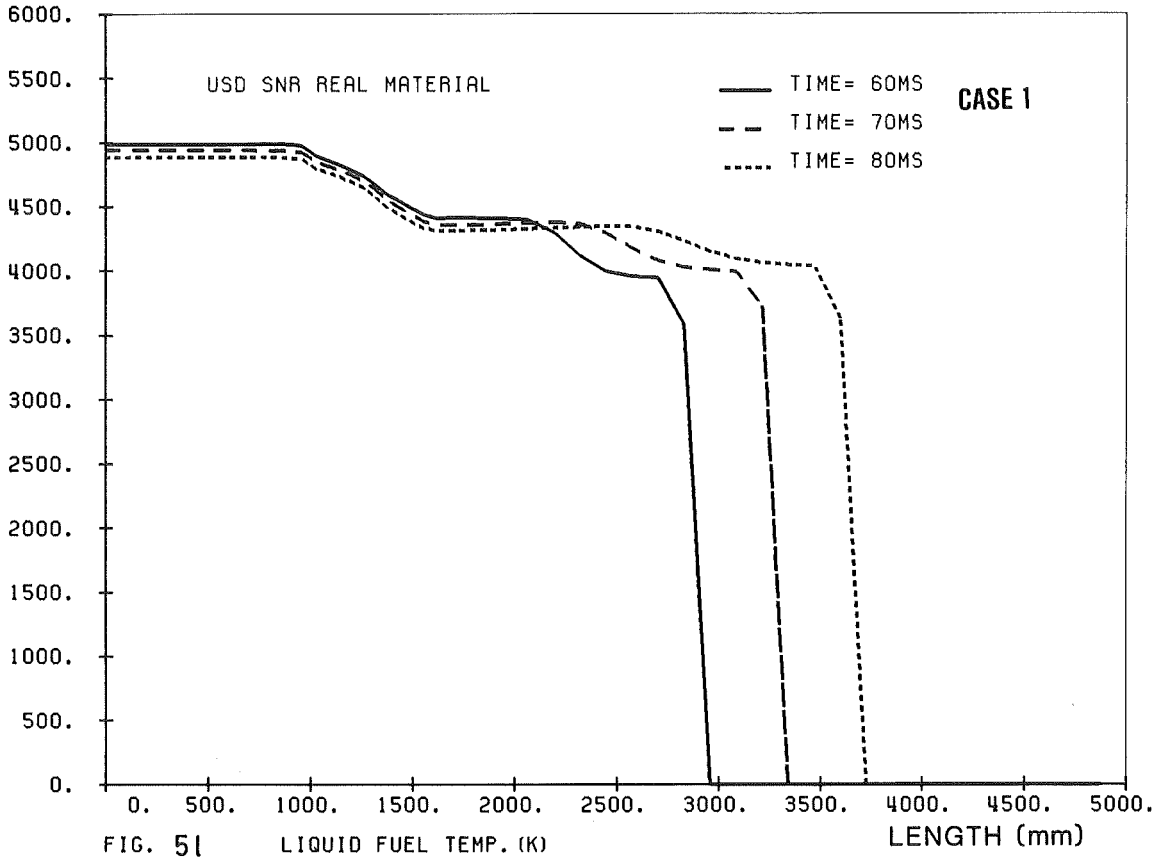

FIG. 5l LIQUID FUEL TEMP. (K)

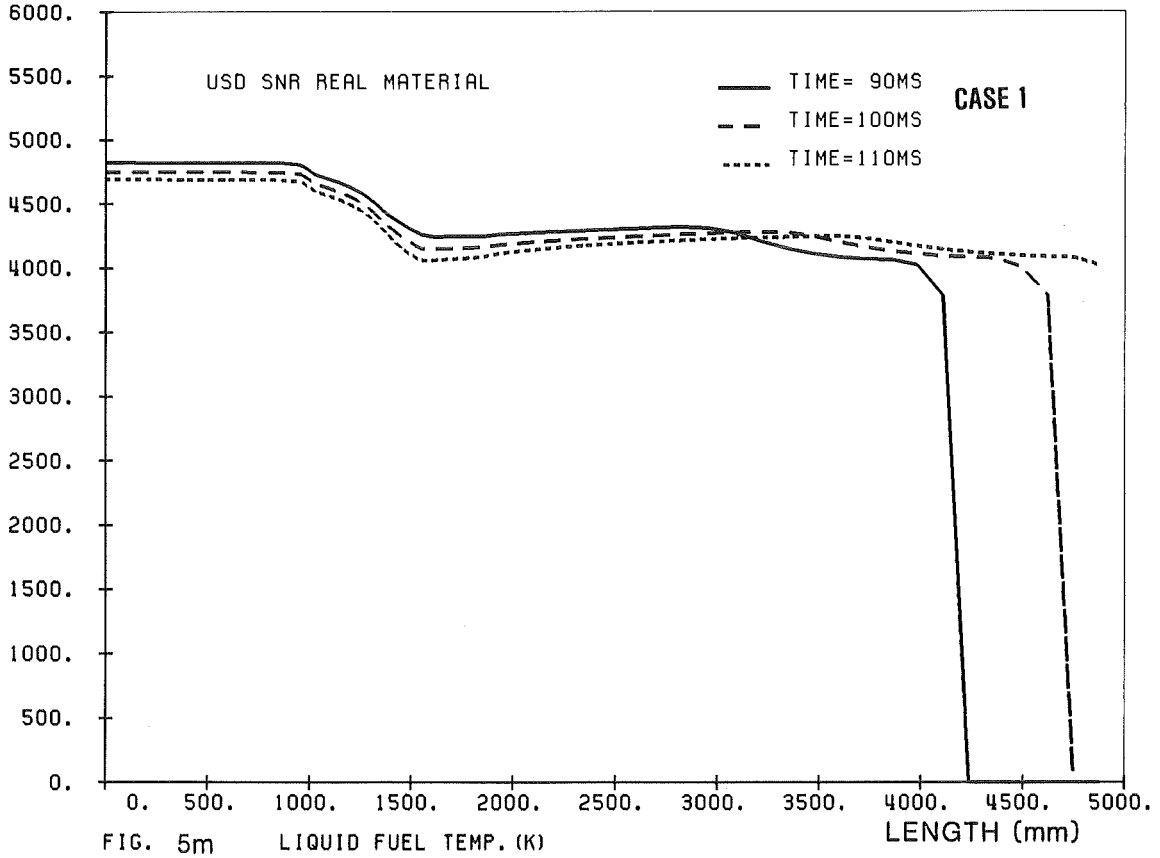

FIG. 5m LIQUID FUEL TEMP. (K)

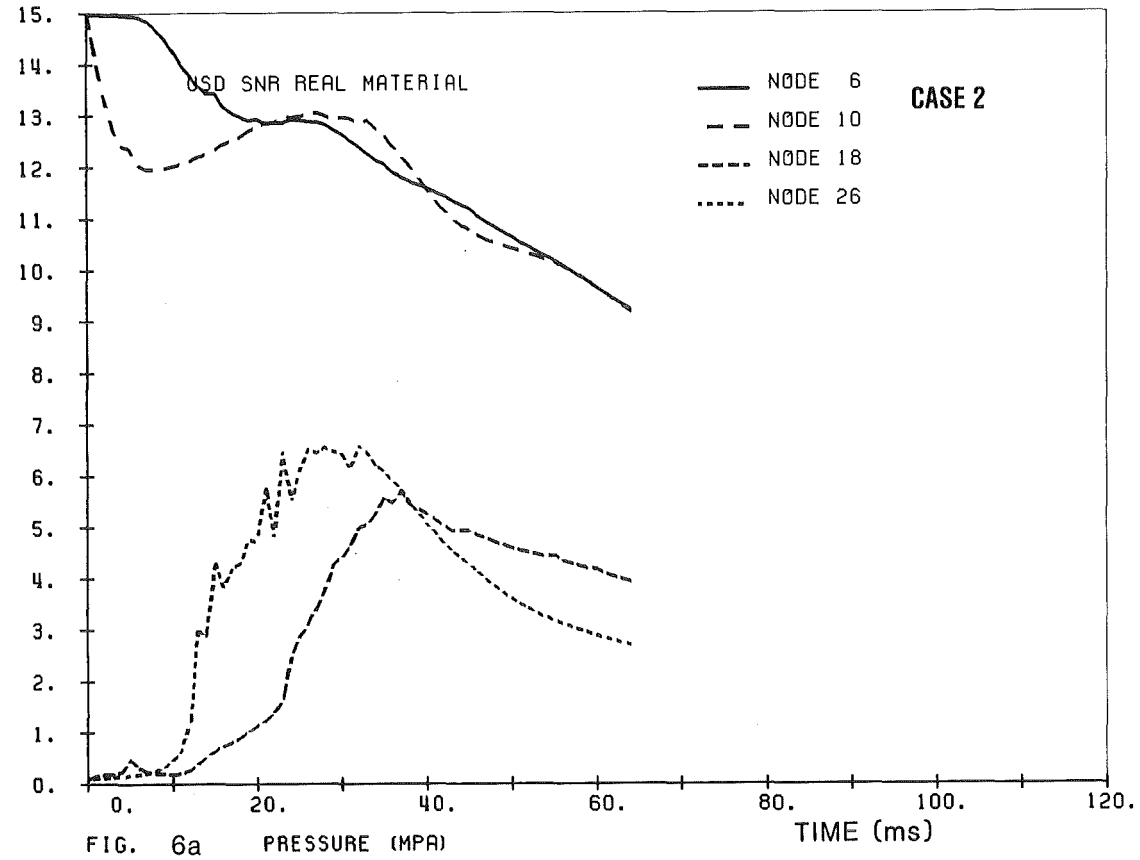

FIG. 6a PRESSURE (MPA)

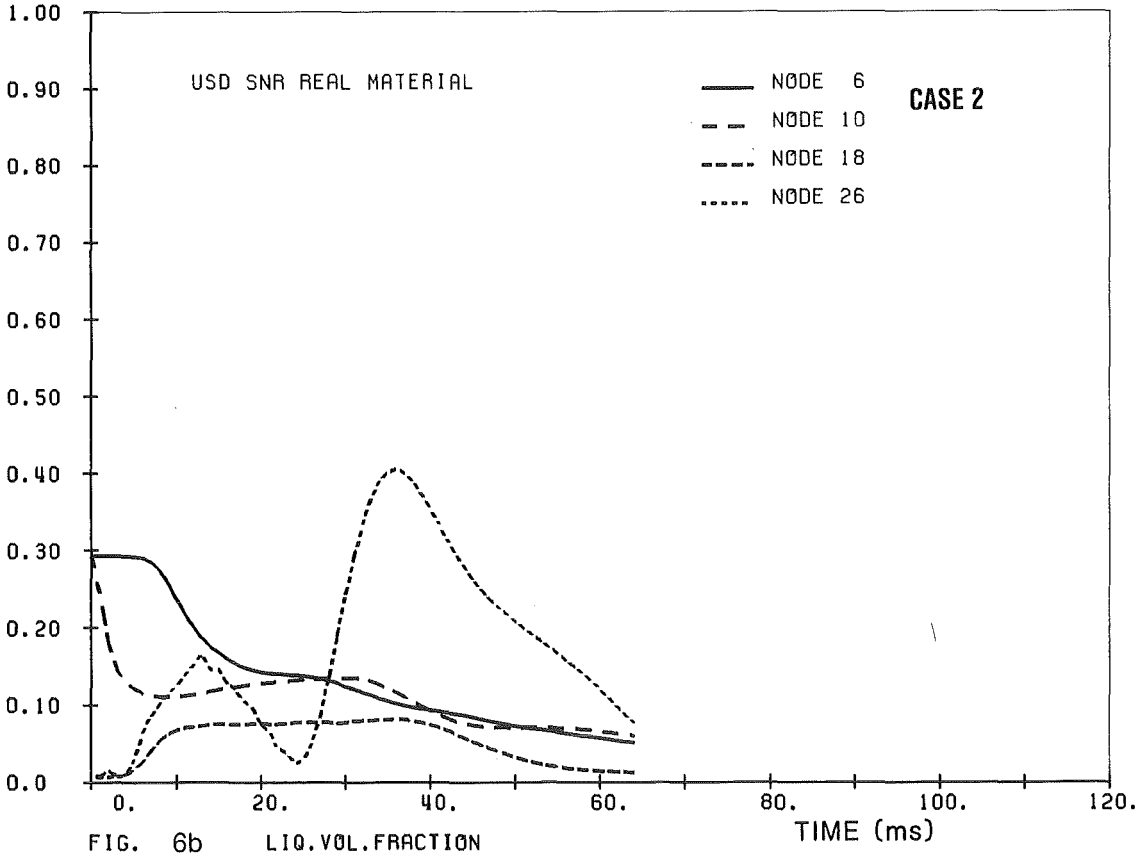

FIG. 6b LIQ.VOL.FRACTION

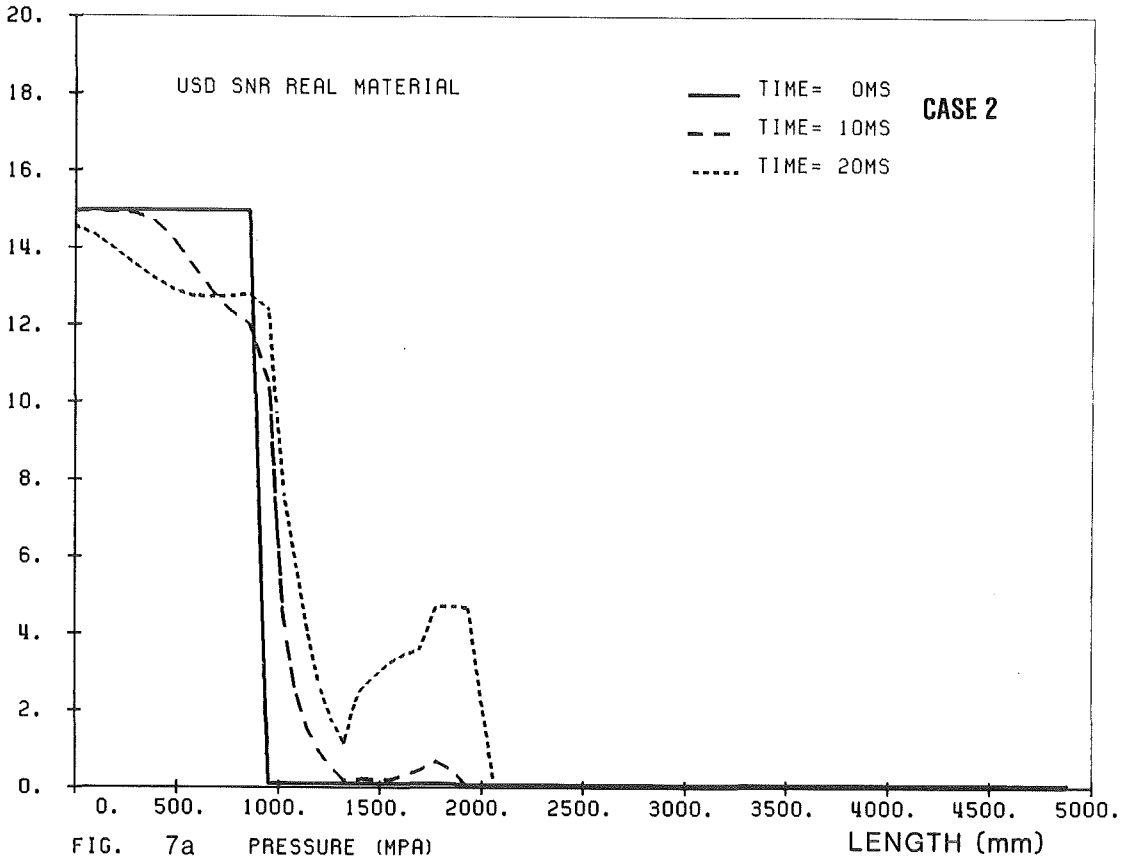
USD SNR REAL MATERIAL
TIME= 0MS
TIME= 10MS
TIME= 20MS
CASE 2
20.
18.
16.
14.
12.
10.
8.
6.
4.
2.
0.
0. 500. 1000. 1500. 2000. 2500. 3000. 3500. 4000. 4500. 5000.
PRESSURE (MPA)
LENGTH (mm)

FIG. 7a

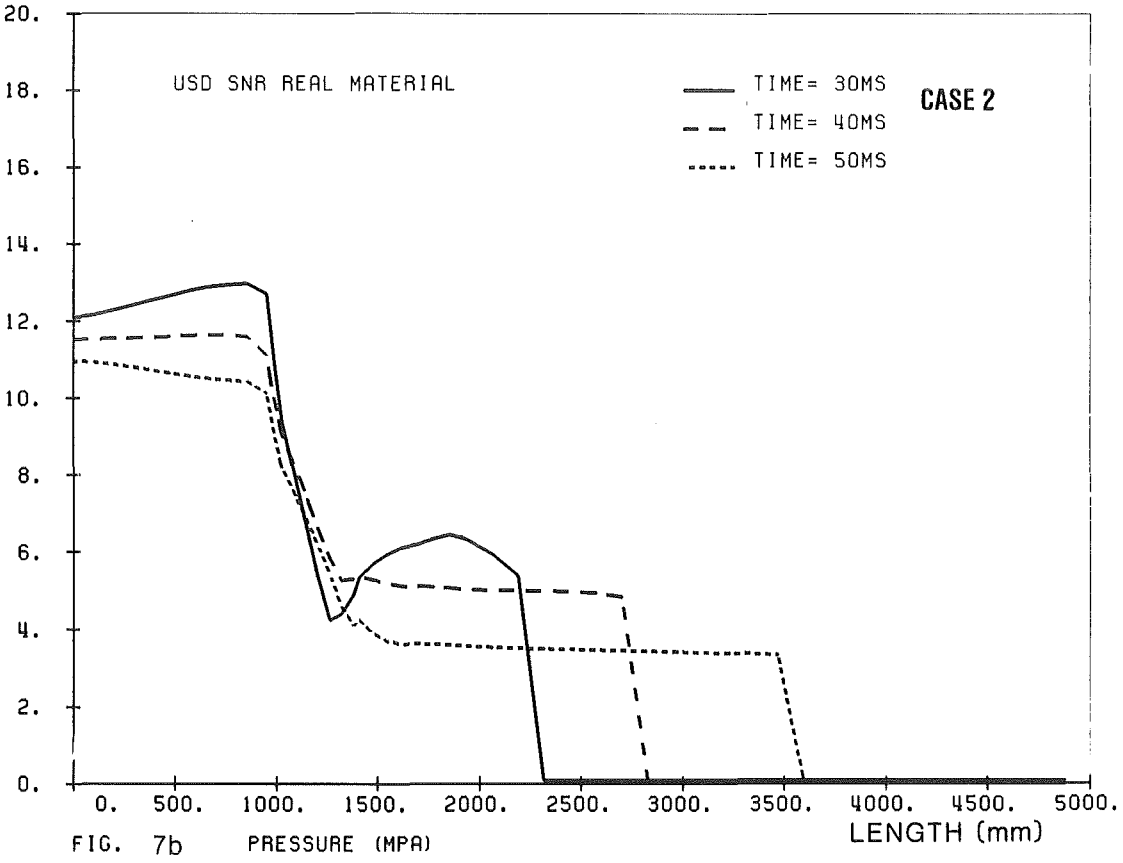
USD SNR REAL MATERIAL
TIME= 30MS
TIME= 40MS
TIME= 50MS
CASE 2
20.
18.
16.
14.
12.
10.
8.
6.
4.
2.
0.
0. 500. 1000. 1500. 2000. 2500. 3000. 3500. 4000. 4500. 5000.
PRESSURE (MPA)
LENGTH (mm)

FIG. 7b

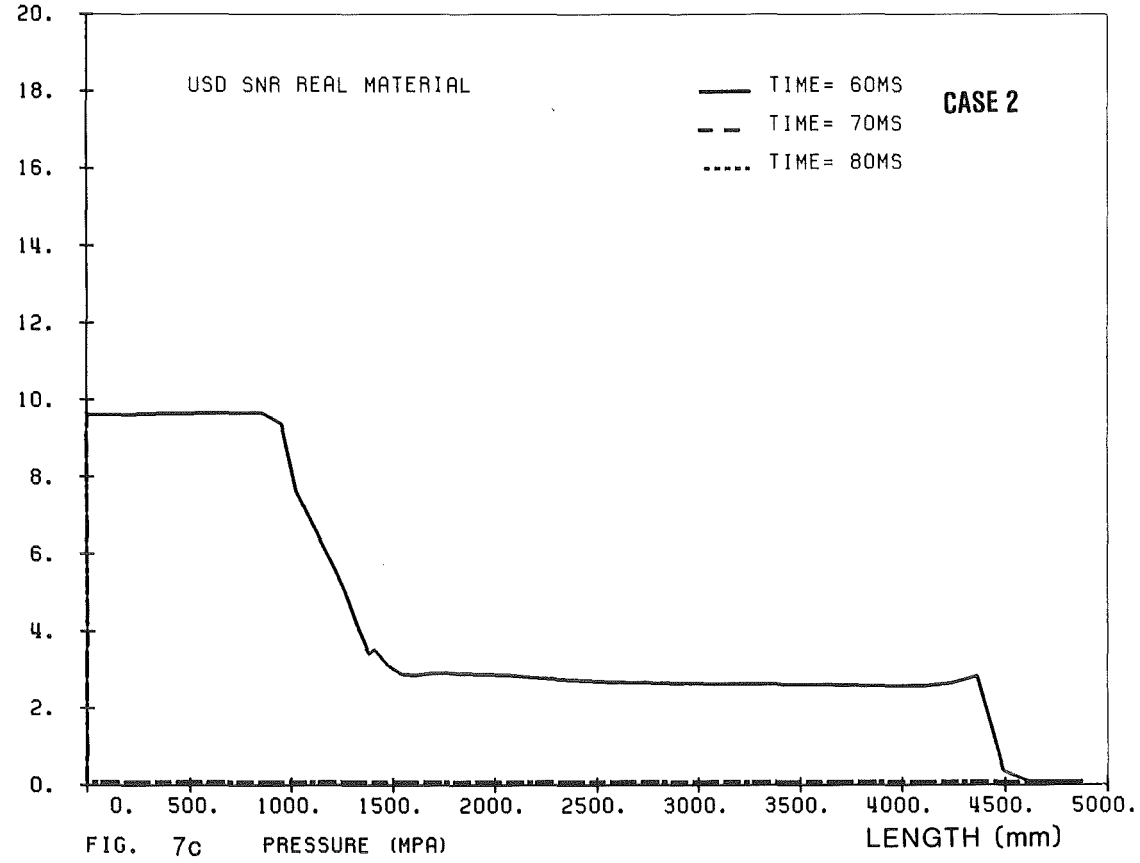

FIG. 7c PRESSURE (MPA)

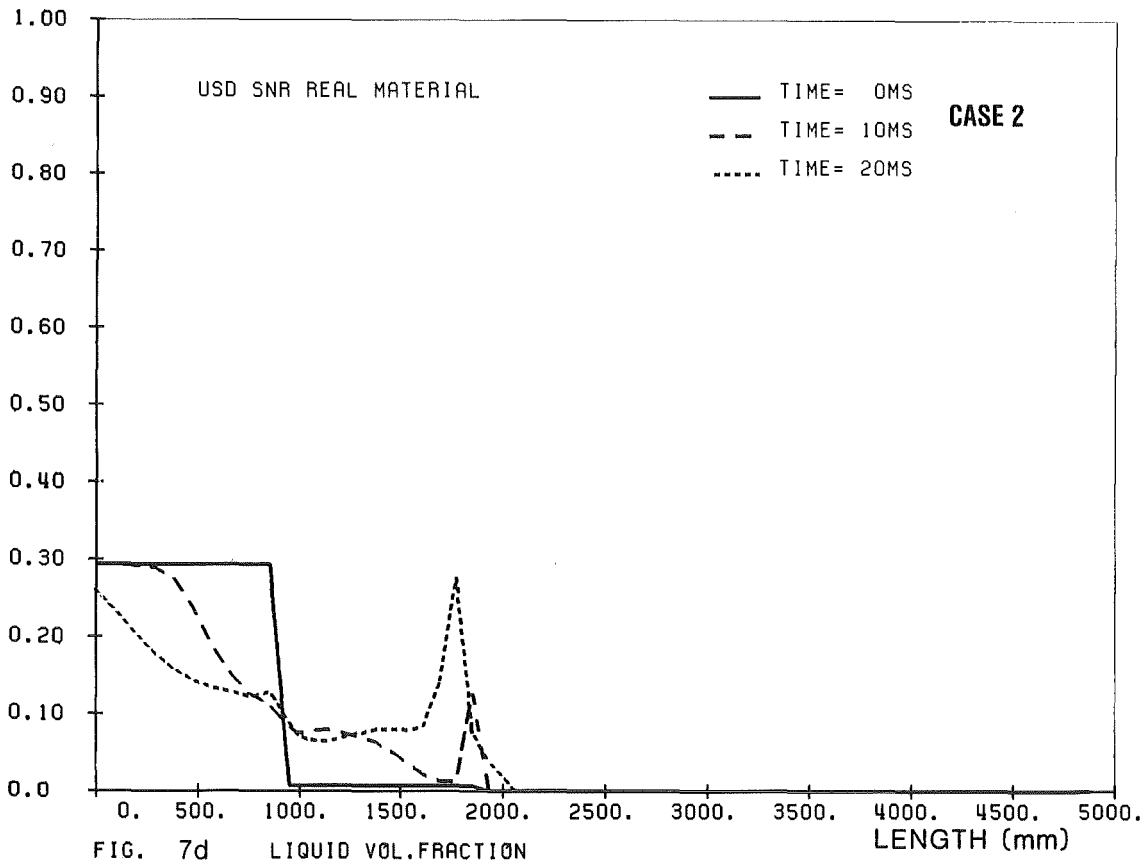

FIG. 7d LIQUID VOL.FRACTION

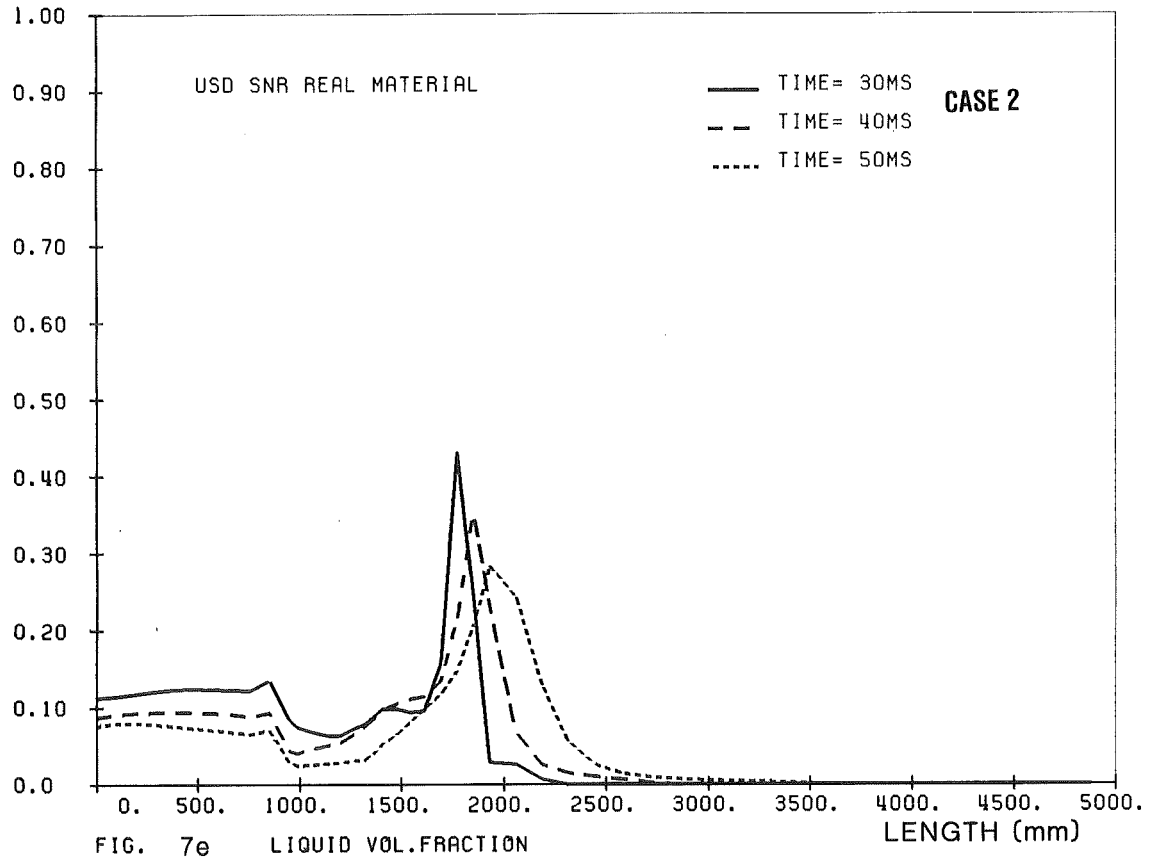

FIG. 7e LIQUID VOL.FRACTION

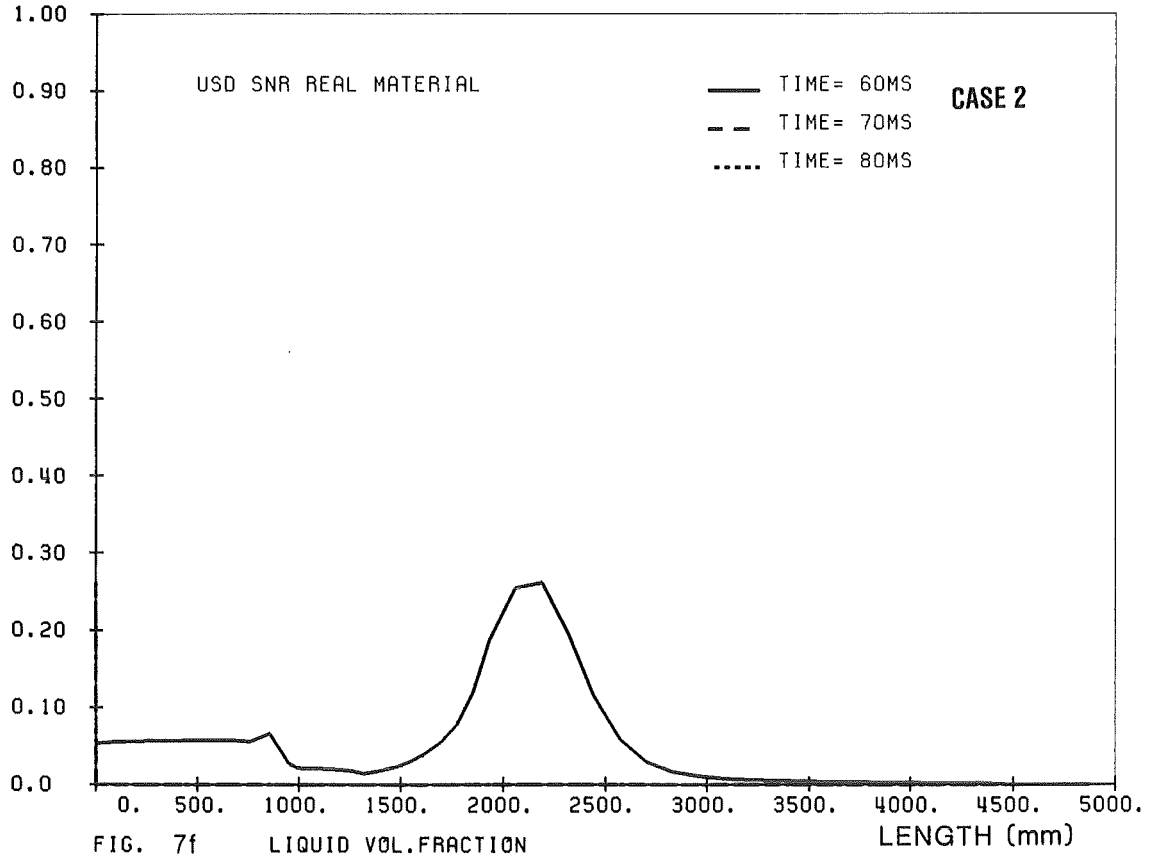

FIG. 7f LIQUID VOL.FRACTION

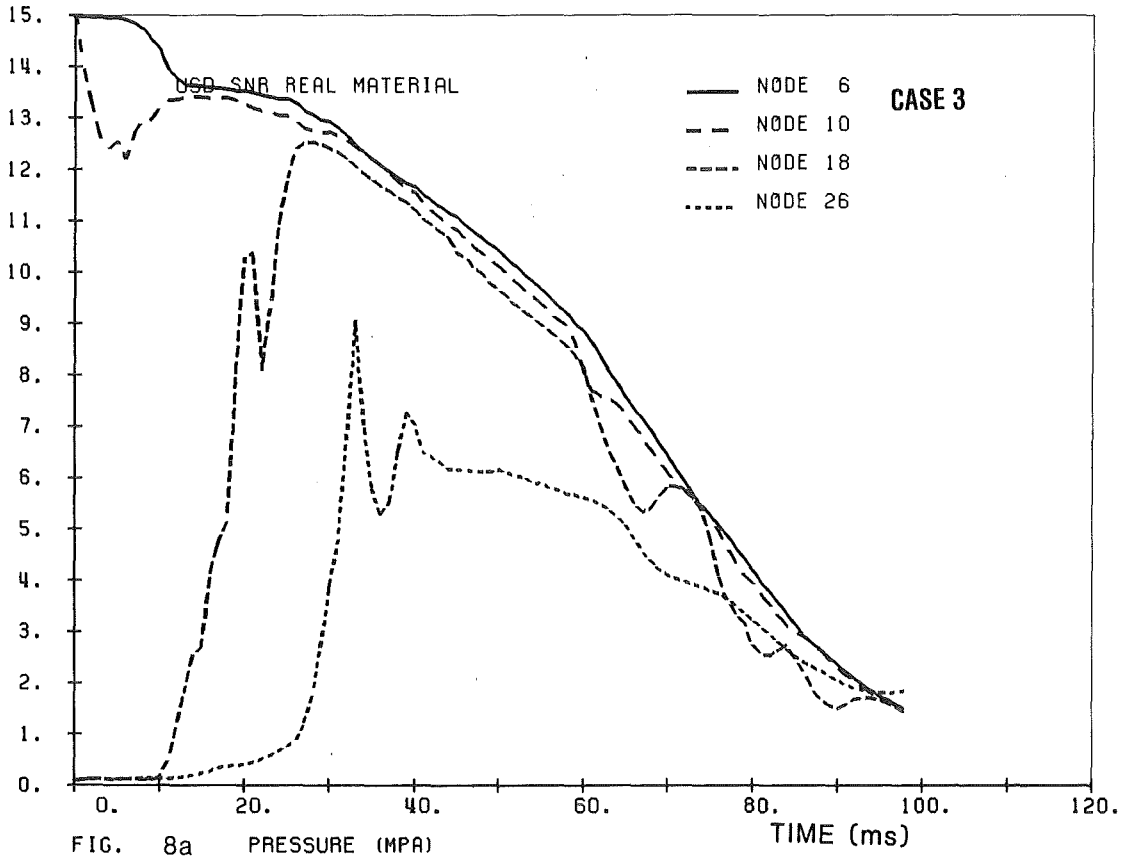

FIG. 8a PRESSURE (MPA)

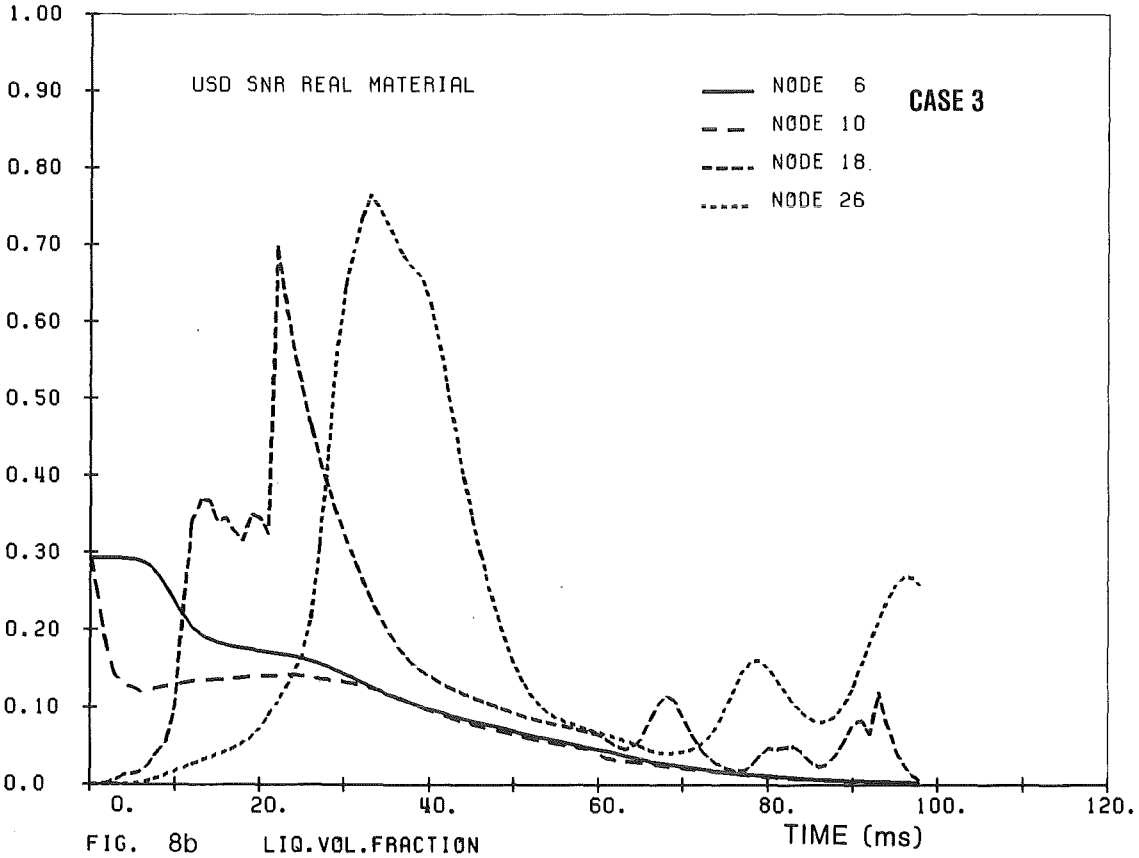

FIG. 8b LIQ.VOL.FRACTION

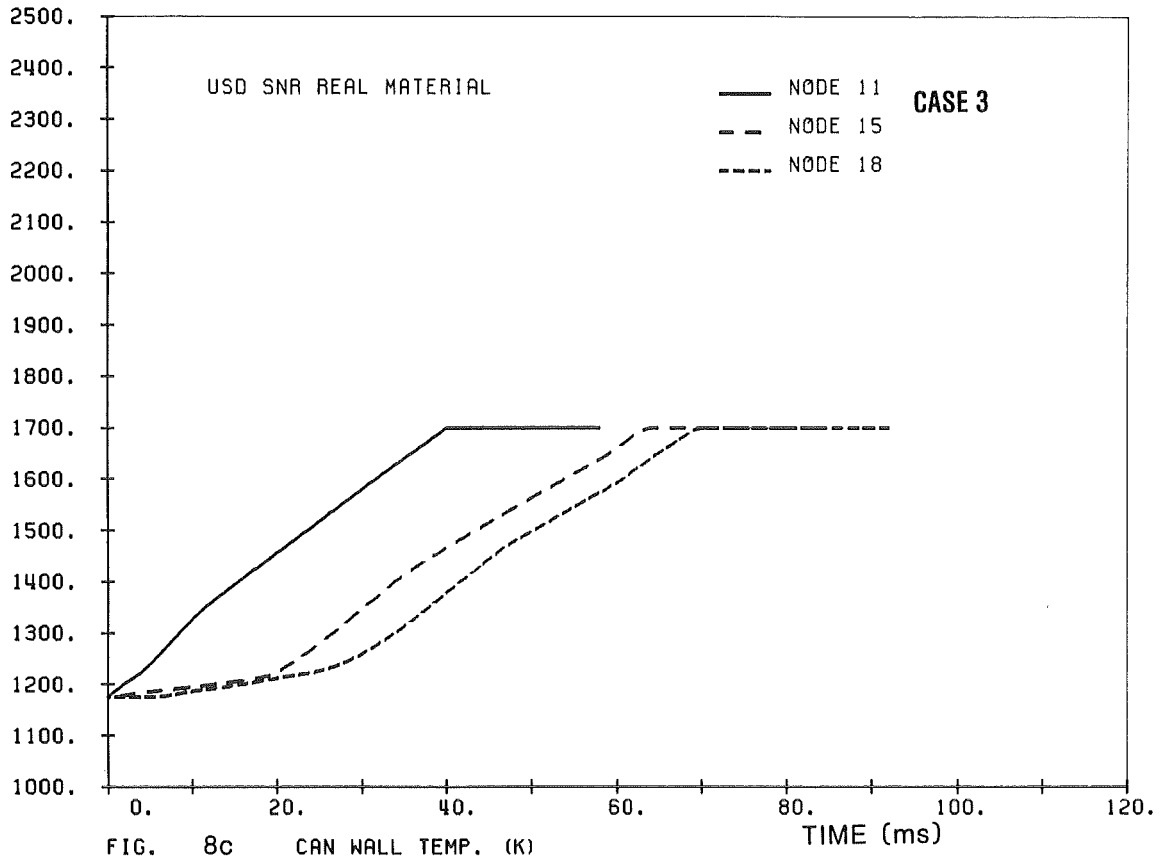

FIG. 8c CAN WALL TEMP. (K)

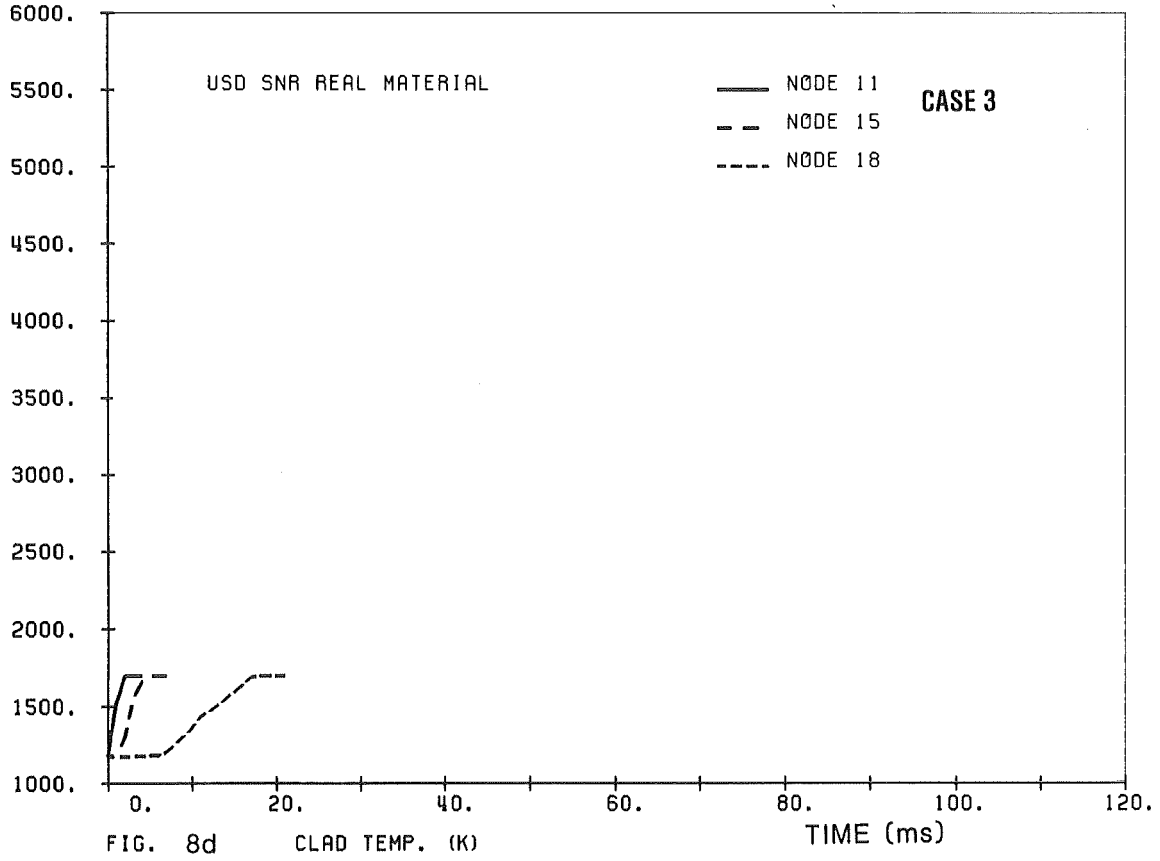

FIG. 8d CLAD TEMP. (K)

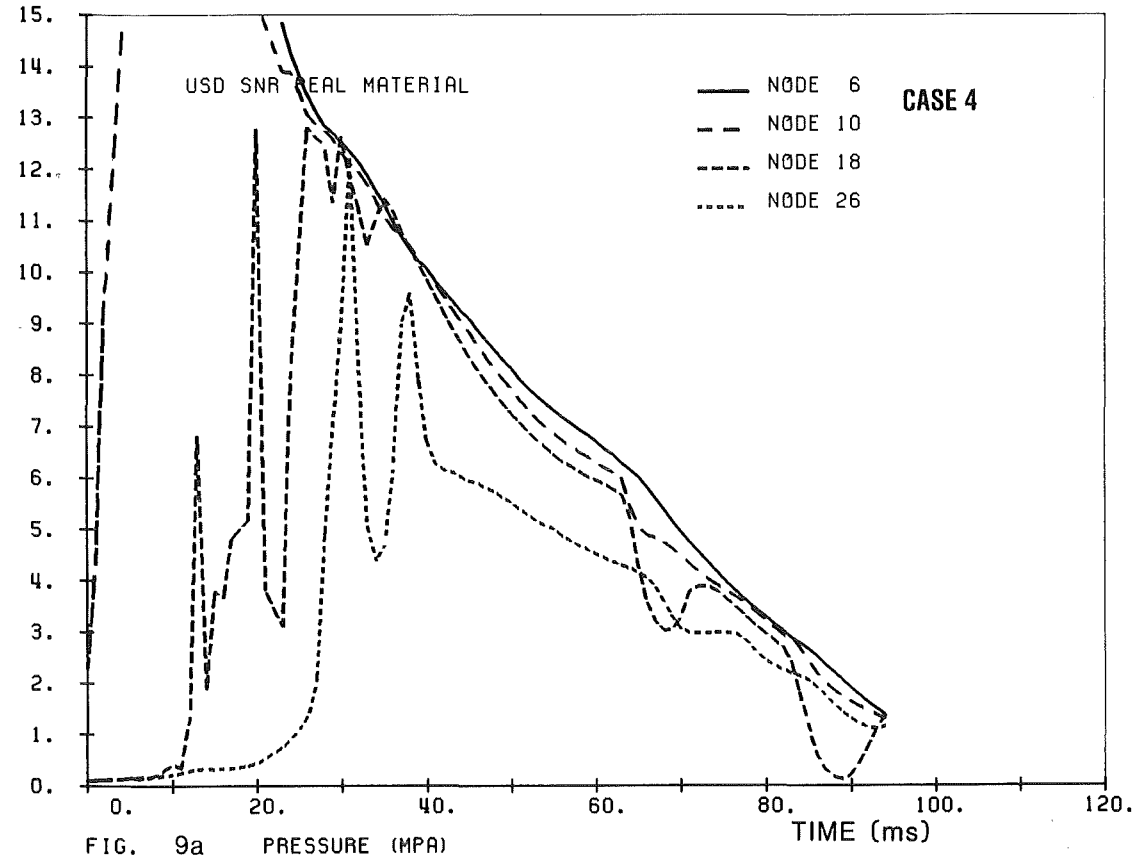

FIG. 9a PRESSURE (MPA)

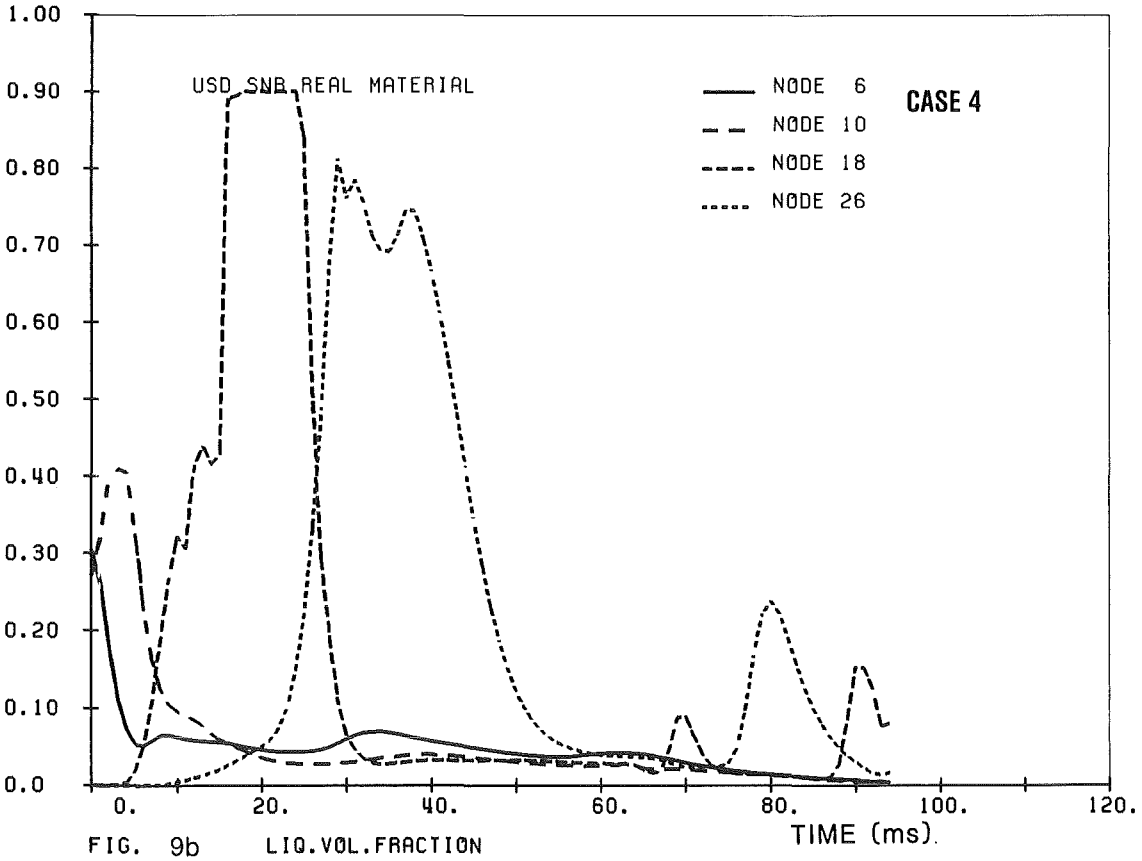

FIG. 9b LIQ.VOL.FRACTION

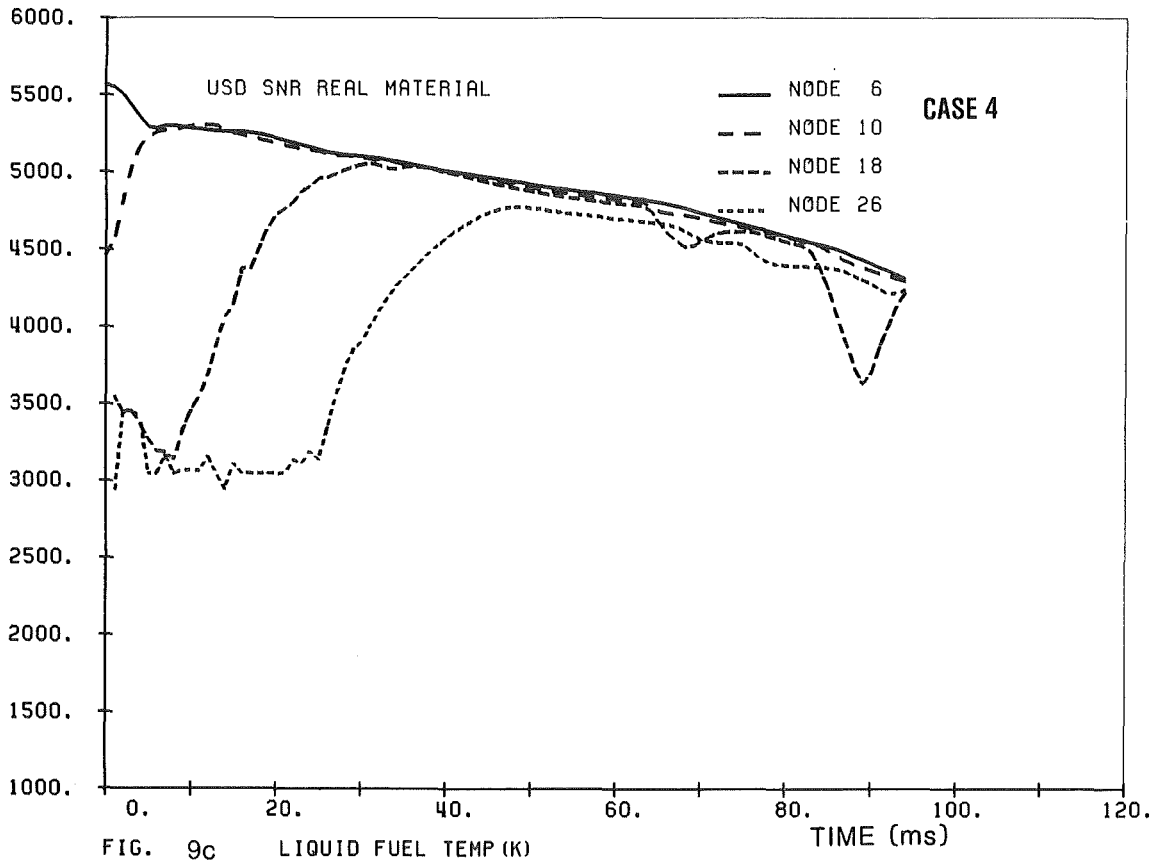

FIG. 9c LIQUID FUEL TEMP (K)

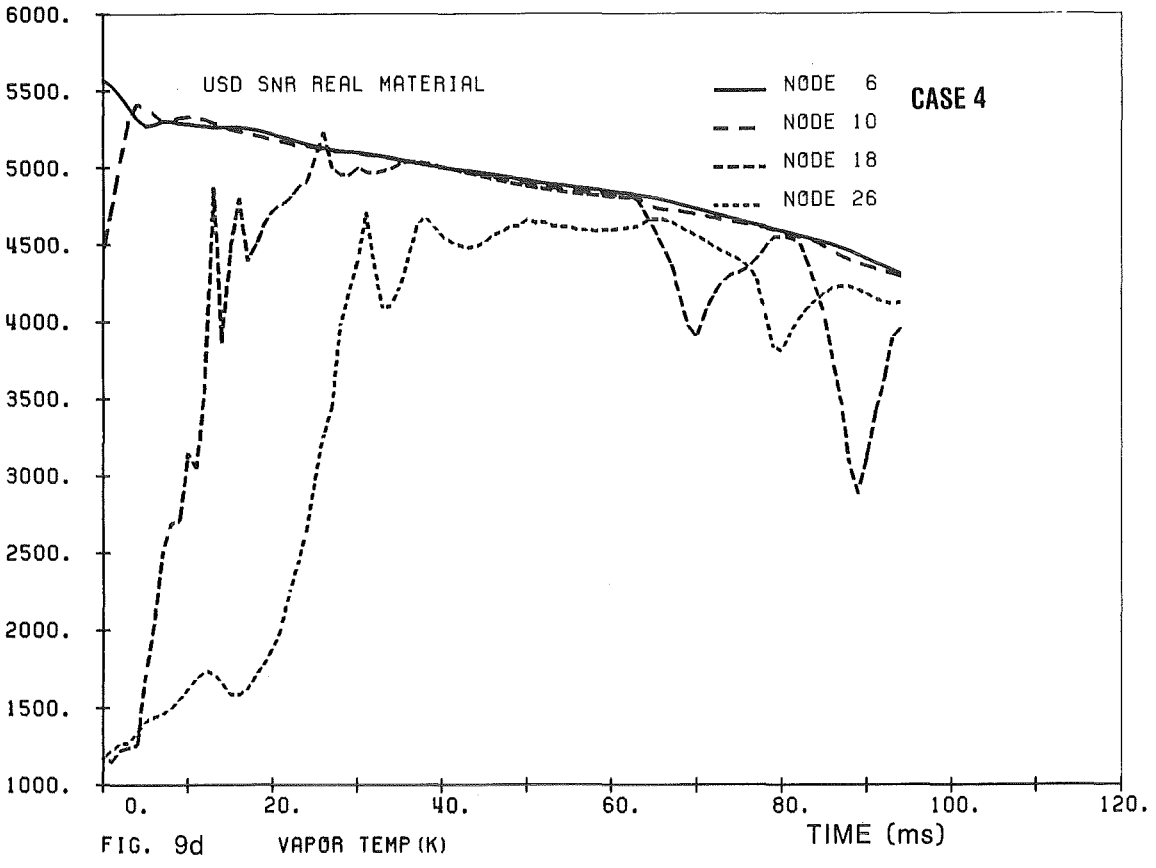

FIG. 9d VAPOR TEMP (K)

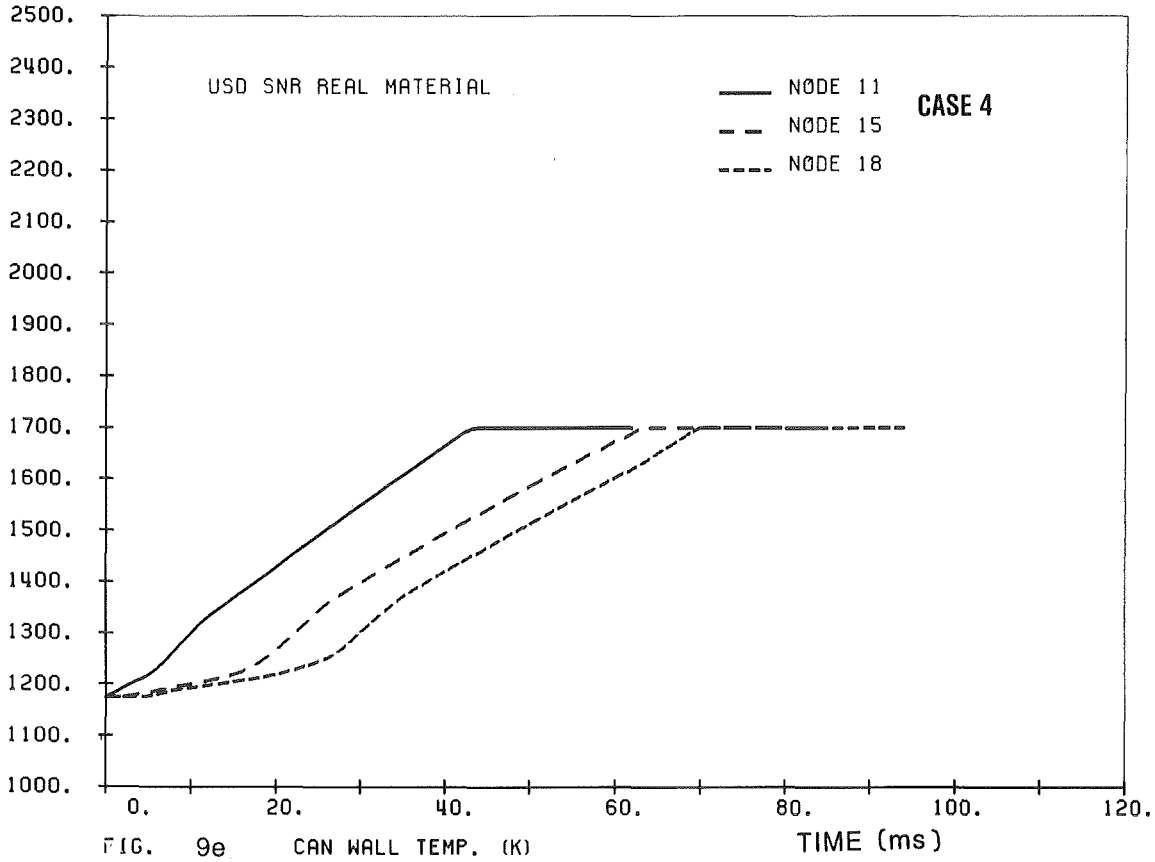

FIG. 9e CAN WALL TEMP. (K)

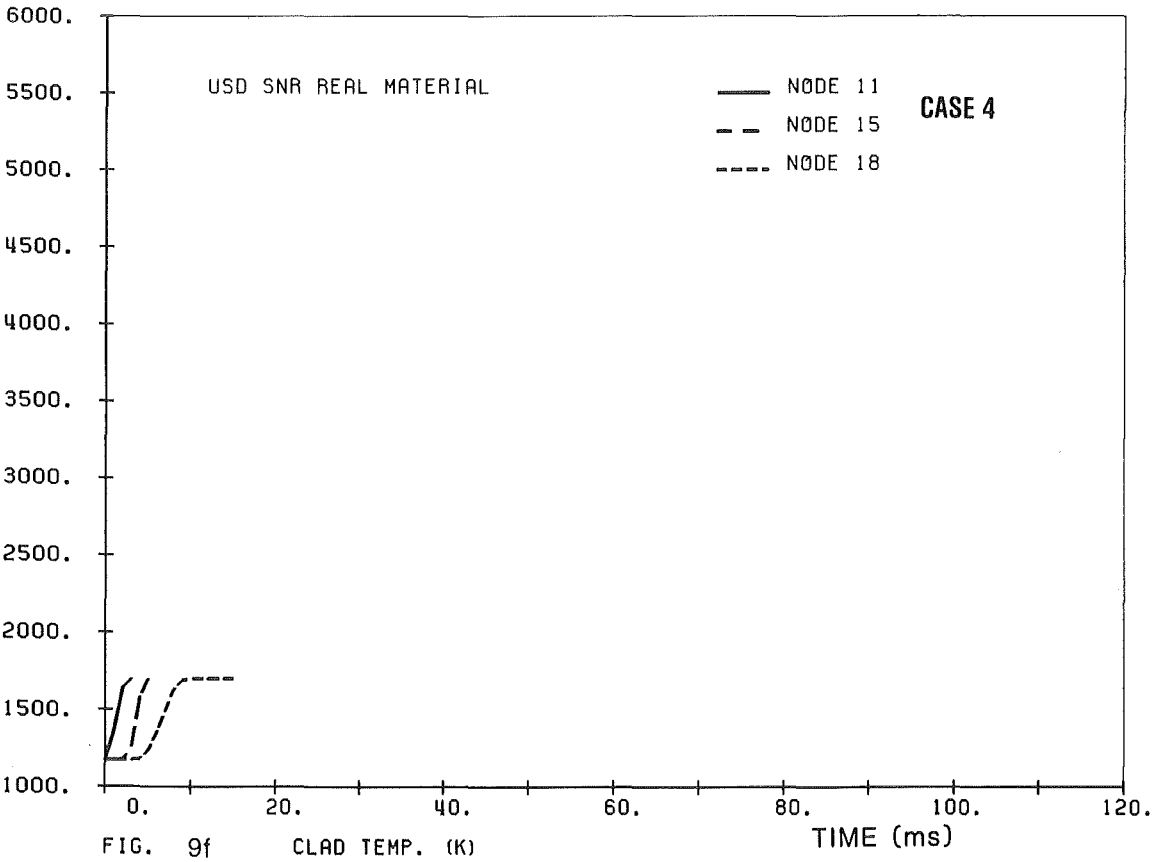

FIG. 9f CLAD TEMP. (K)

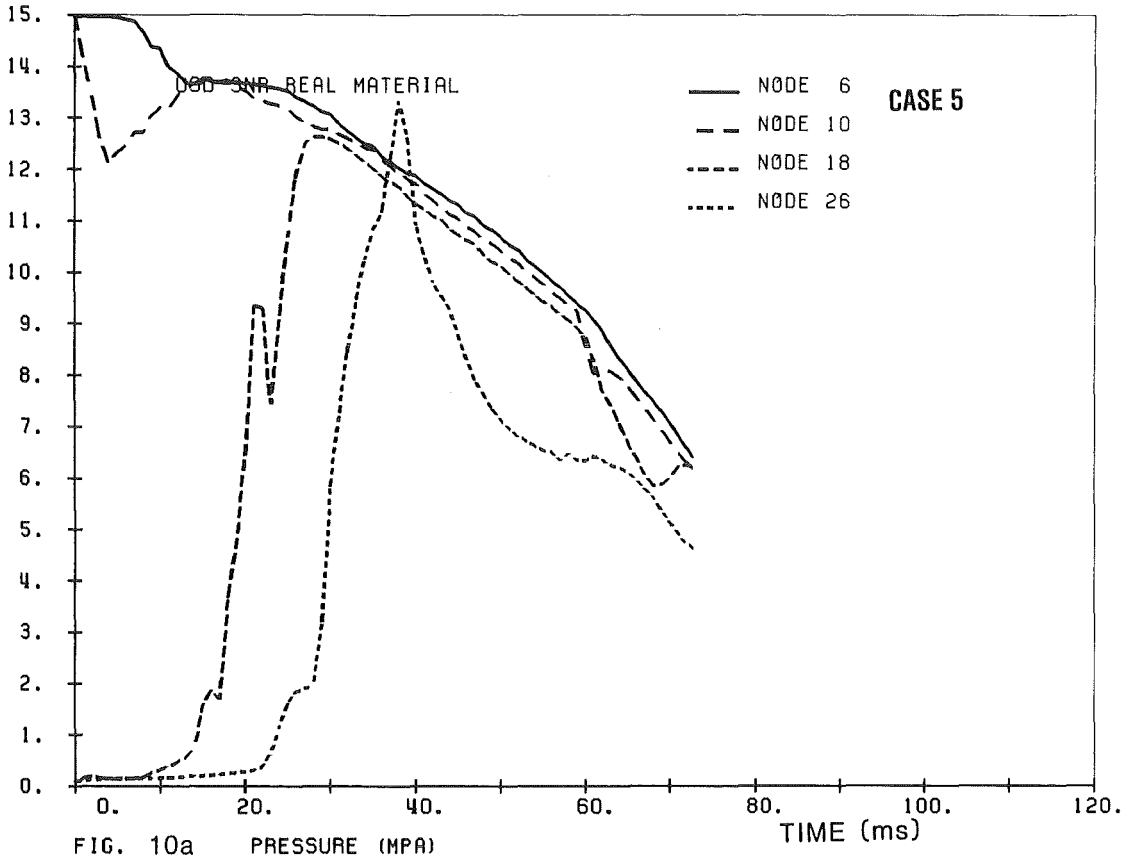

FIG. 10a PRESSURE (MPA)

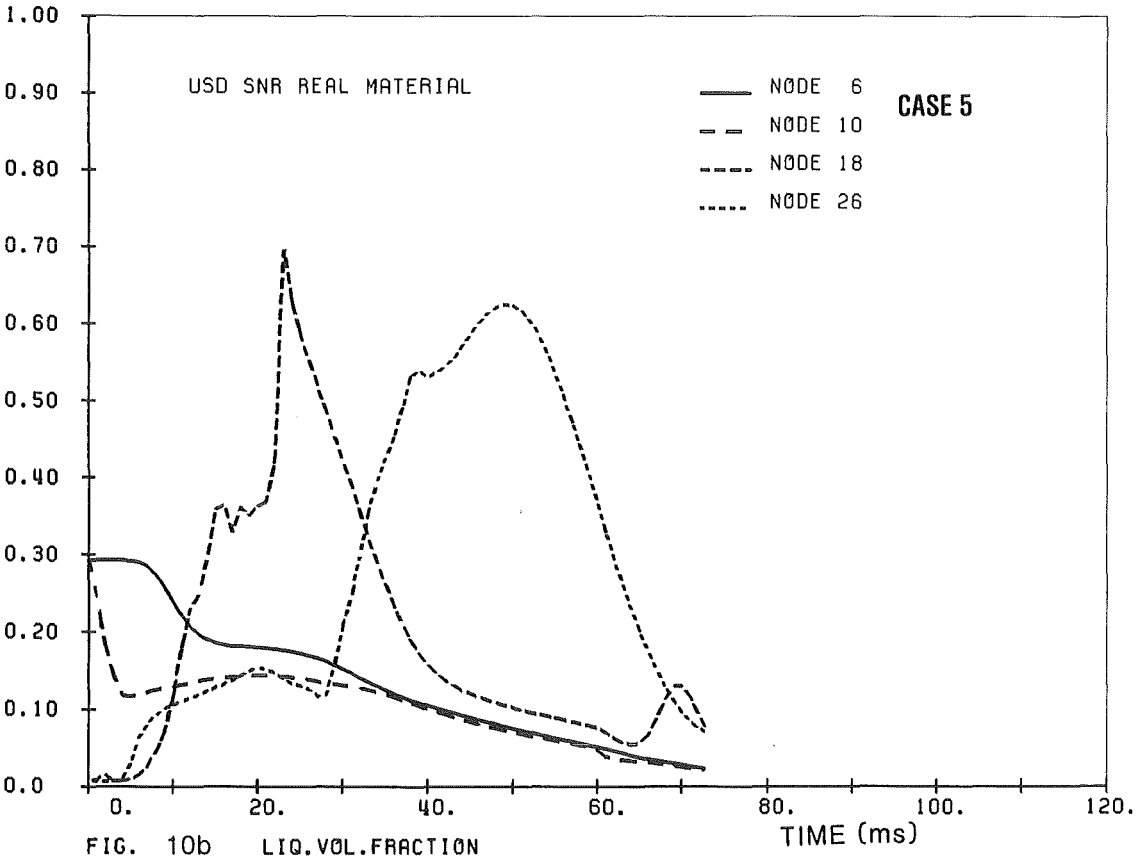

FIG. 10b LIQ.VOL.FRACTION

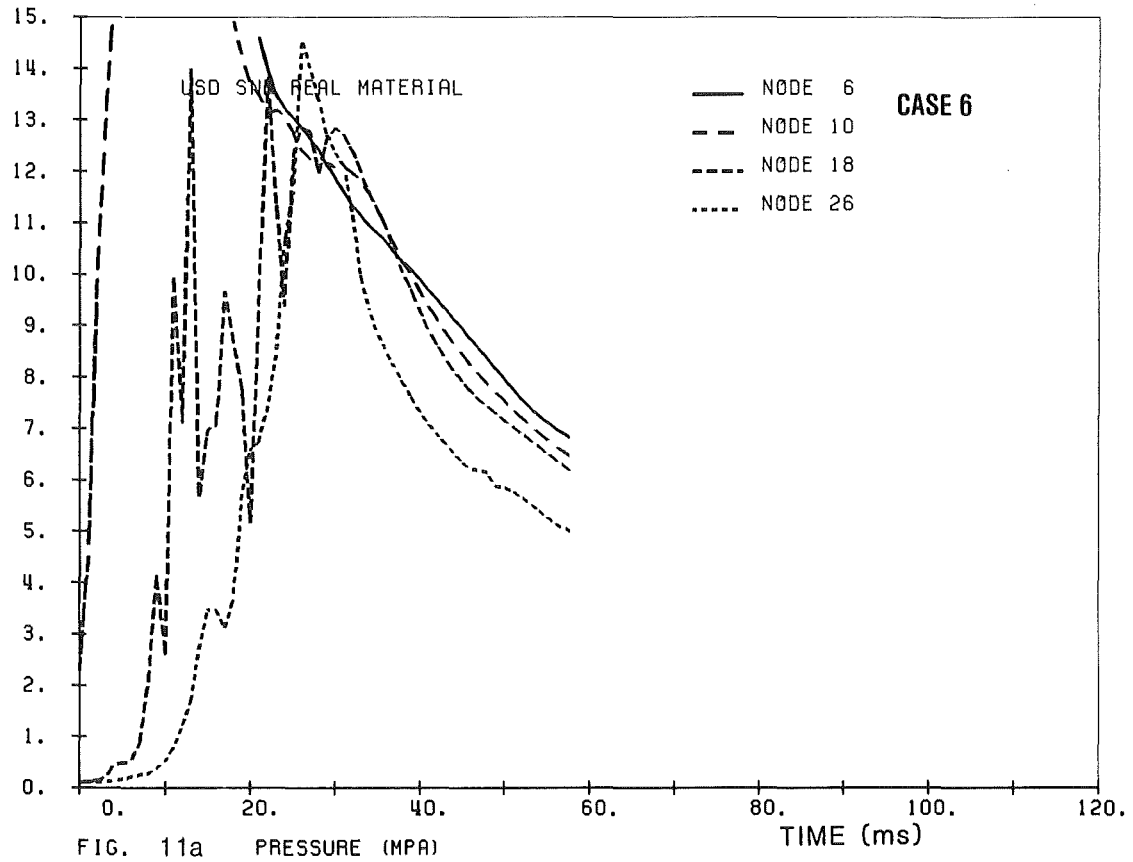

FIG. 11a PRESSURE (MPA)

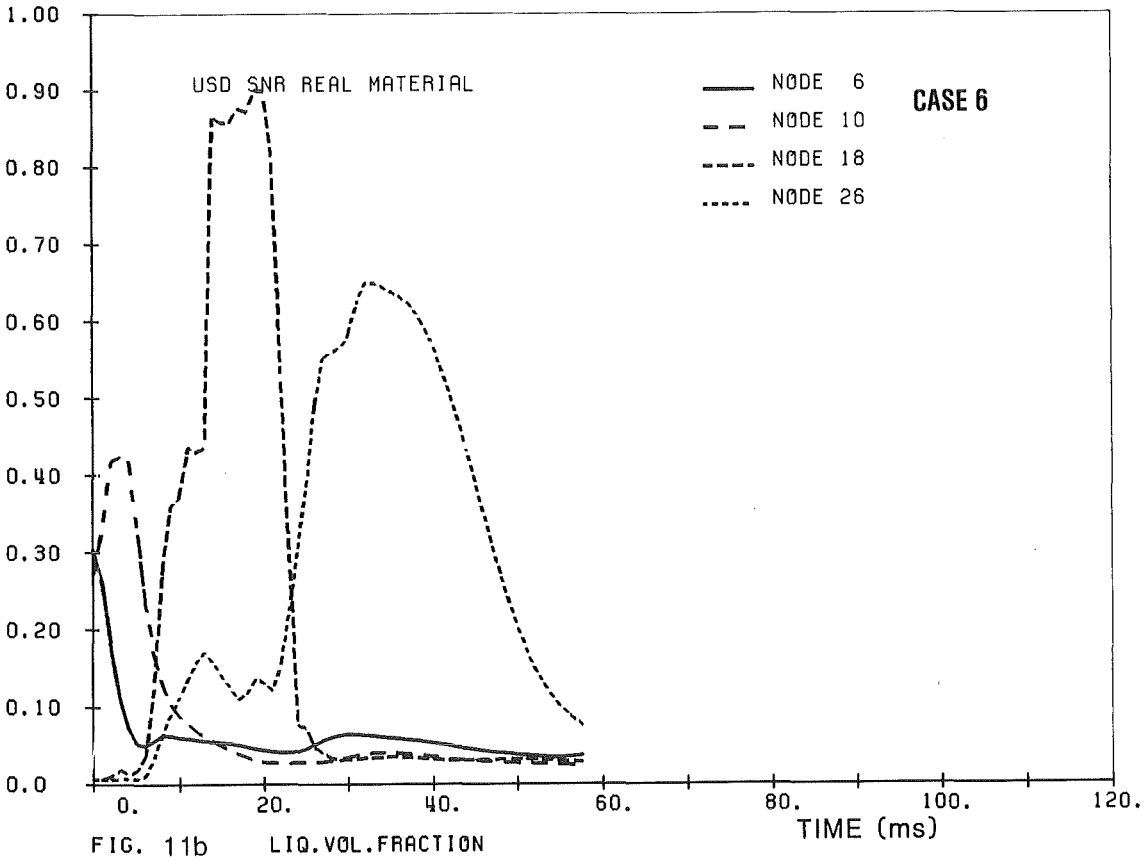

FIG. 11b LIQ.VOL.FRACTION

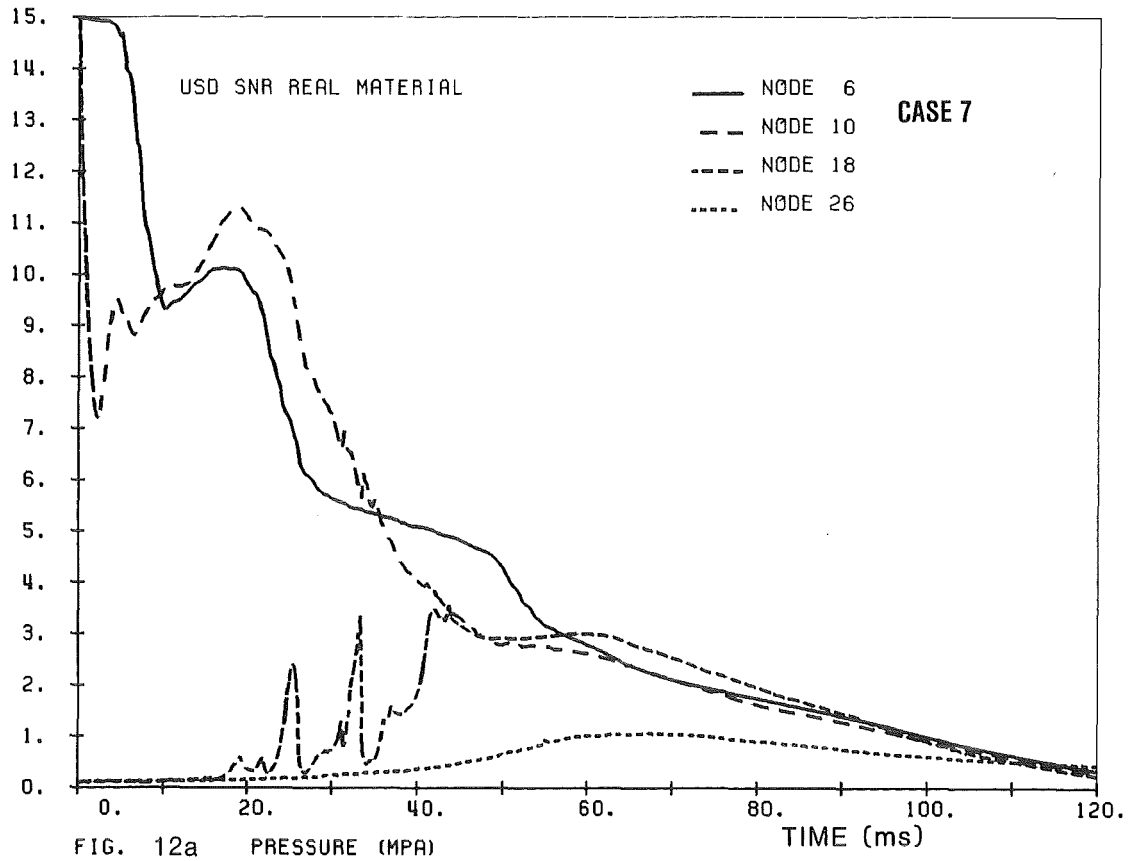

FIG. 12a PRESSURE (MPA)

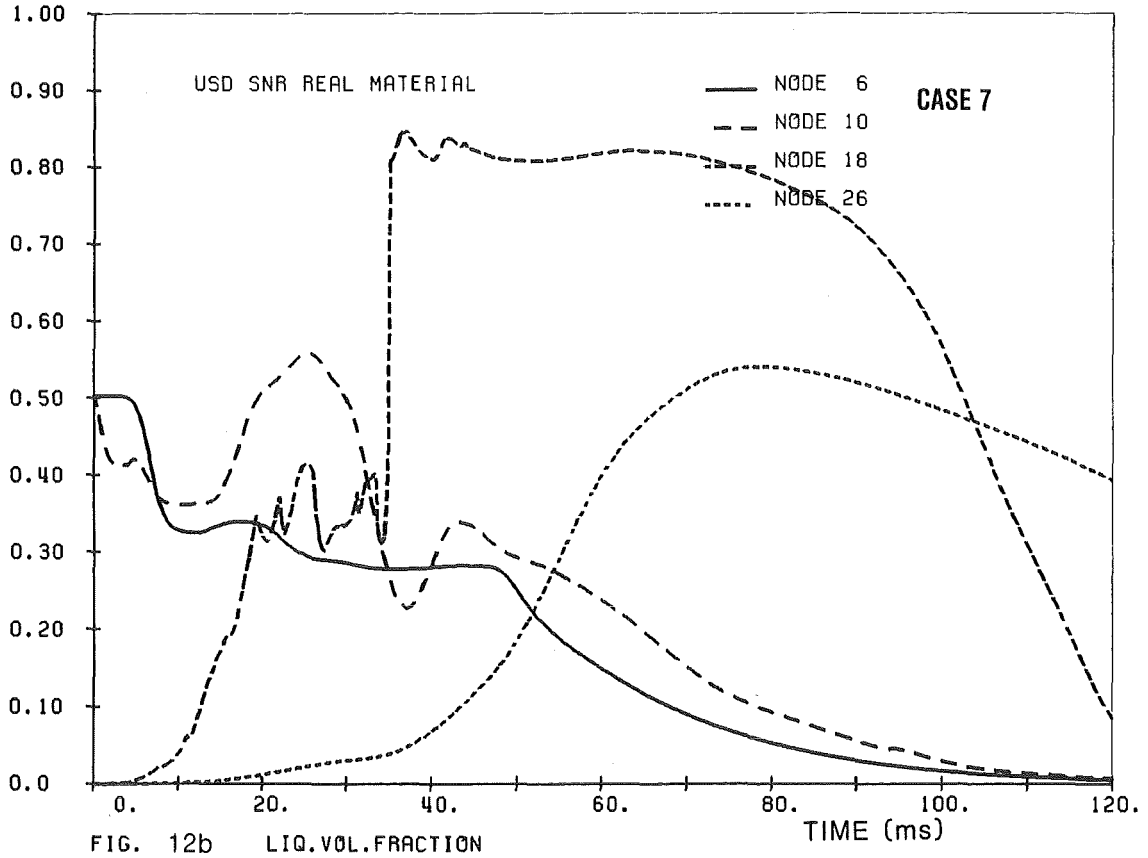

FIG. 12b LIQ.VOL.FRACTION

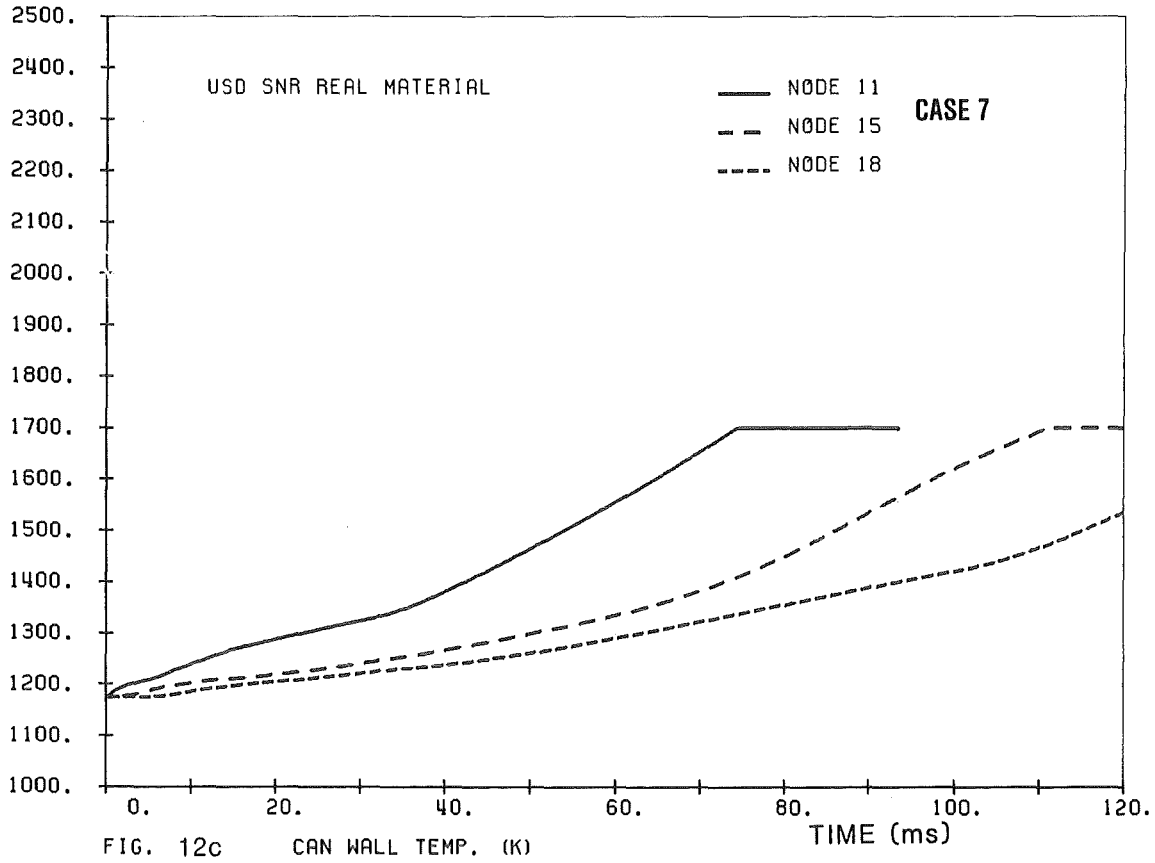

FIG. 12c CAN WALL TEMP. (K)

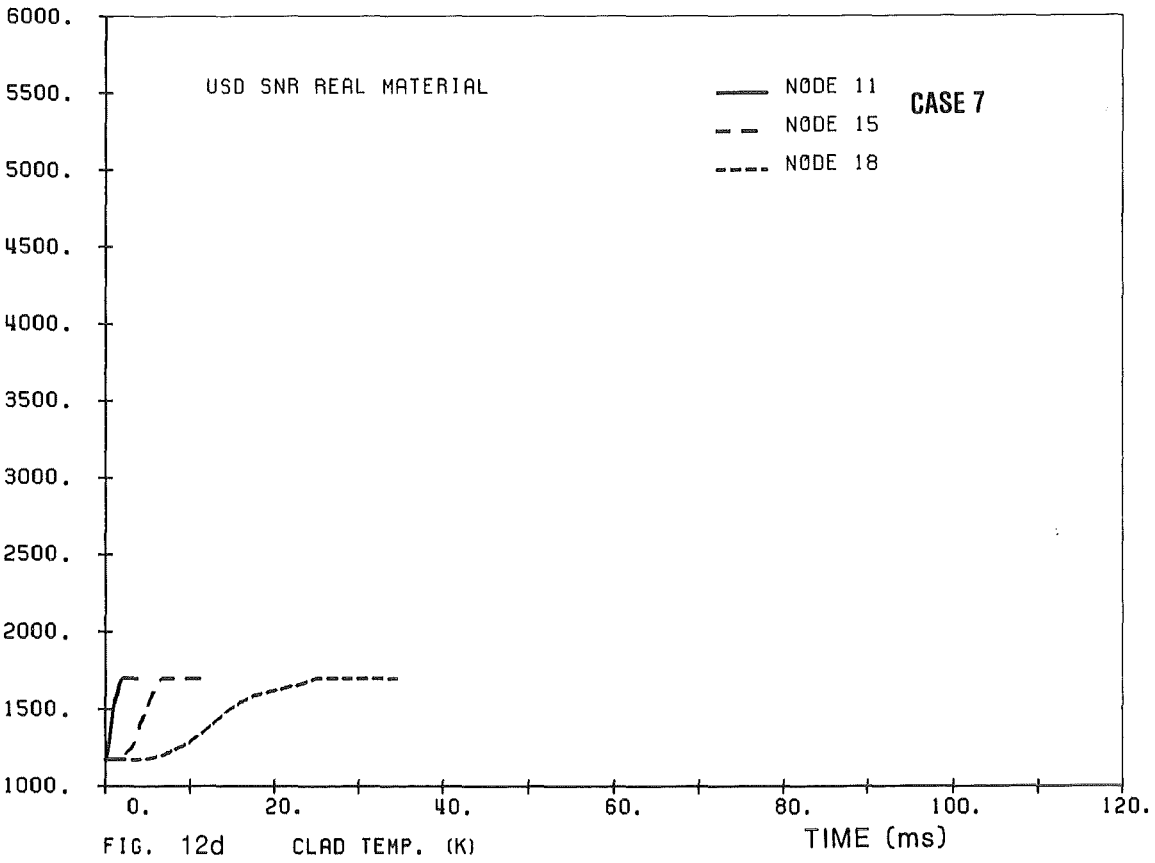

FIG. 12d CLAD TEMP. (K)

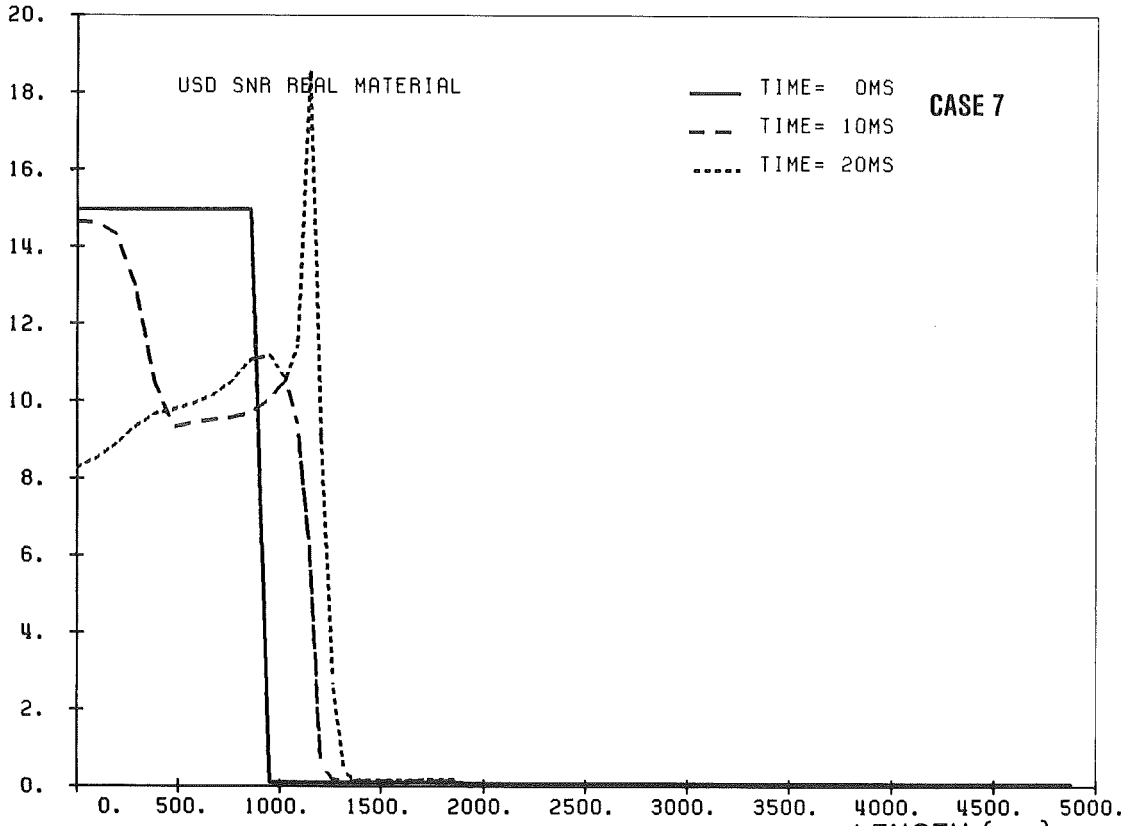

FIG. 13a

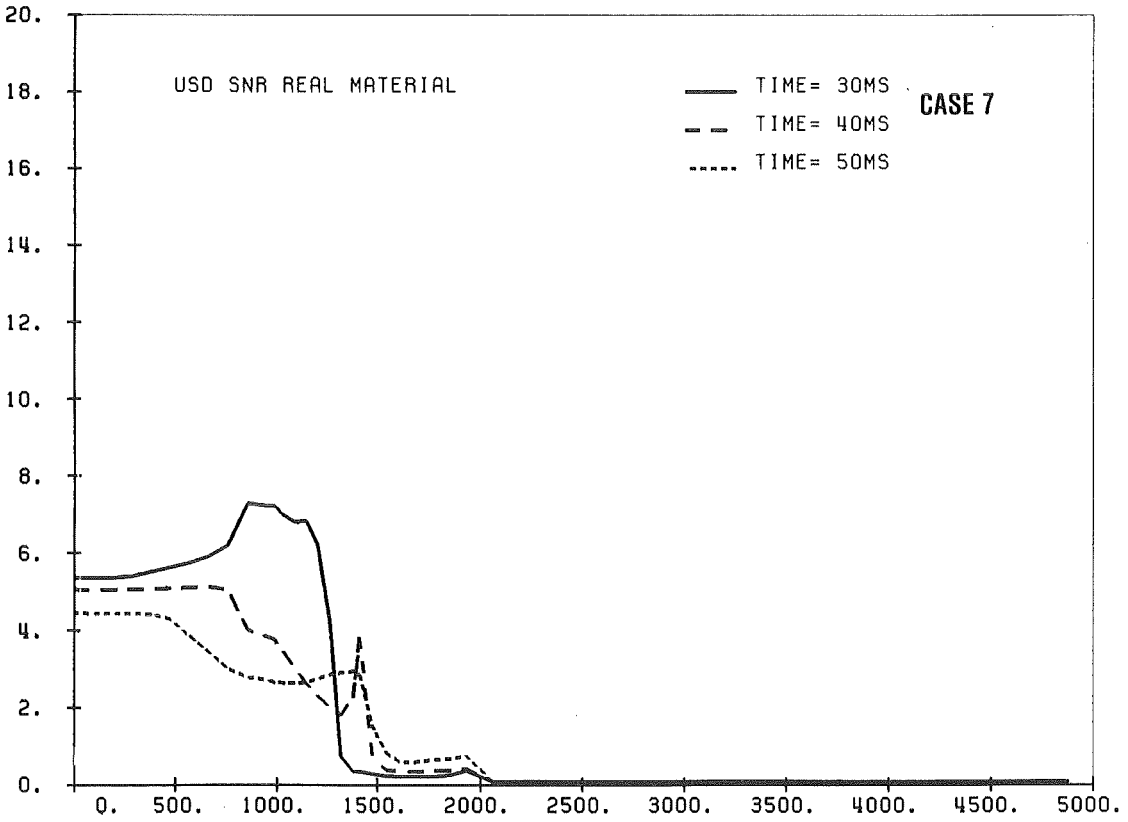

FIG. 13b

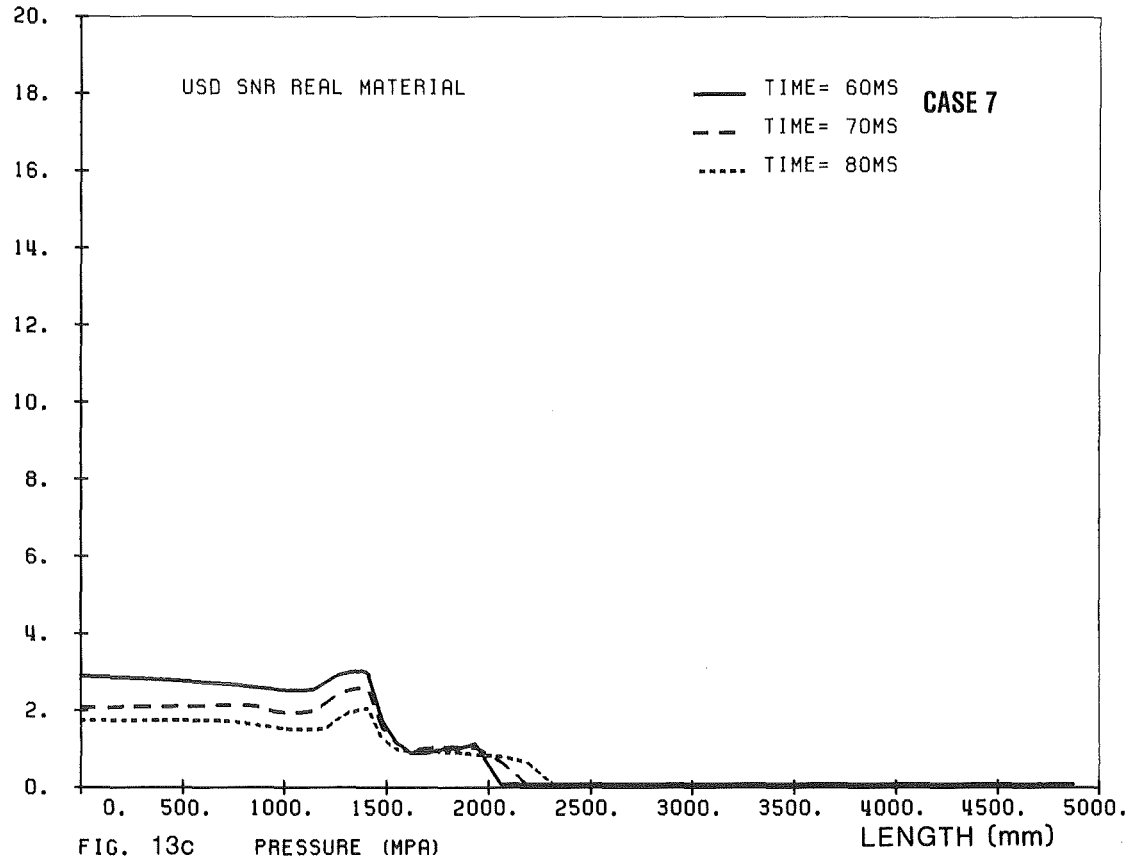

FIG. 13c PRESSURE (MPA)

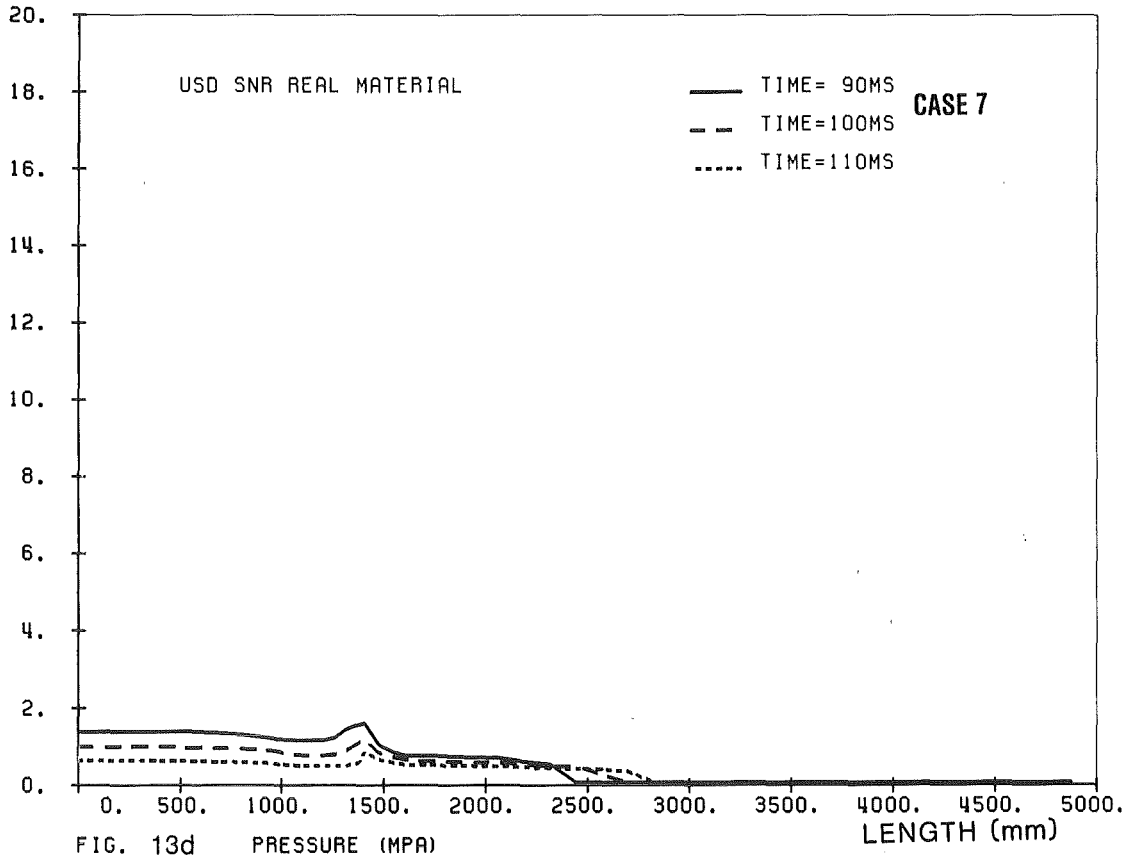

FIG. 13d PRESSURE (MPA)

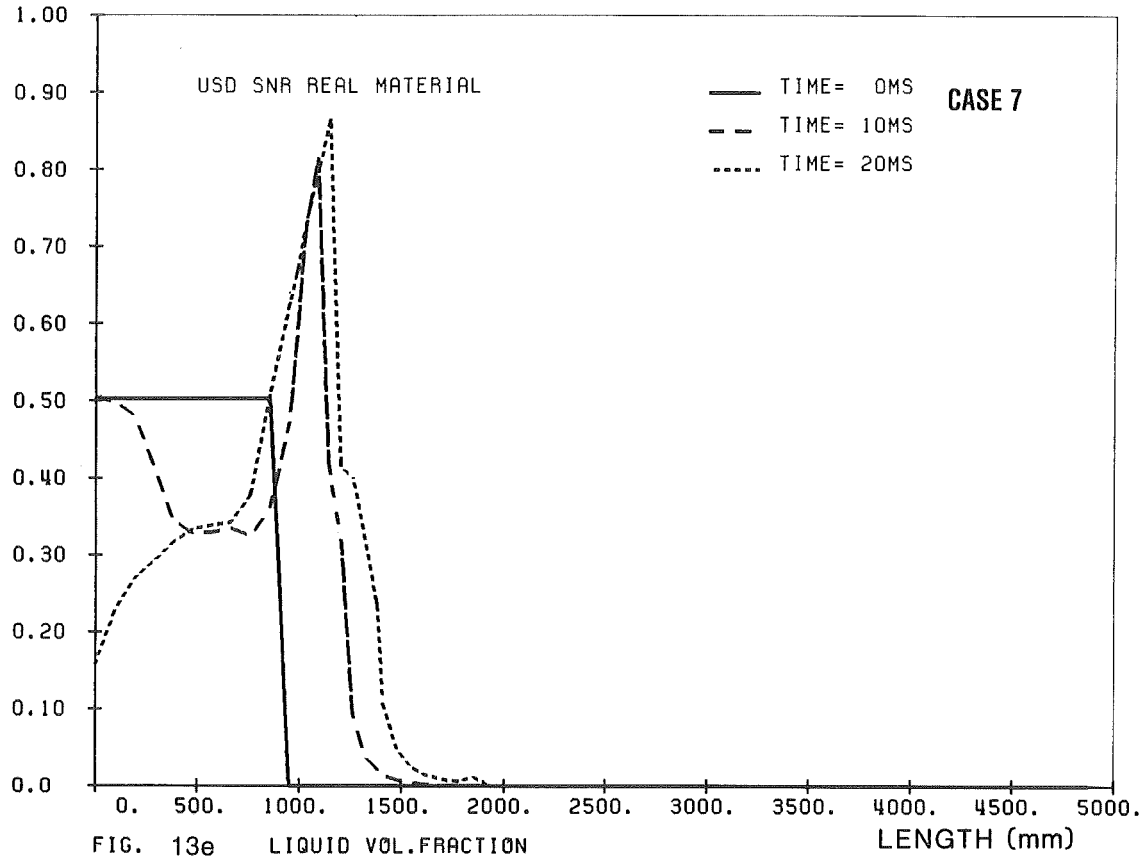

FIG. 13e LIQUID VOL.FRACTION

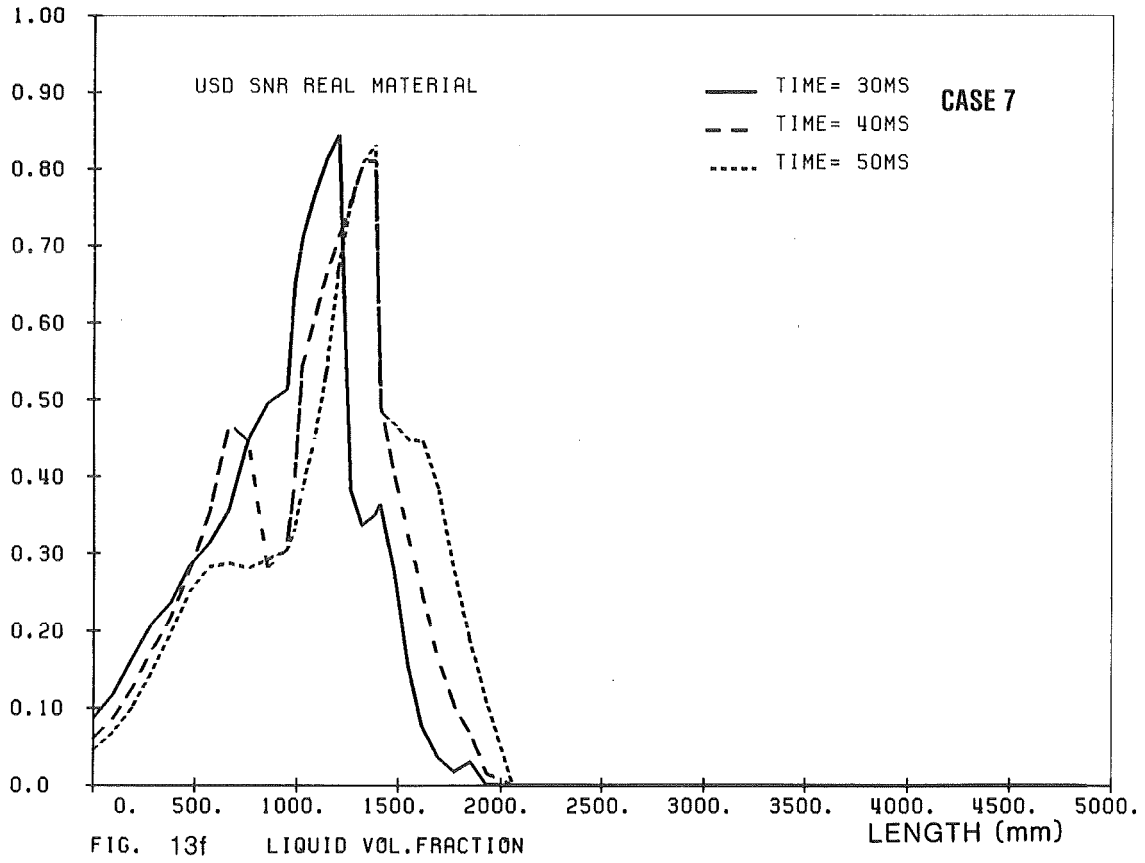

FIG. 13f LIQUID VOL.FRACTION

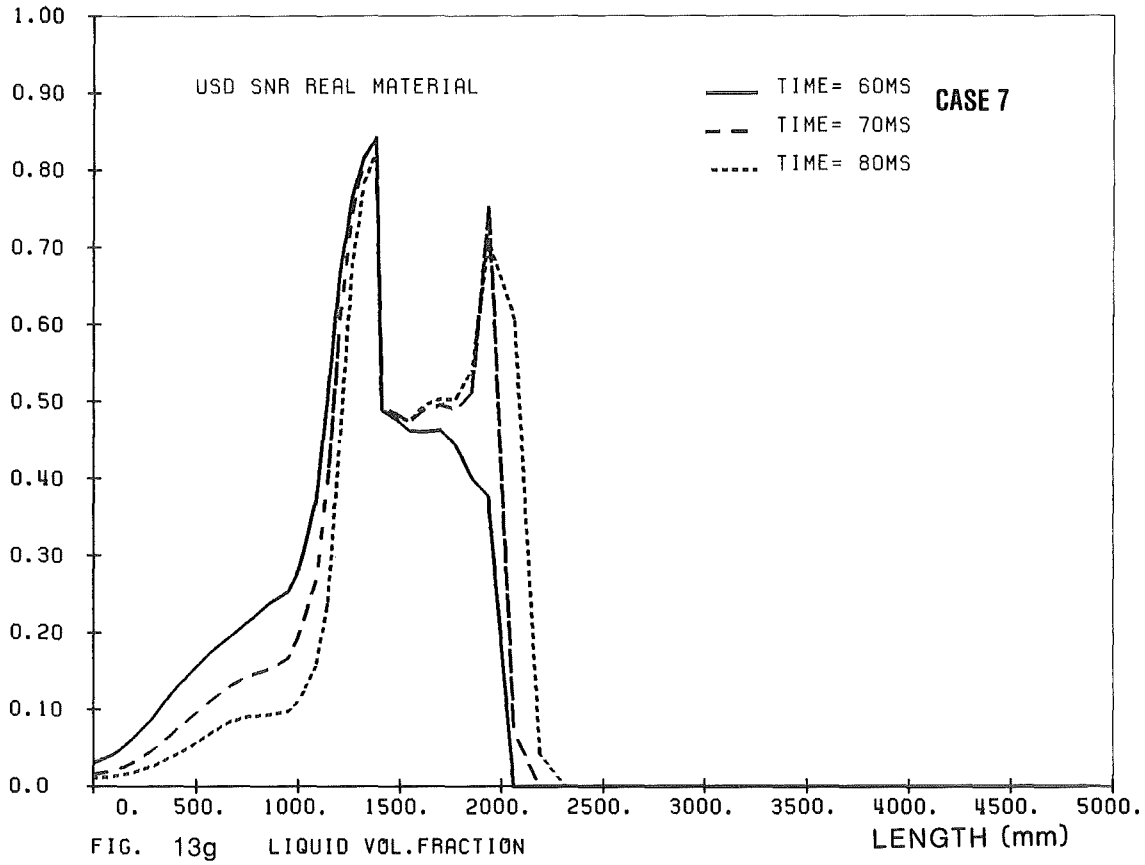

FIG. 13g LIQUID VOL.FRACTION

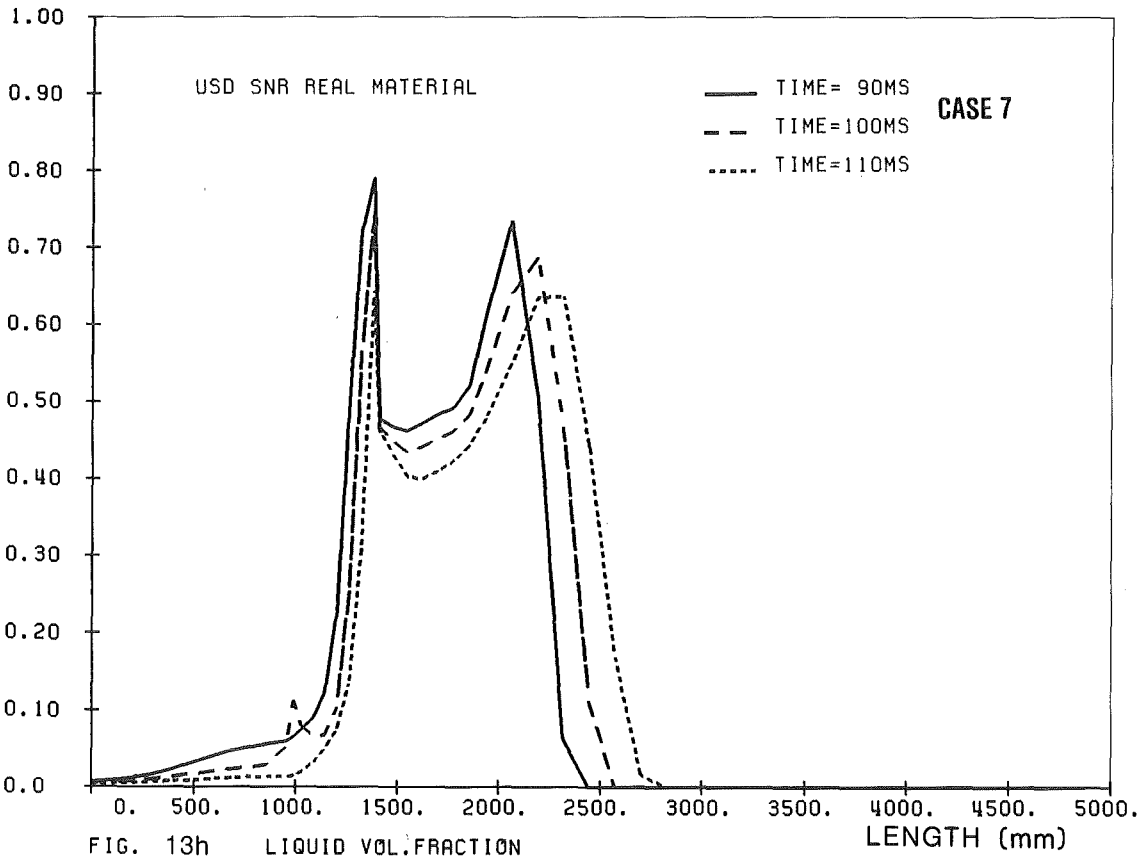

FIG. 13h LIQUID VOL.FRACTION

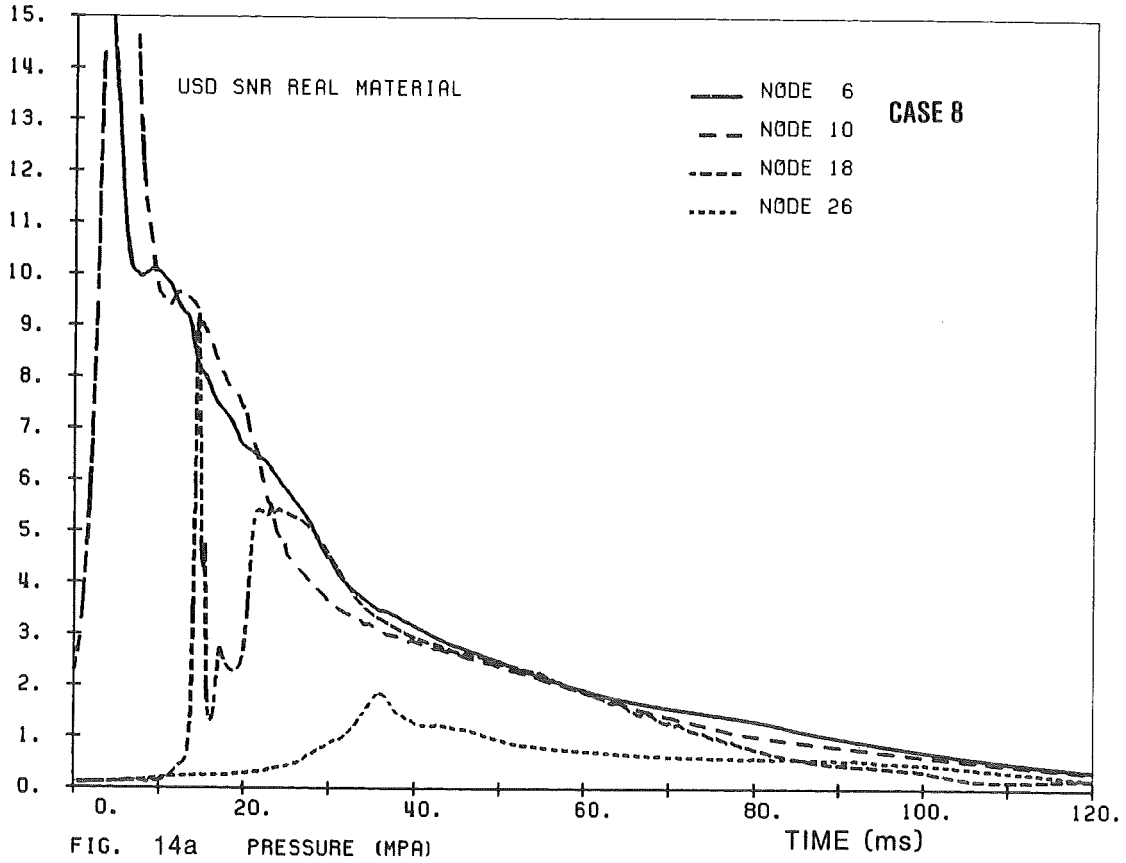

FIG. 14a PRESSURE (MPA)

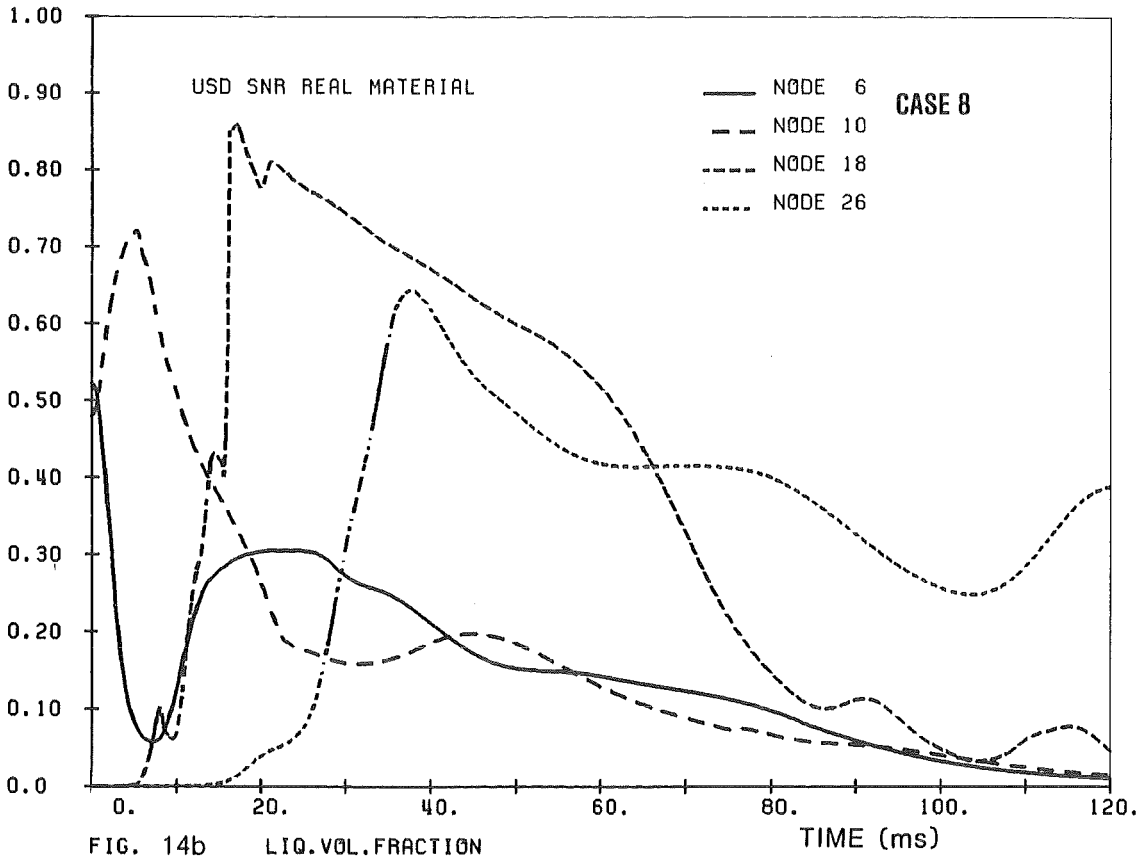

FIG. 14b LIQ.VOL.FRACTION

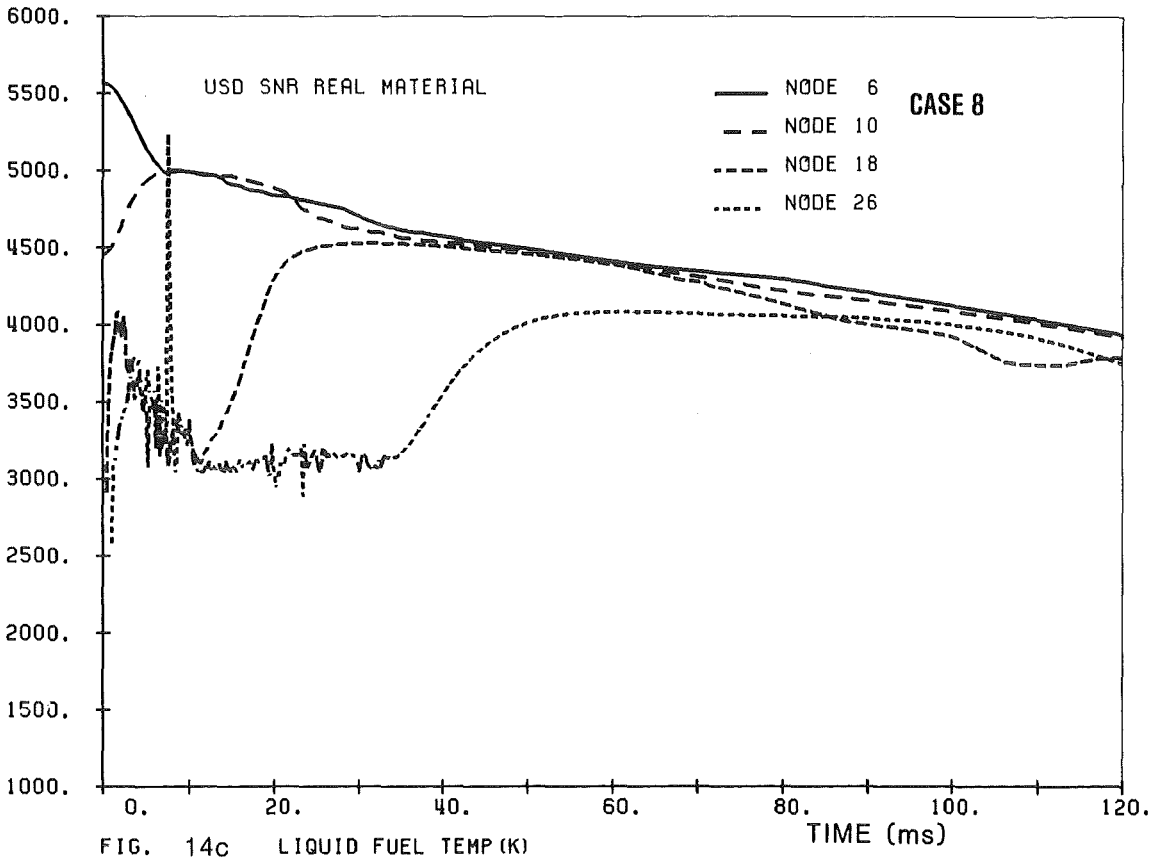

FIG. 14c LIQUID FUEL TEMP (K)

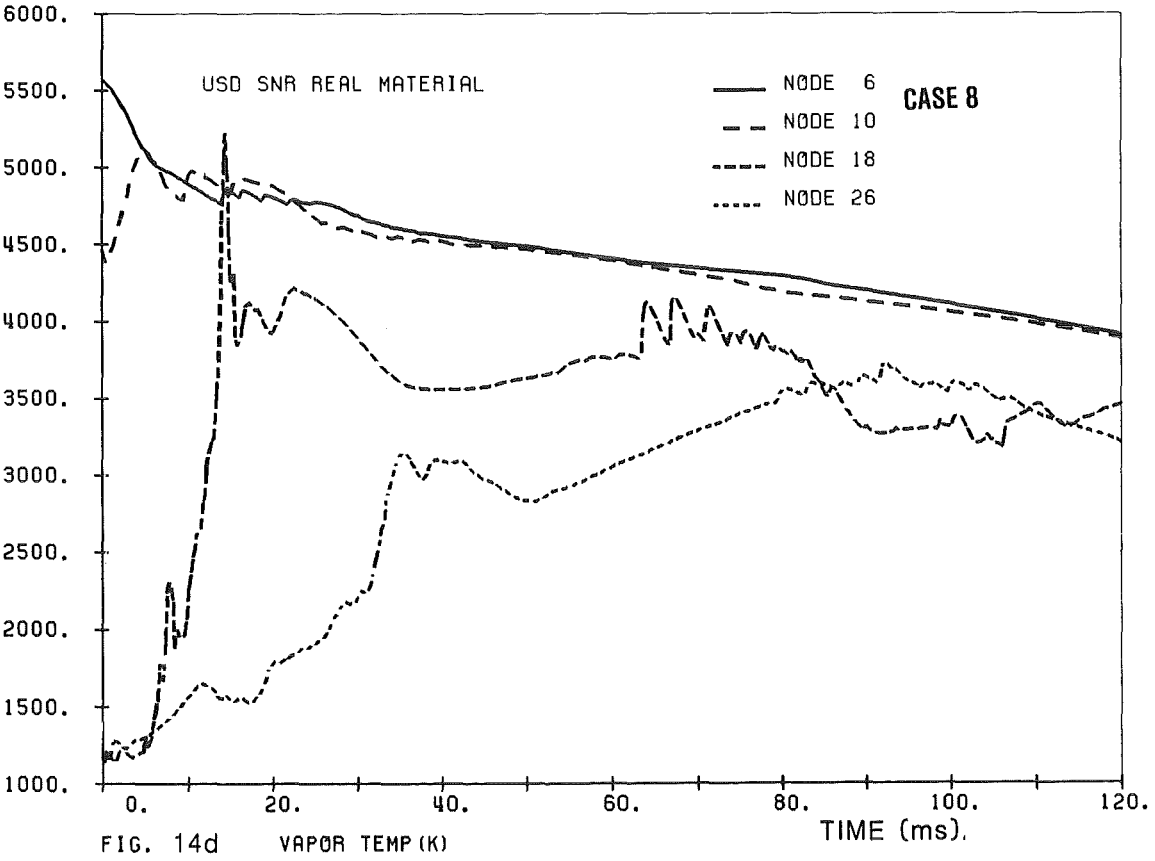

FIG. 14d VAPOR TEMP (K)

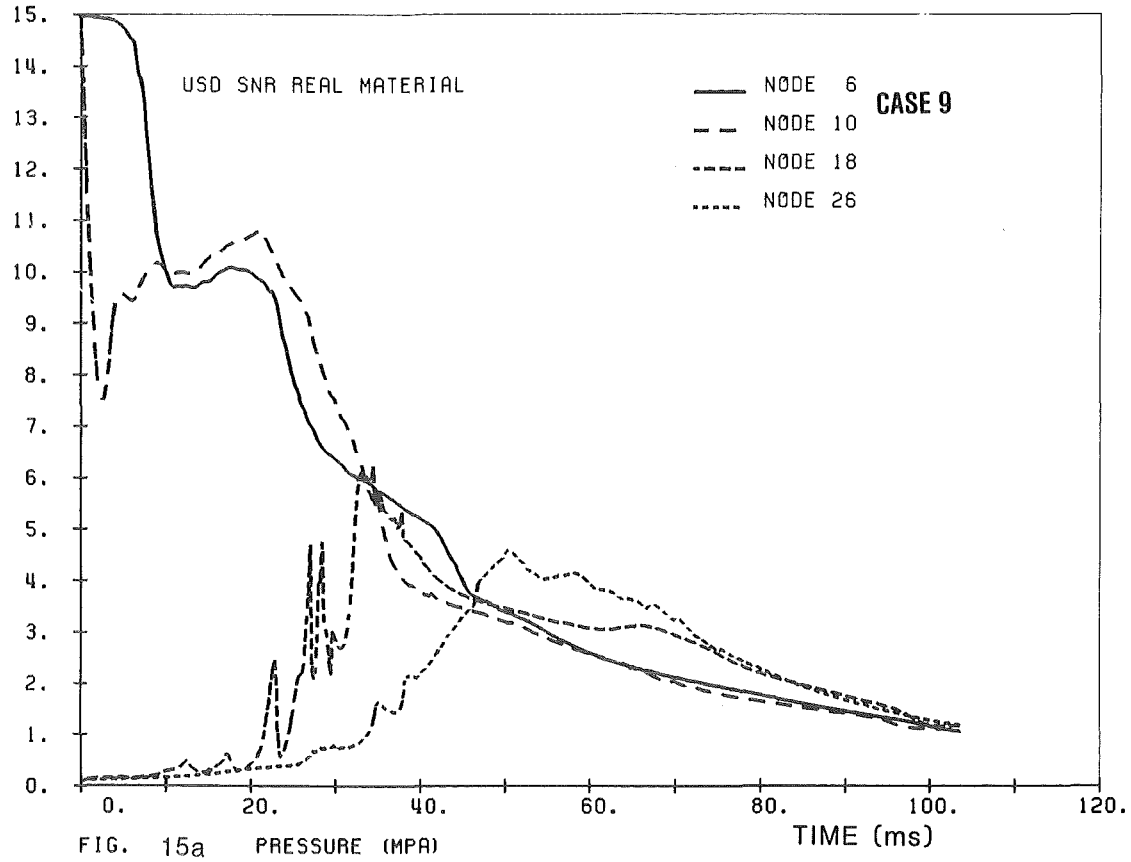

FIG. 15a PRESSURE (MPA)

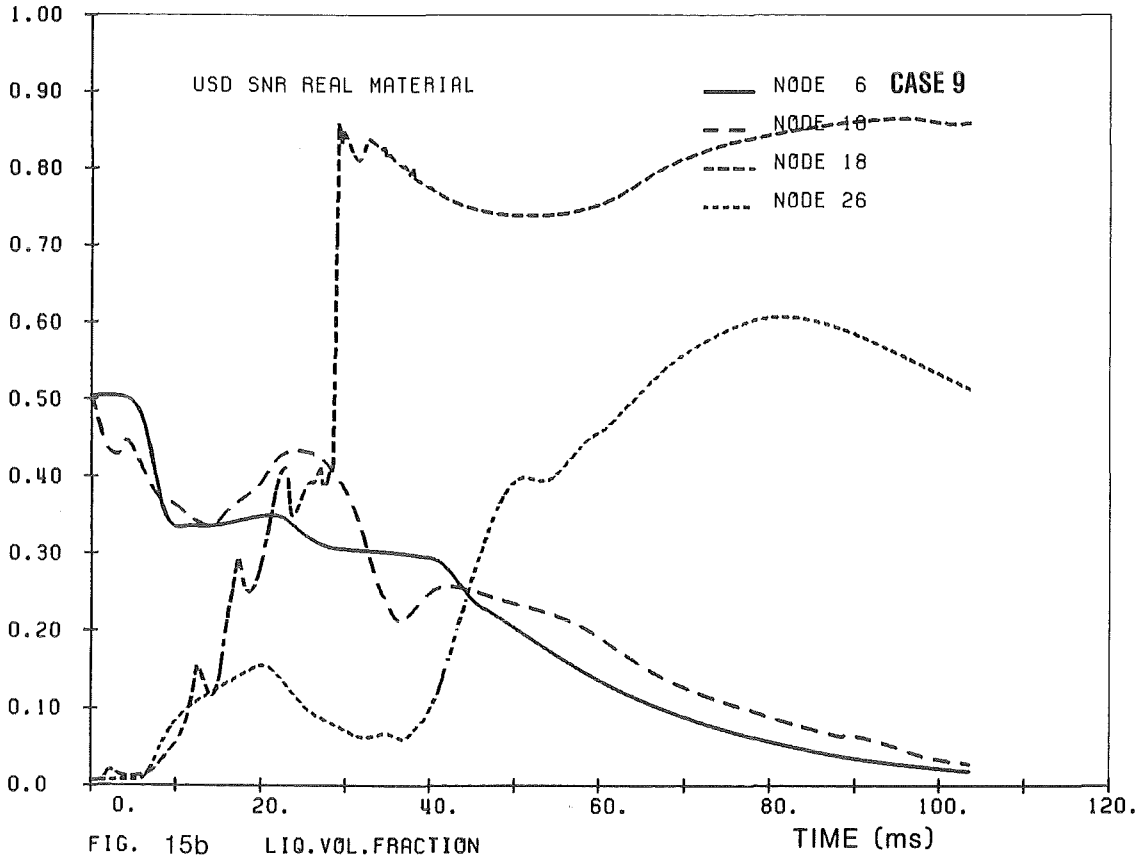

FIG. 15b LIQ.VOL.FRACTION

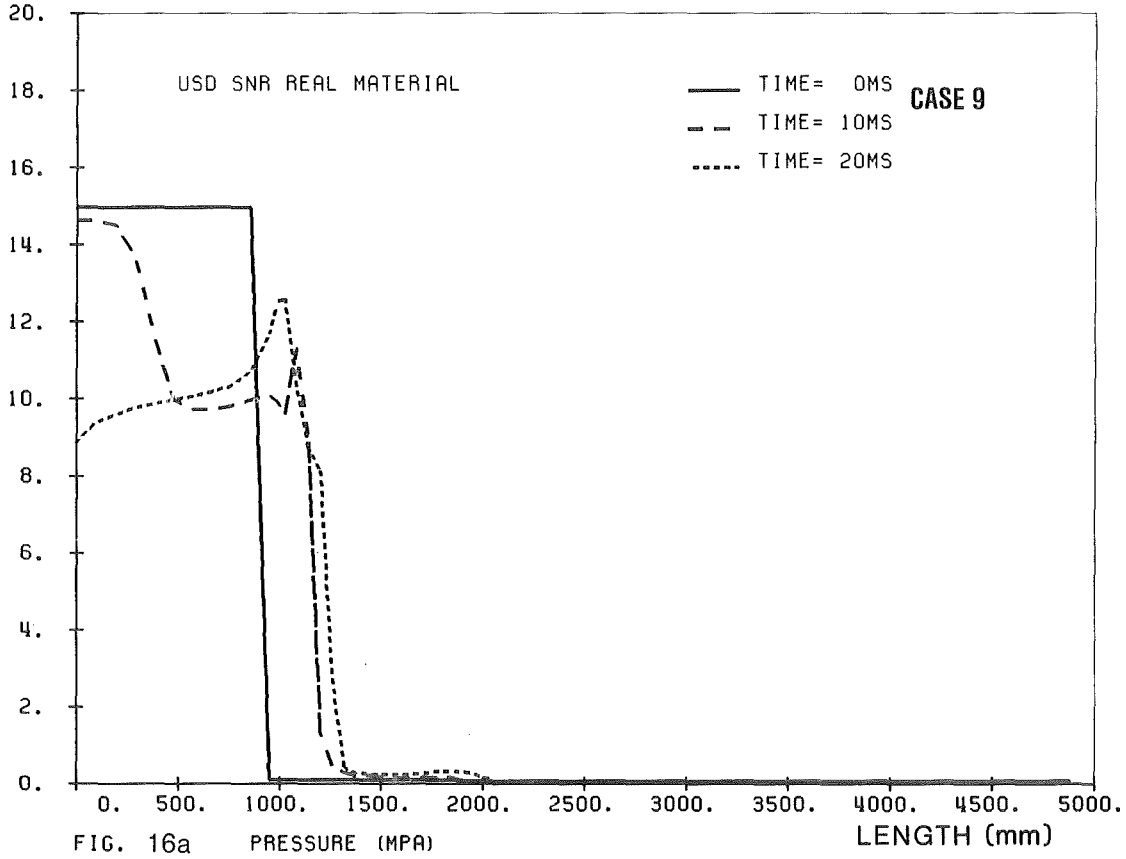

FIG. 16a

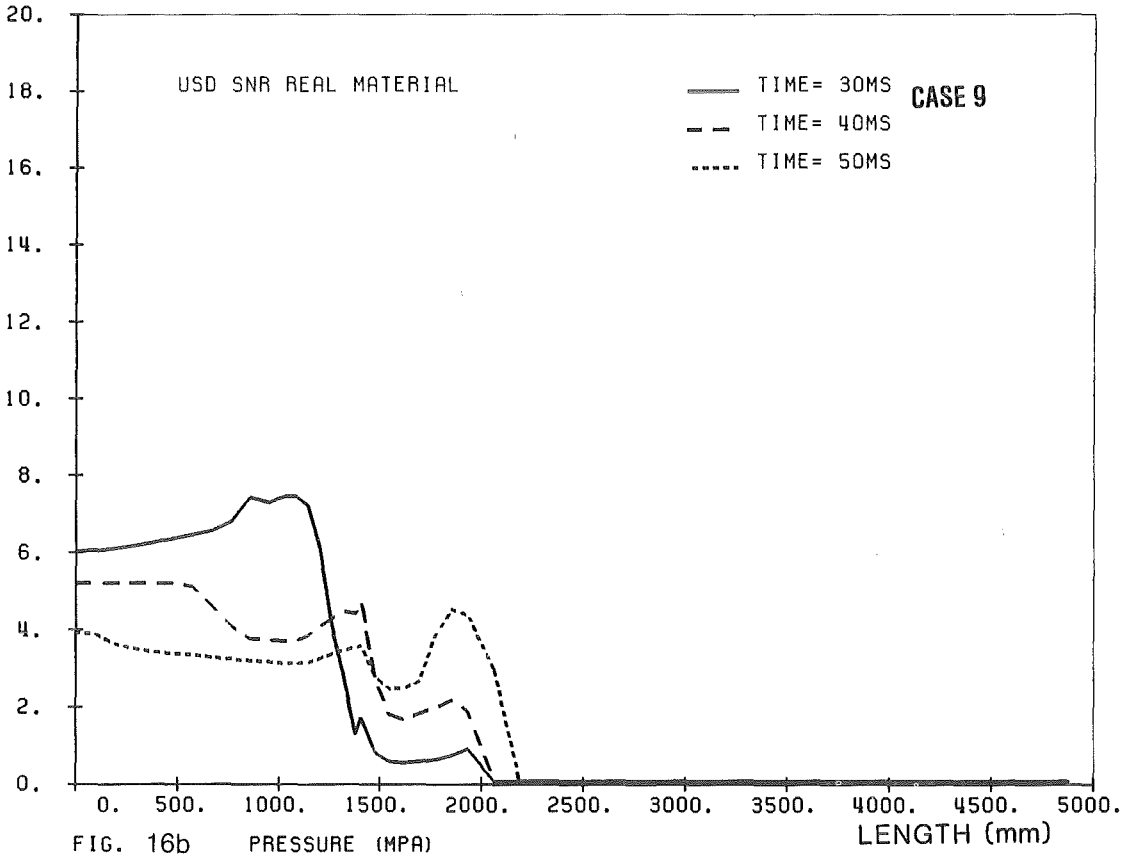

FIG. 16b

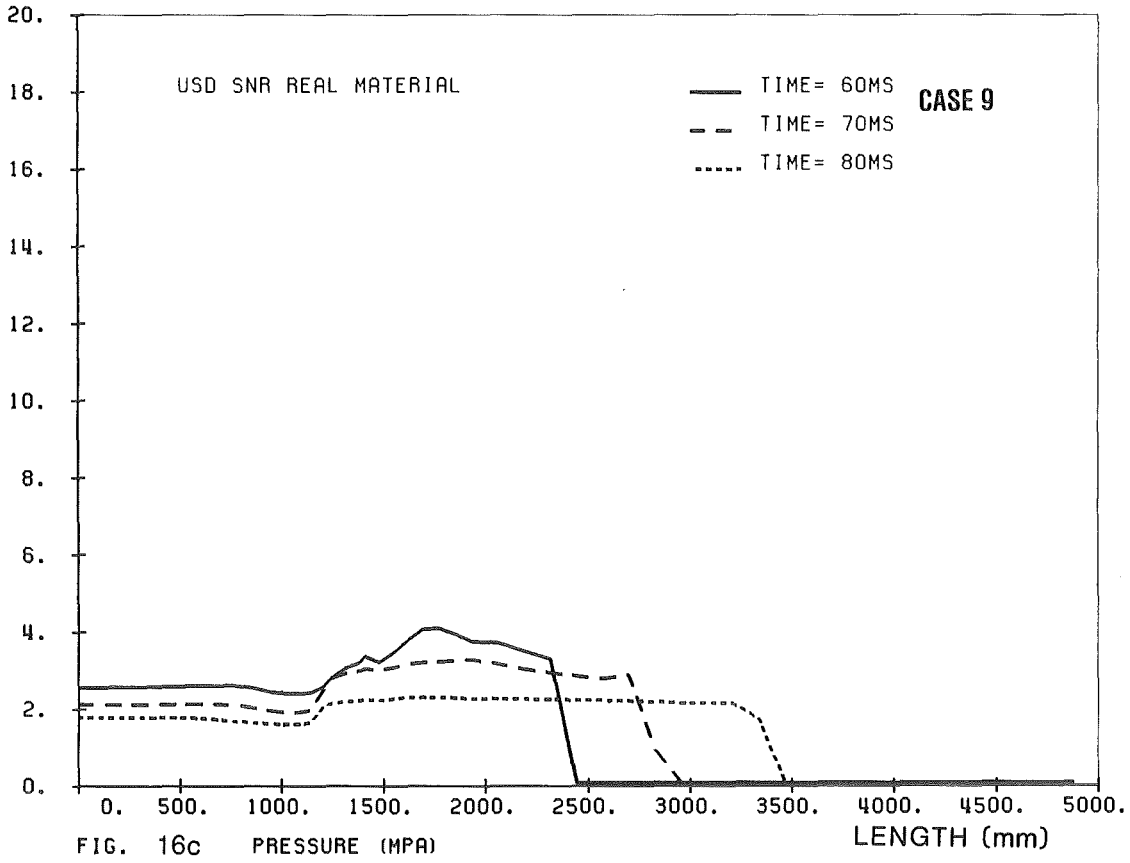

FIG. 16c

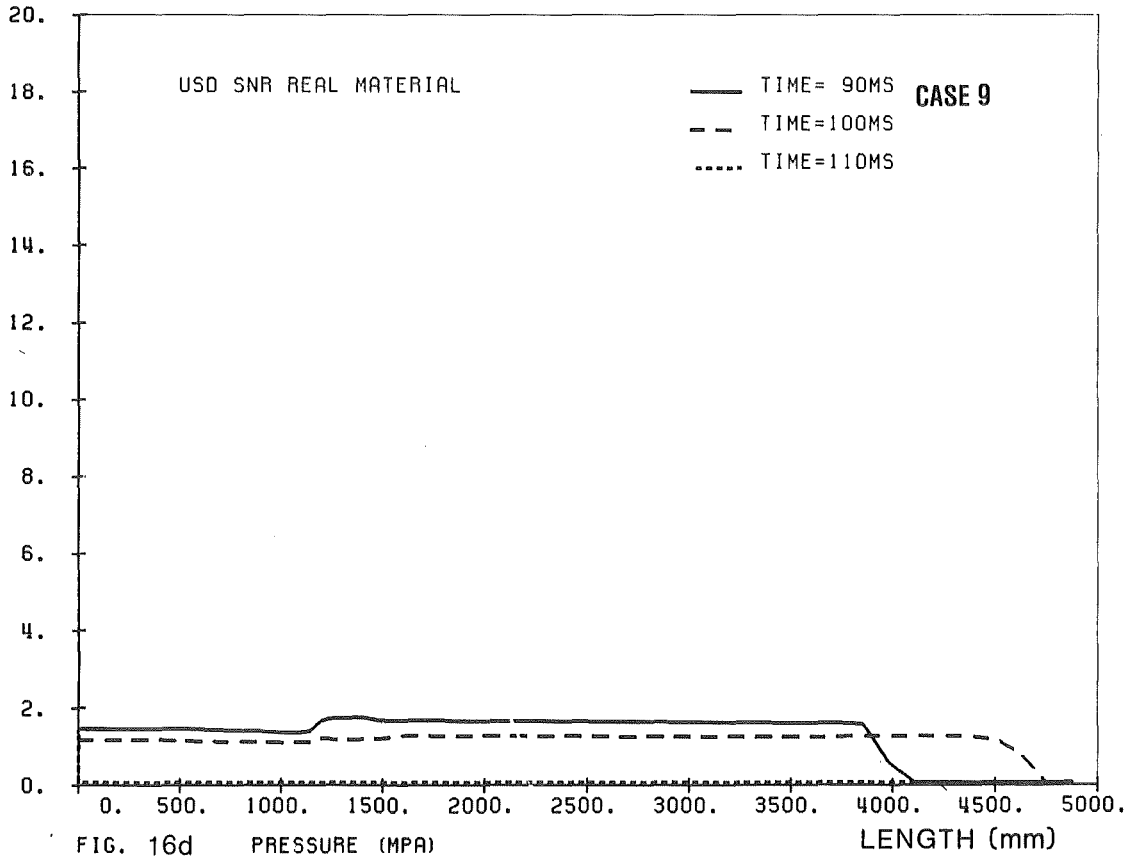

FIG. 16d

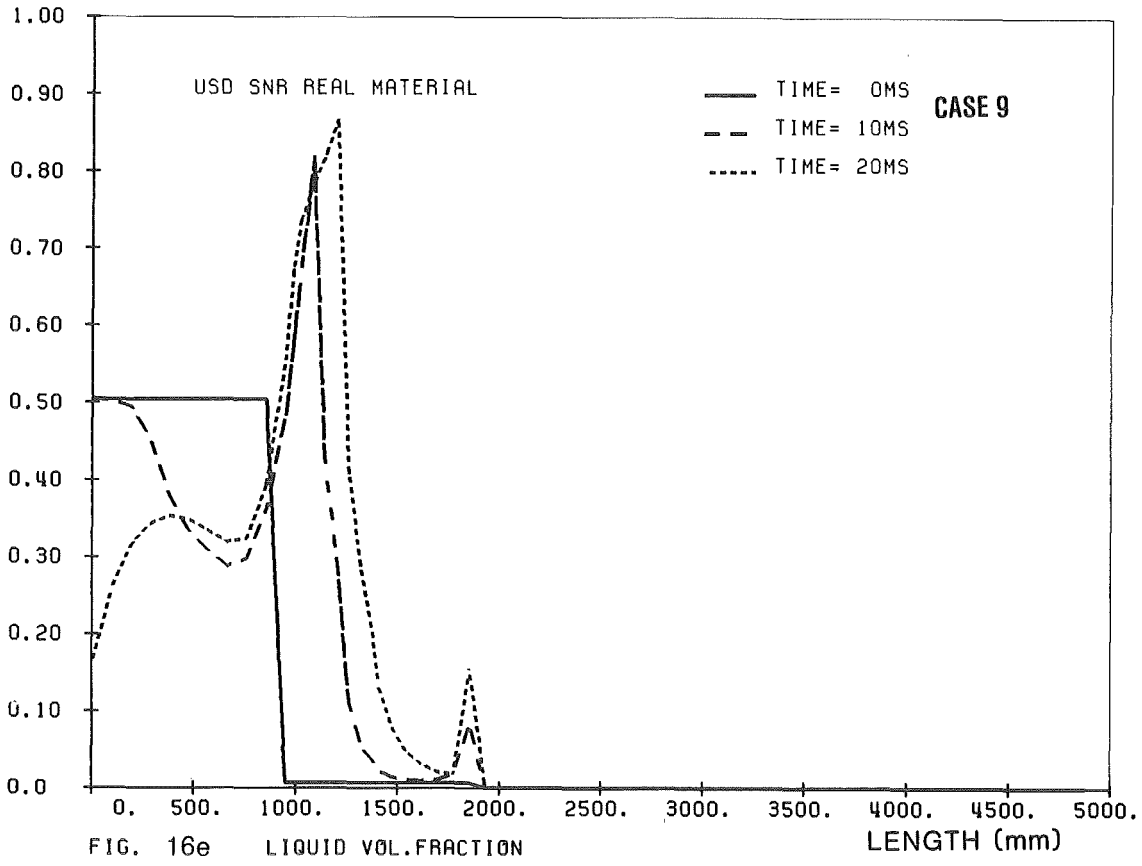

FIG. 16e LIQUID VOL.FRACTION

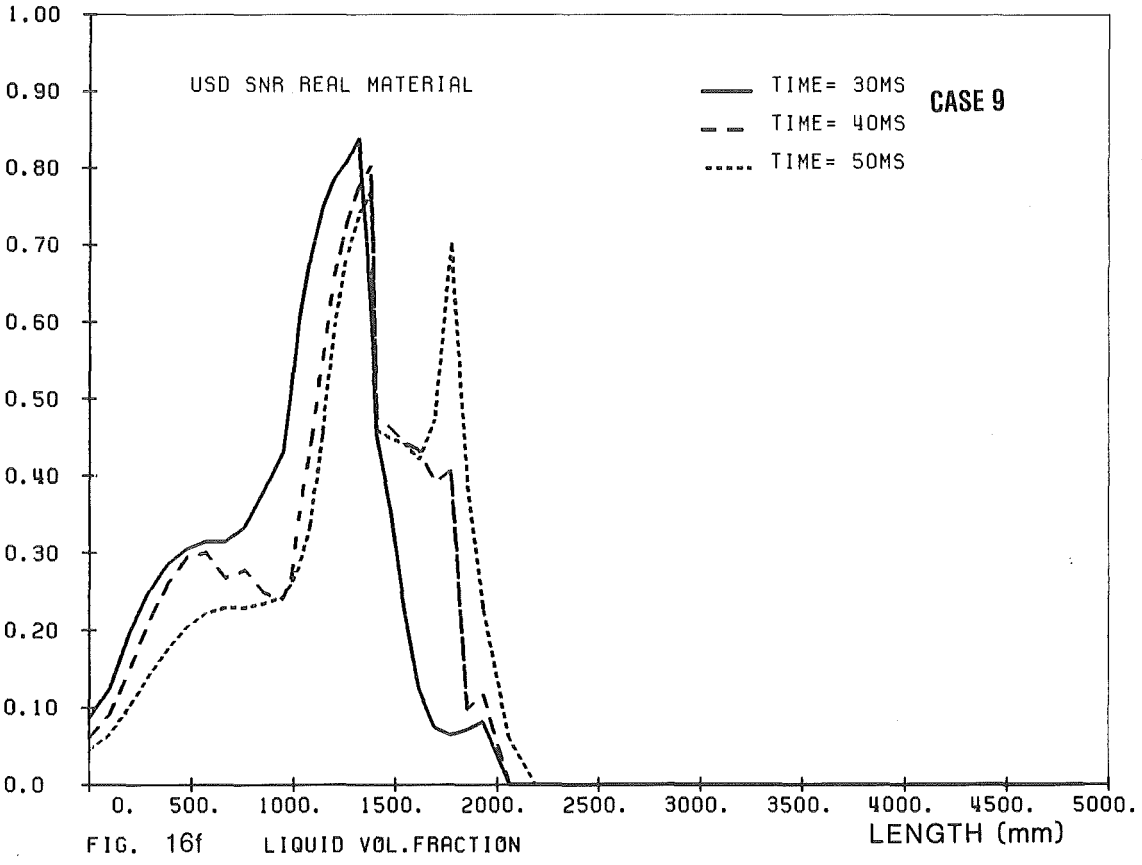

FIG. 16f LIQUID VOL.FRACTION

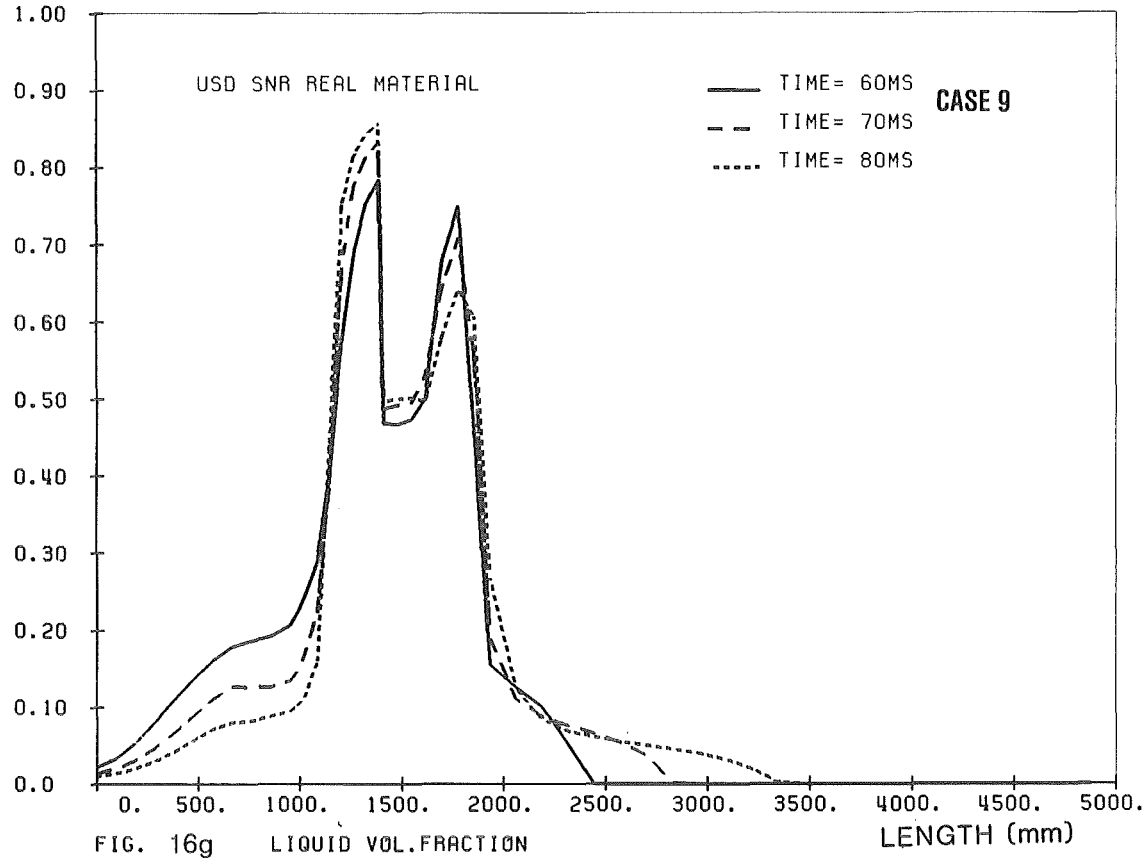

FIG. 16g LIQUID VOL.FRACTION

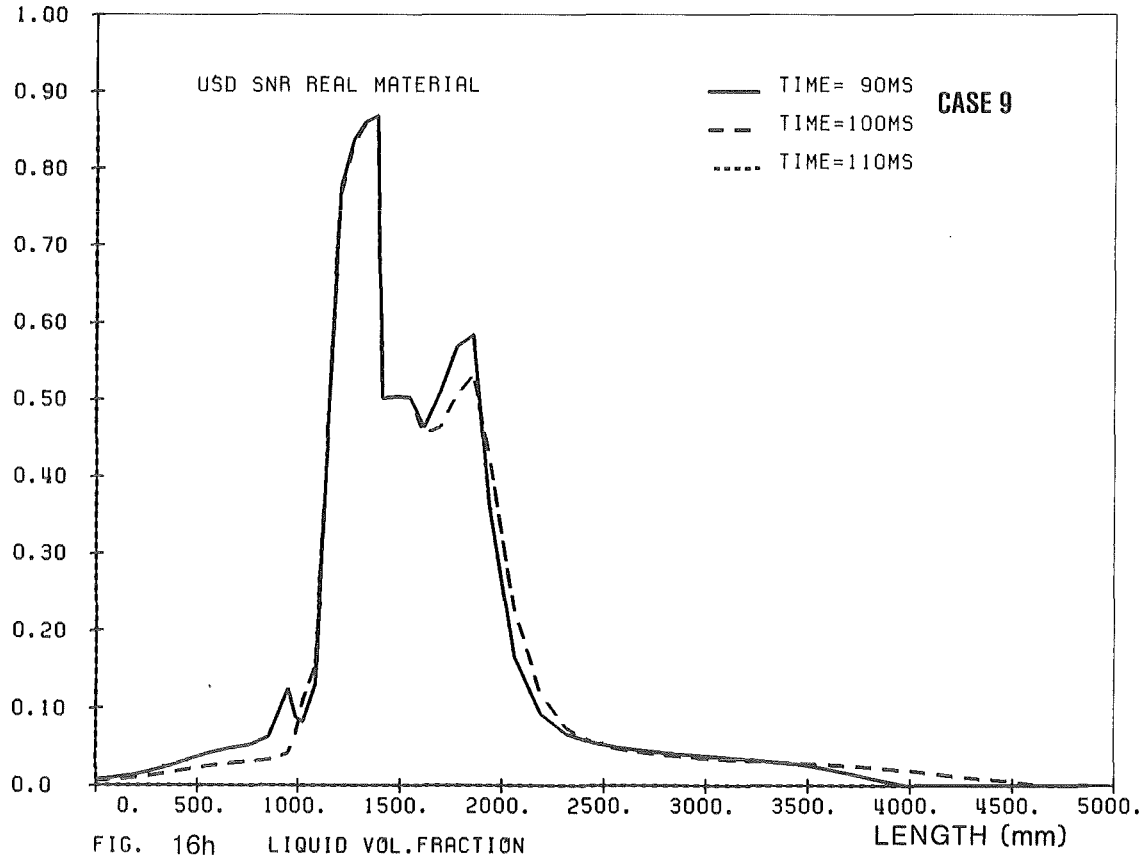

FIG. 16h LIQUID VOL.FRACTION

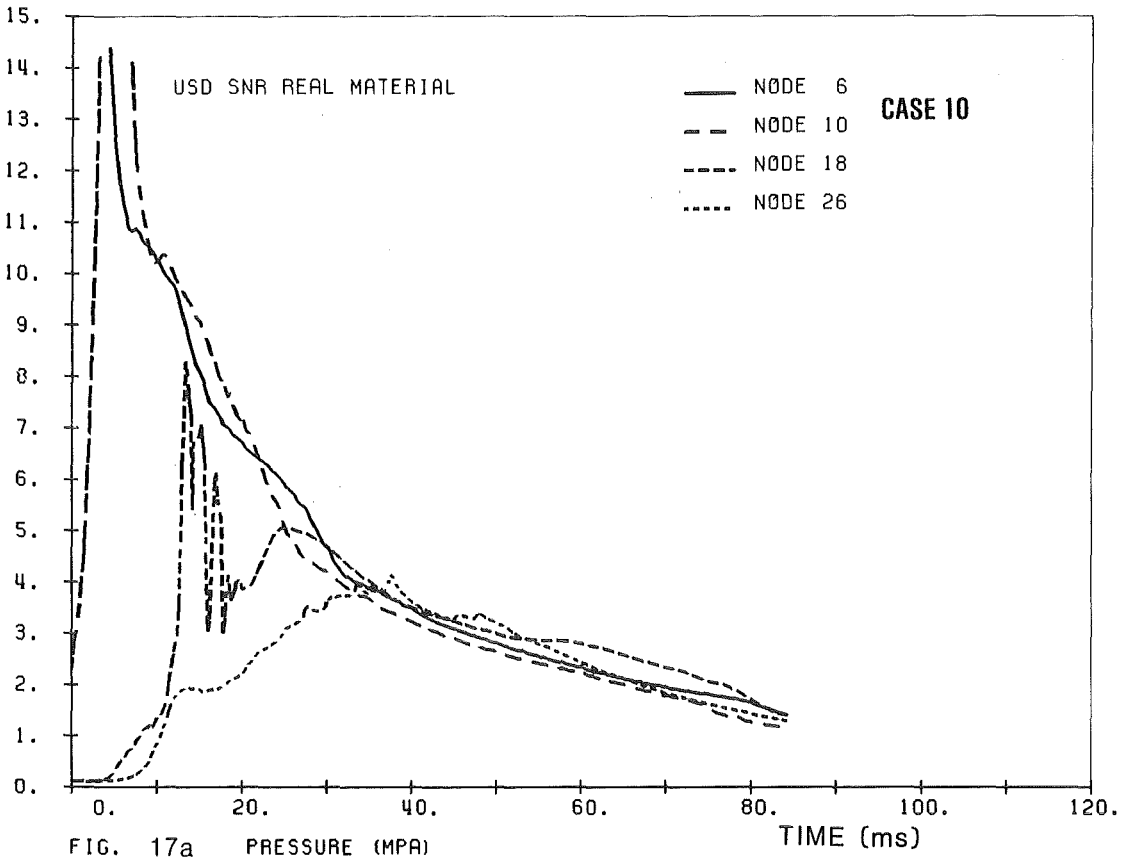

FIG. 17a PRESSURE (MPA)

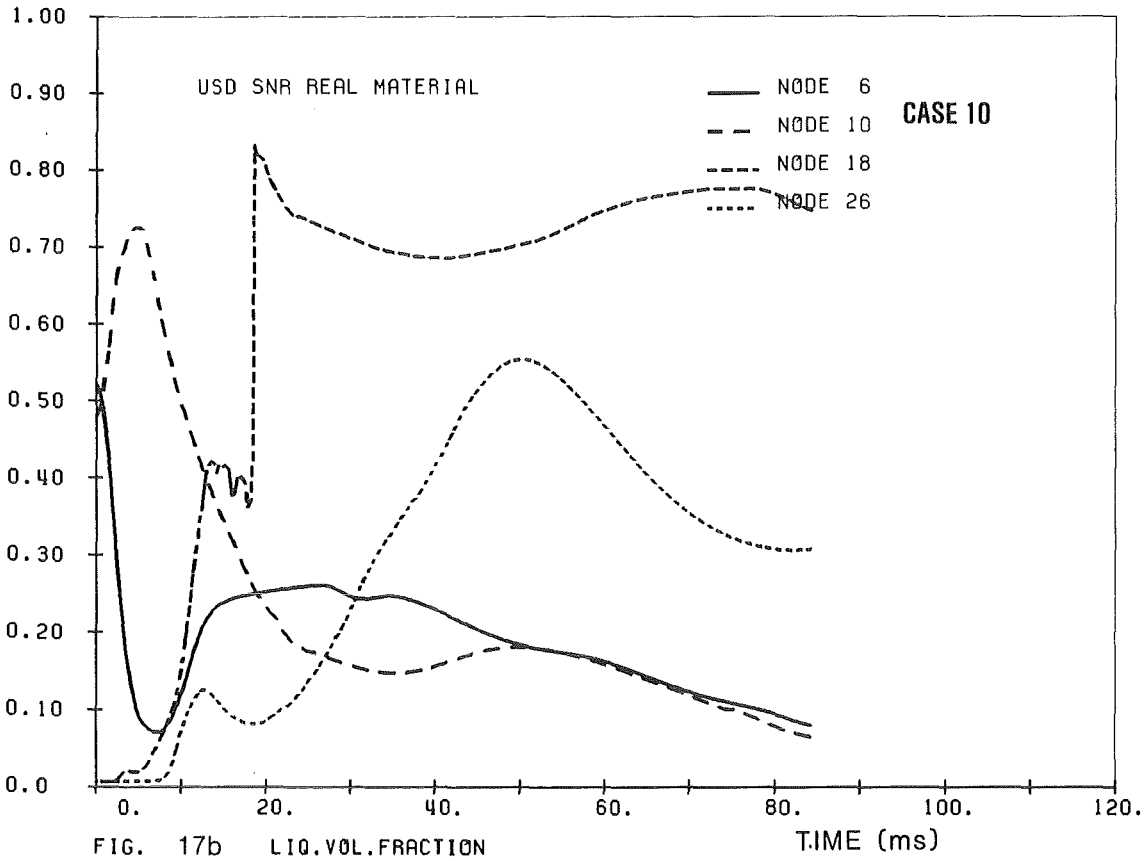

FIG. 17b LIQ.VOL.FRACTION

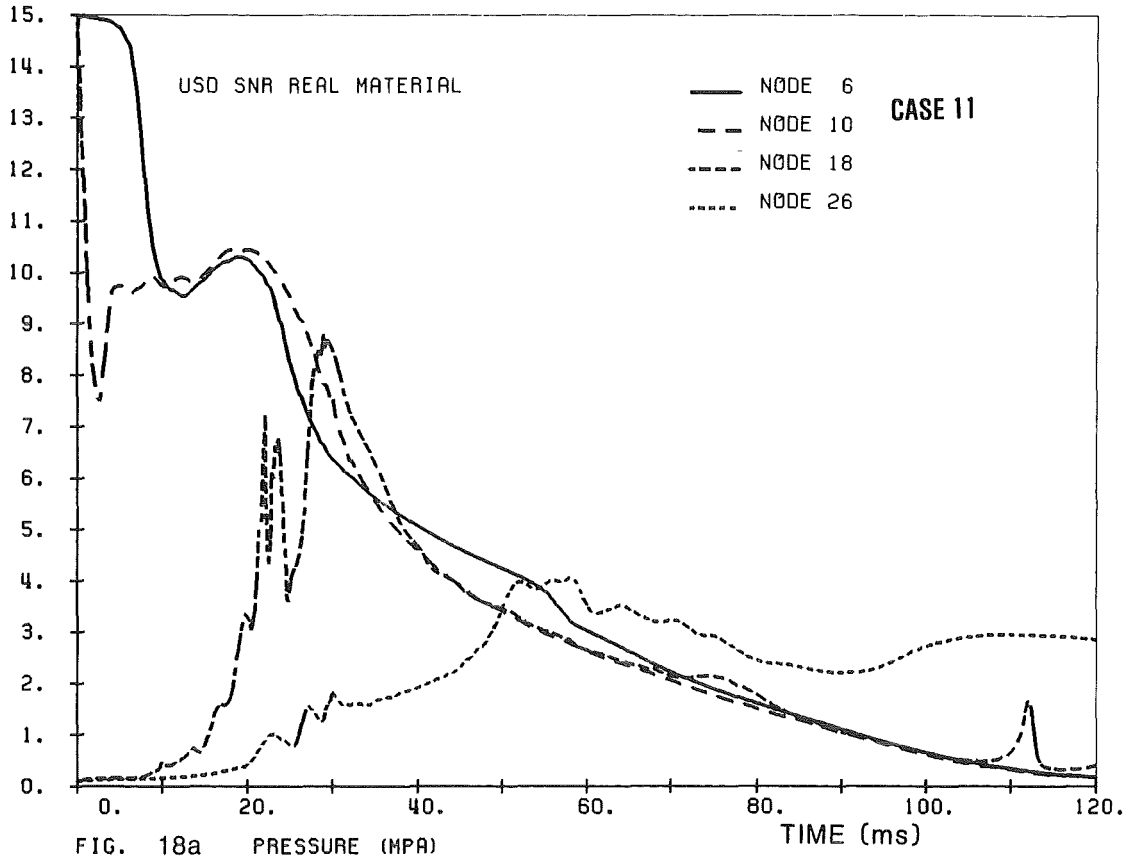

FIG. 18a PRESSURE (MPA)

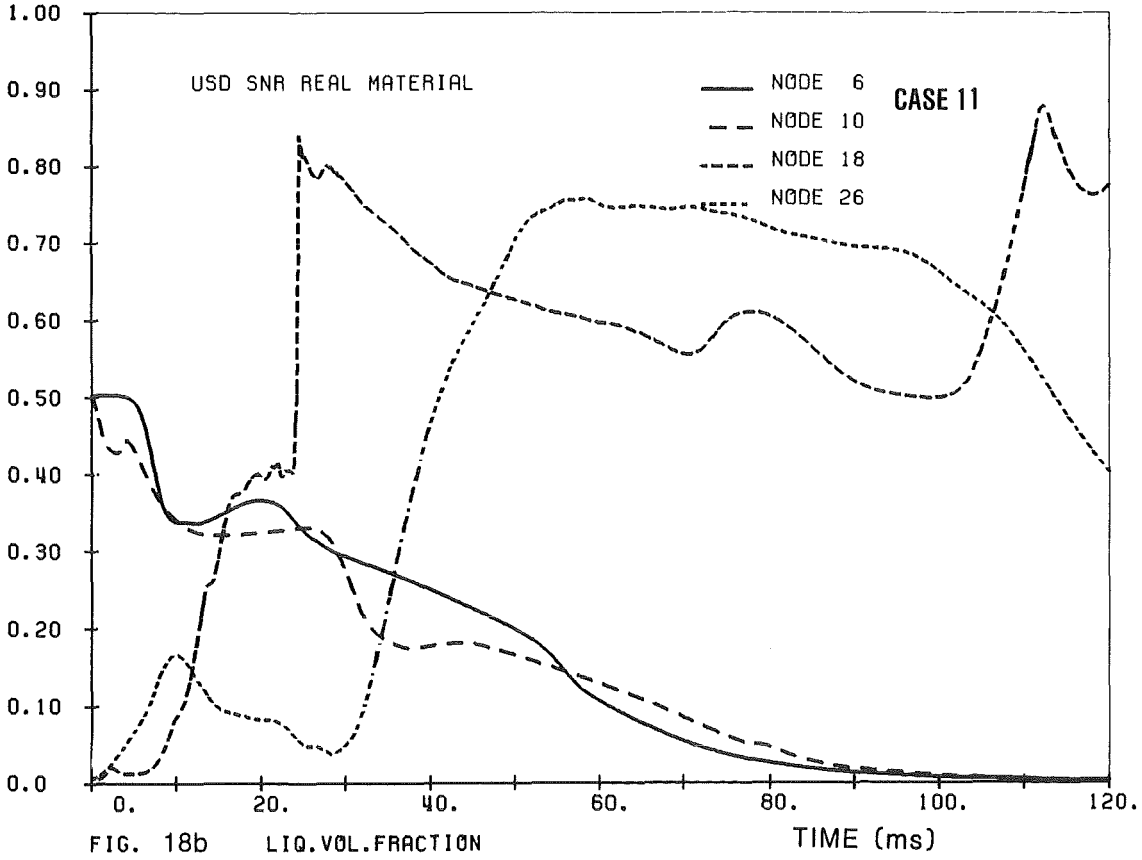

FIG. 18b LIQ.VOL.FRACTION

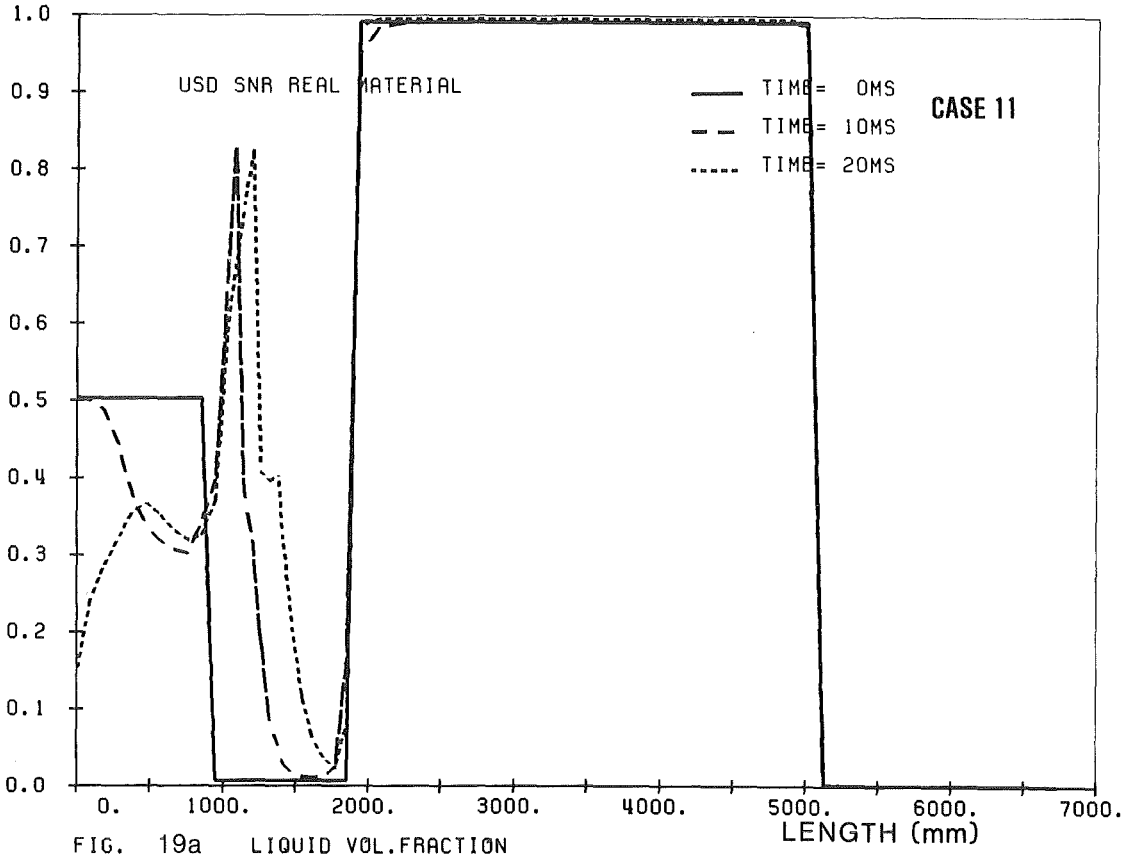

FIG. 19a LIQUID VOL.FRACTION

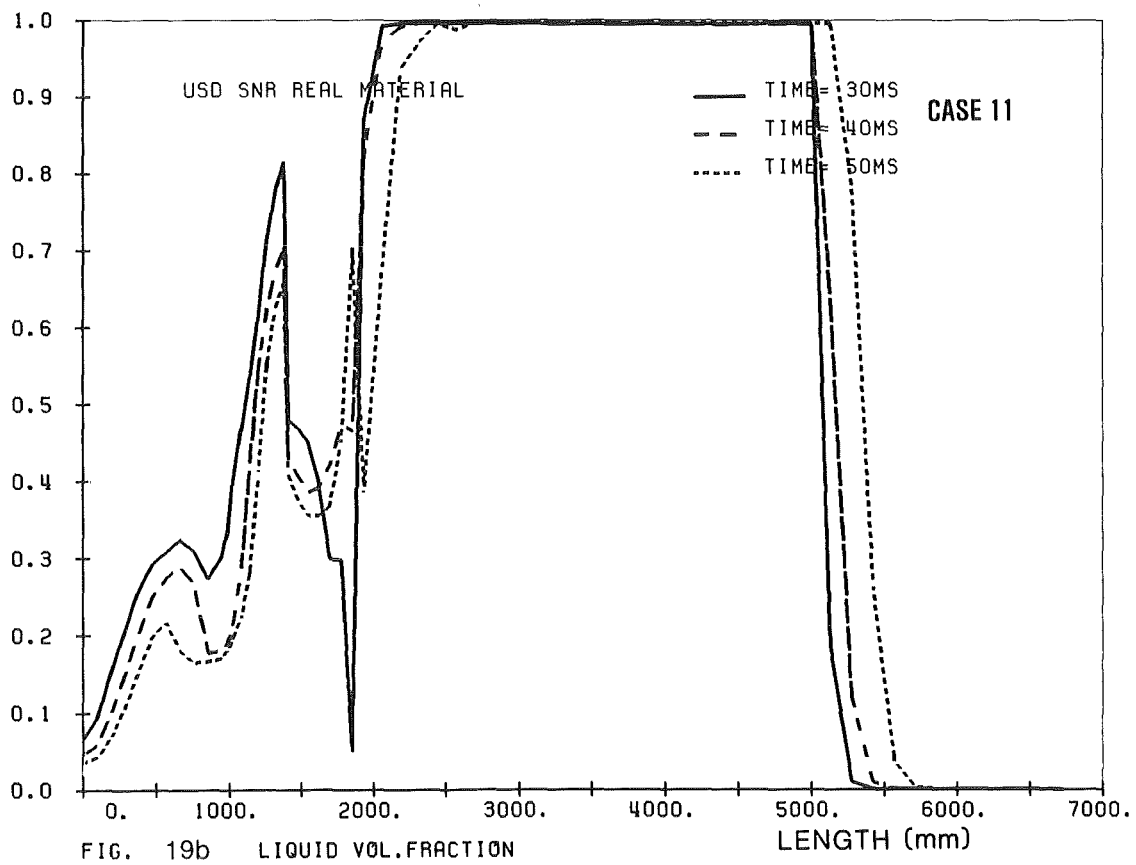

FIG. 19b LIQUID VOL.FRACTION

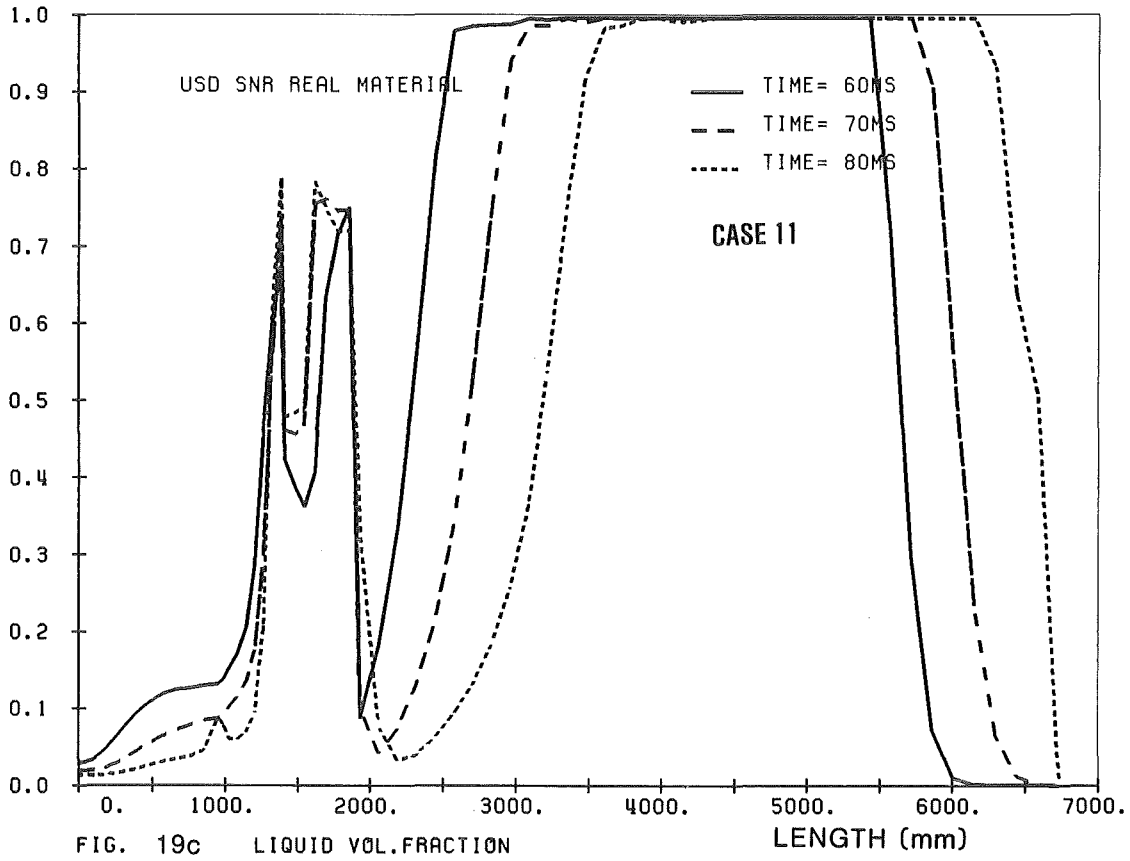

FIG. 19c LIQUID VOL.FRACTION

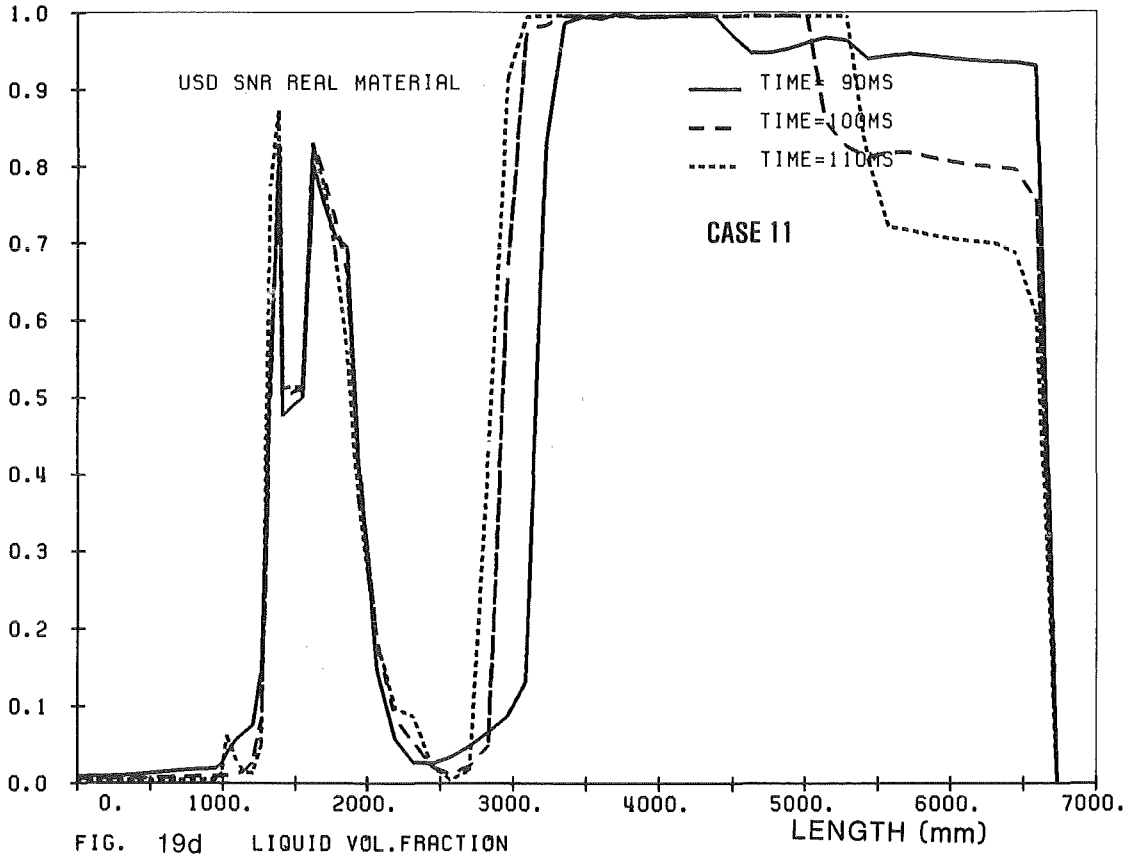

FIG. 19d LIQUID VOL.FRACTION

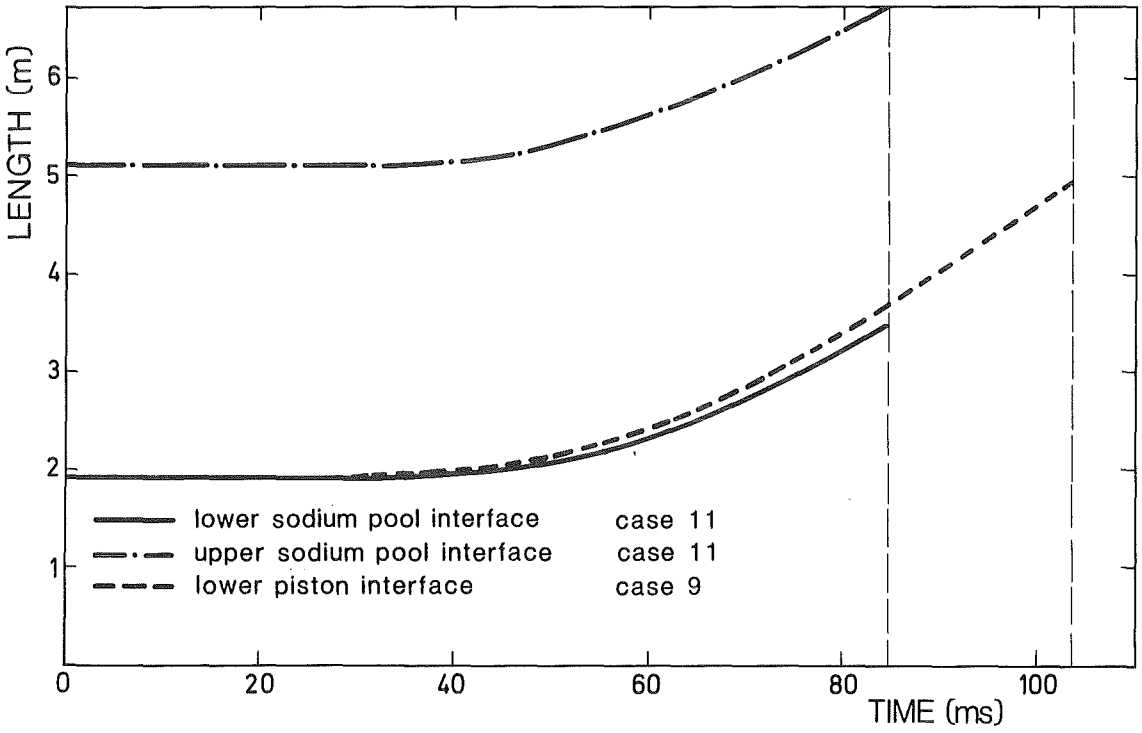

Fig. 20. Piston displacement as a function of time in comparison with the moving sodium pool interface for case 9 and 11.

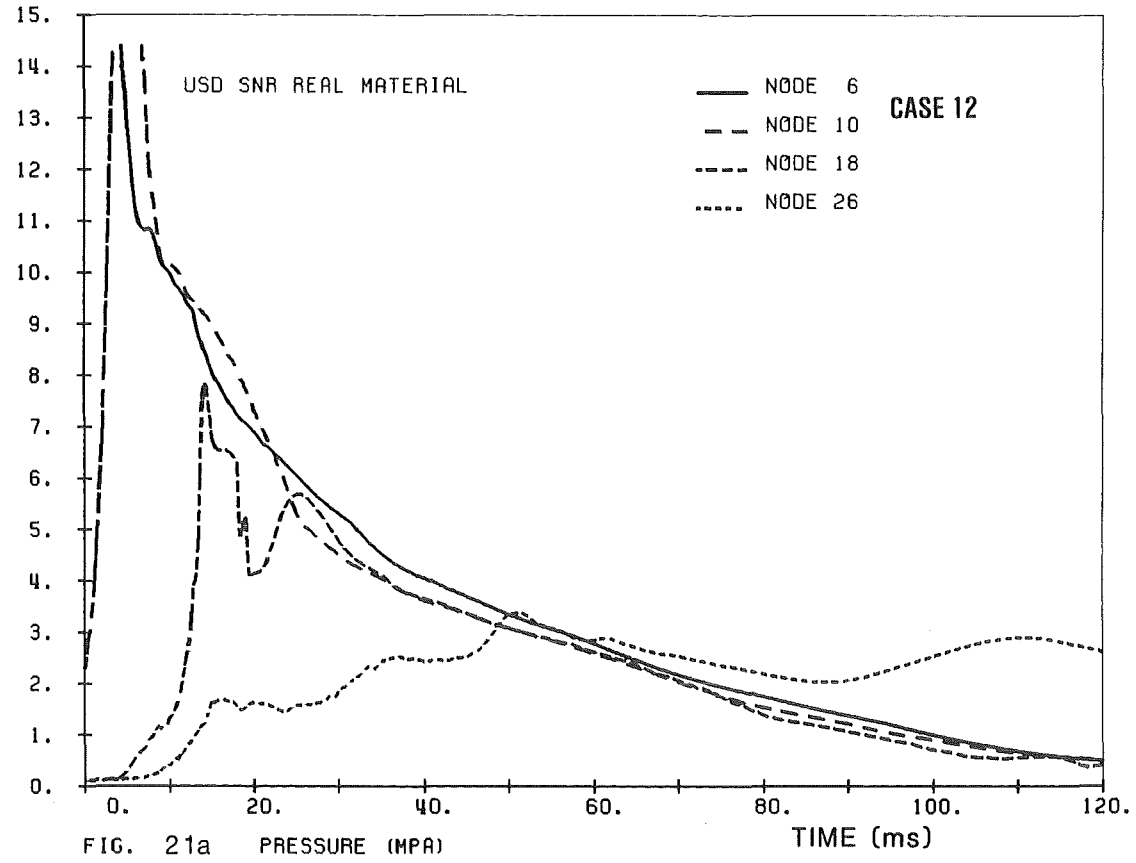

FIG. 21a PRESSURE (MPA)

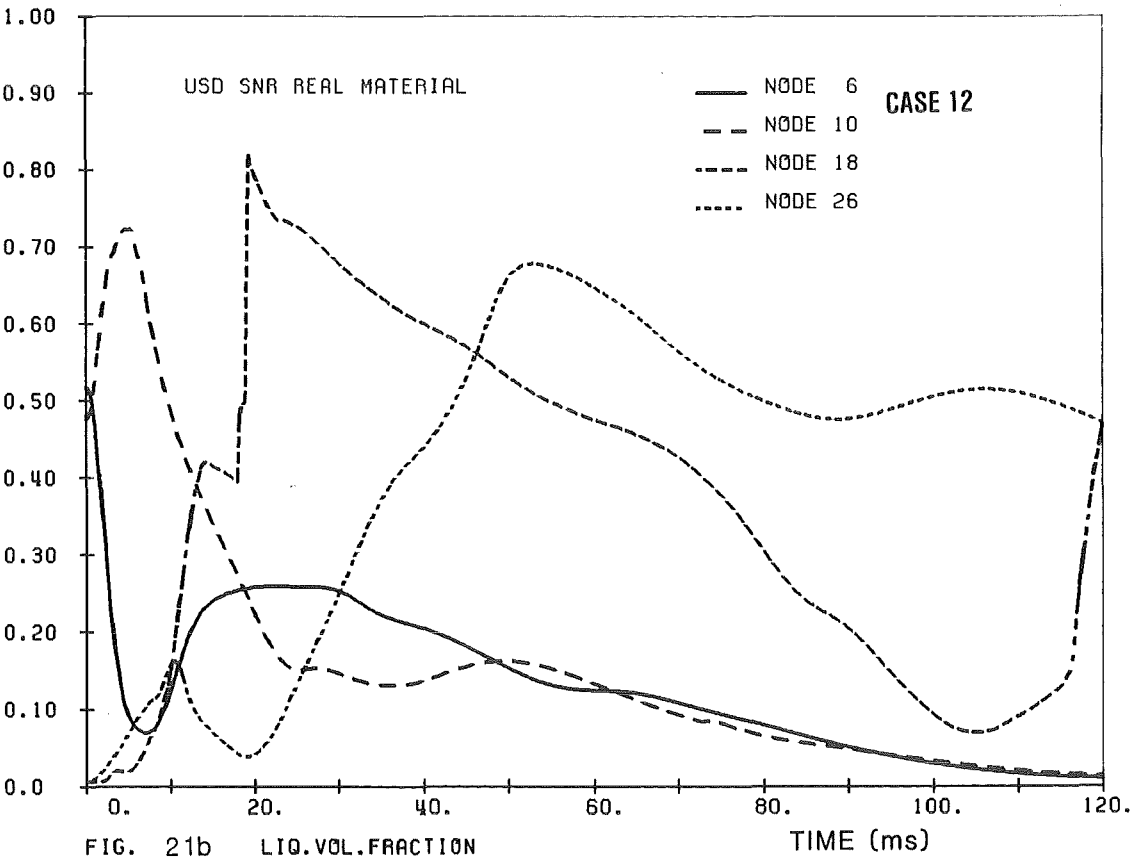

FIG. 21b LIQ.VOL.FRACTION

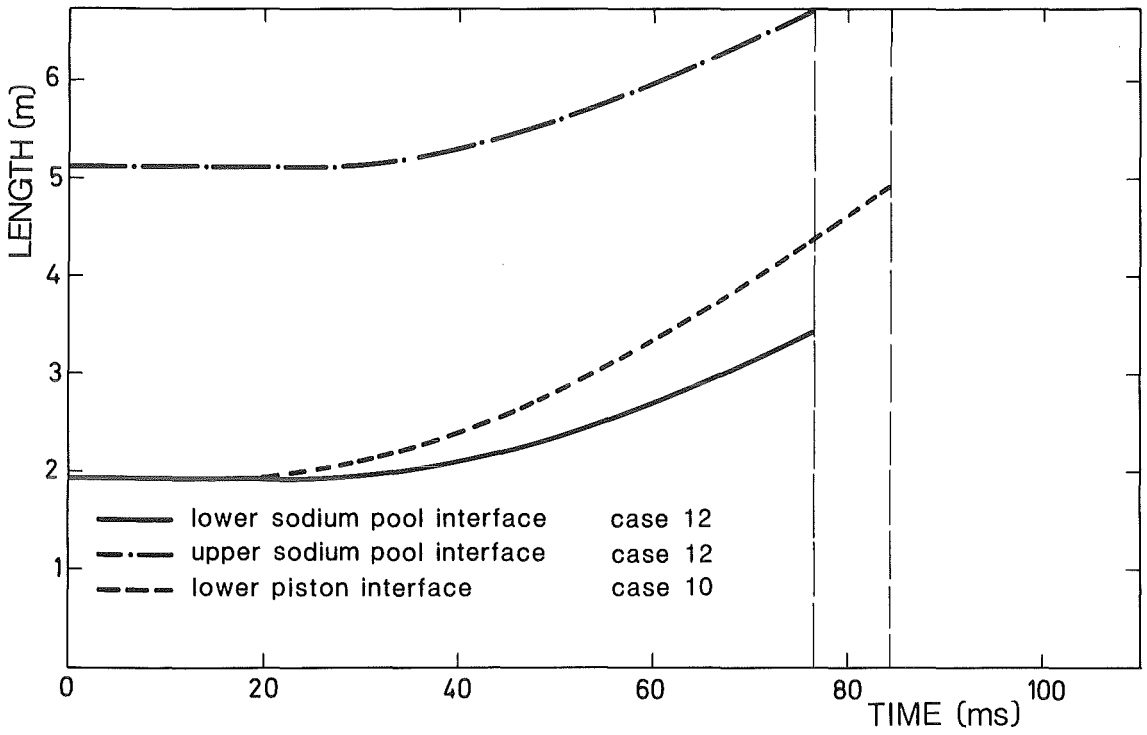

Fig. 22. Piston displacement as a function of time in comparison with the moving sodium pool interface for case 10 and 12.

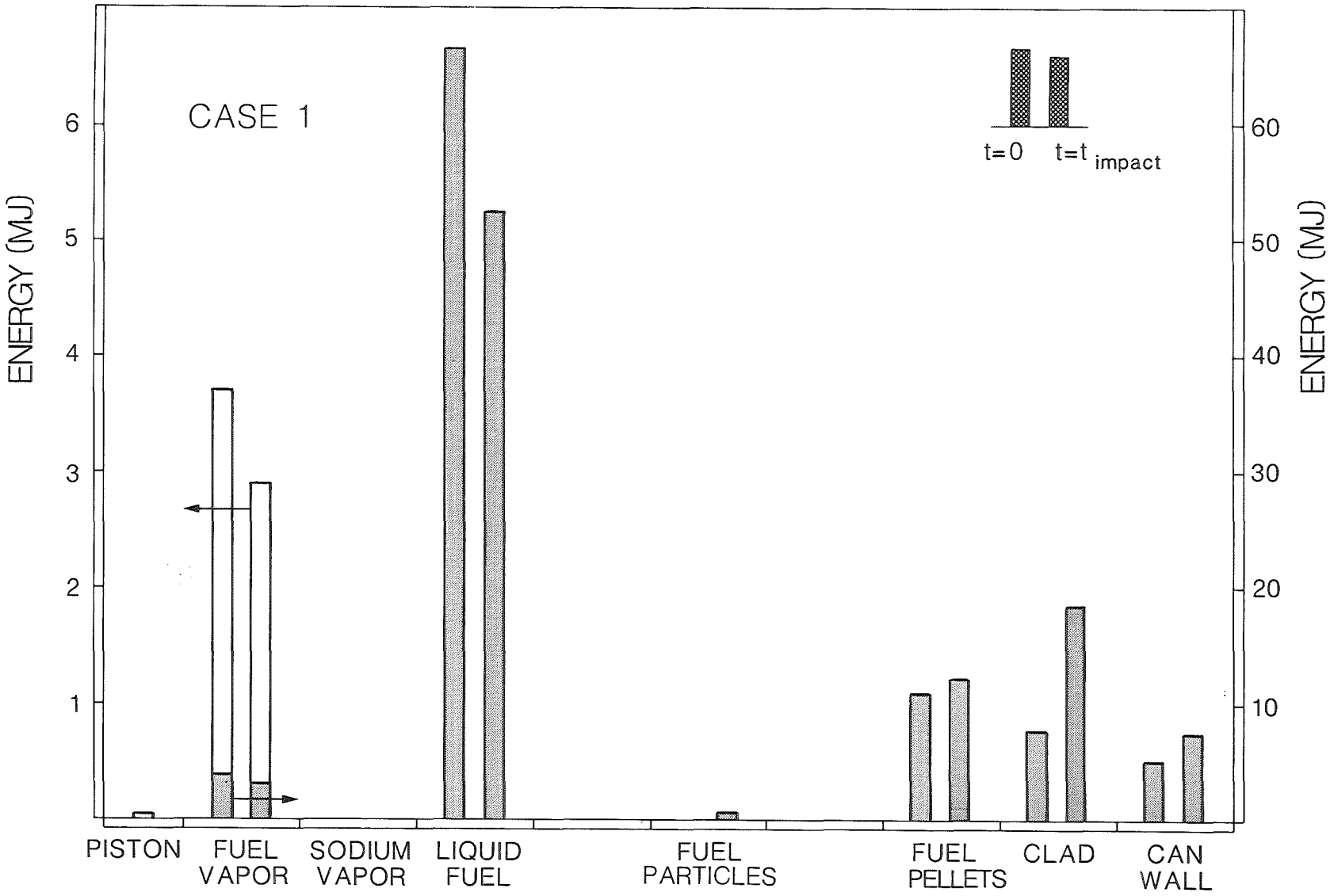

Fig. 23. Total energy summations at two times for Case 1.

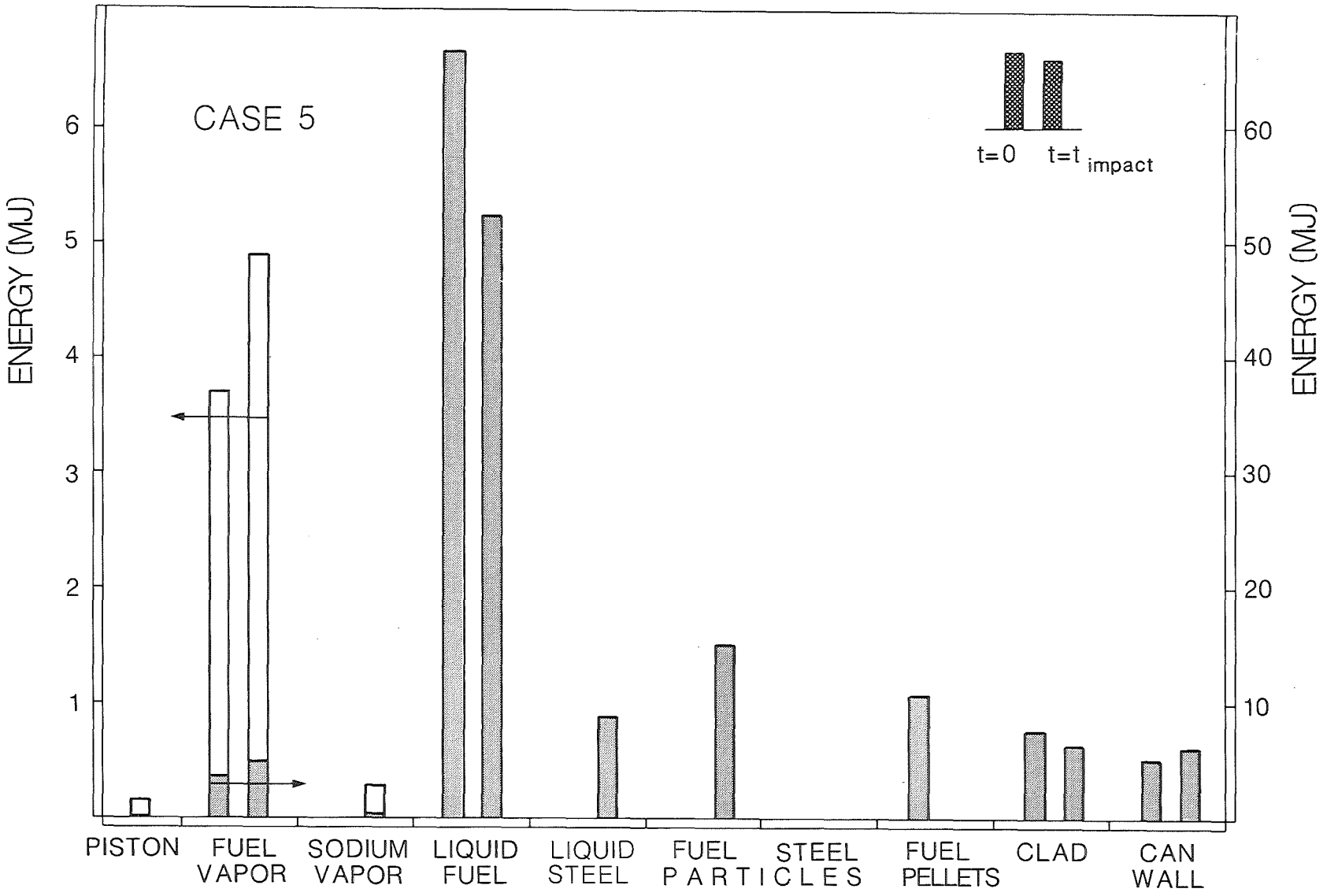

Fig. 24. Total energy summations at two times for Case 5.

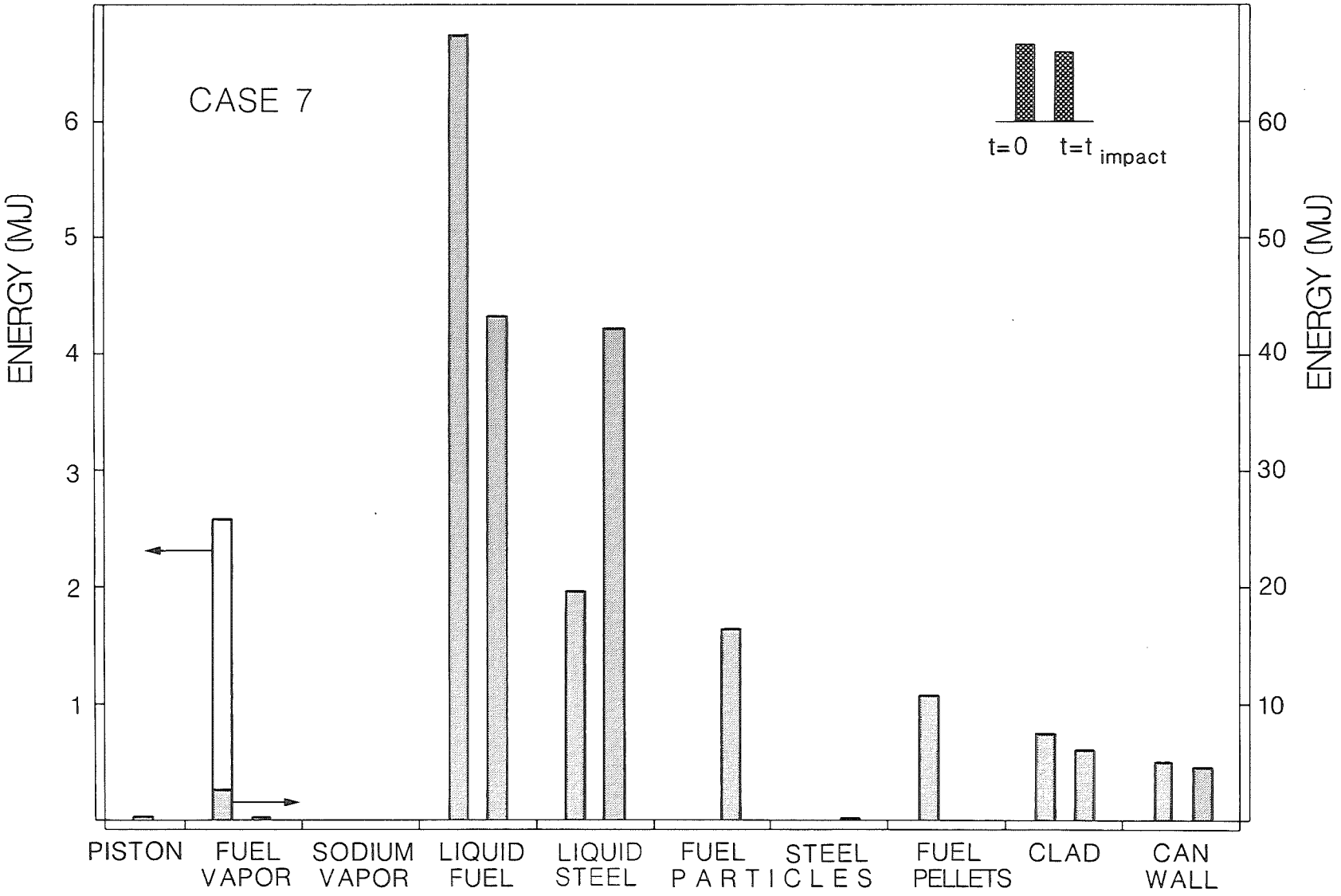

Fig. 25. Total energy summations at two times for Case 7.

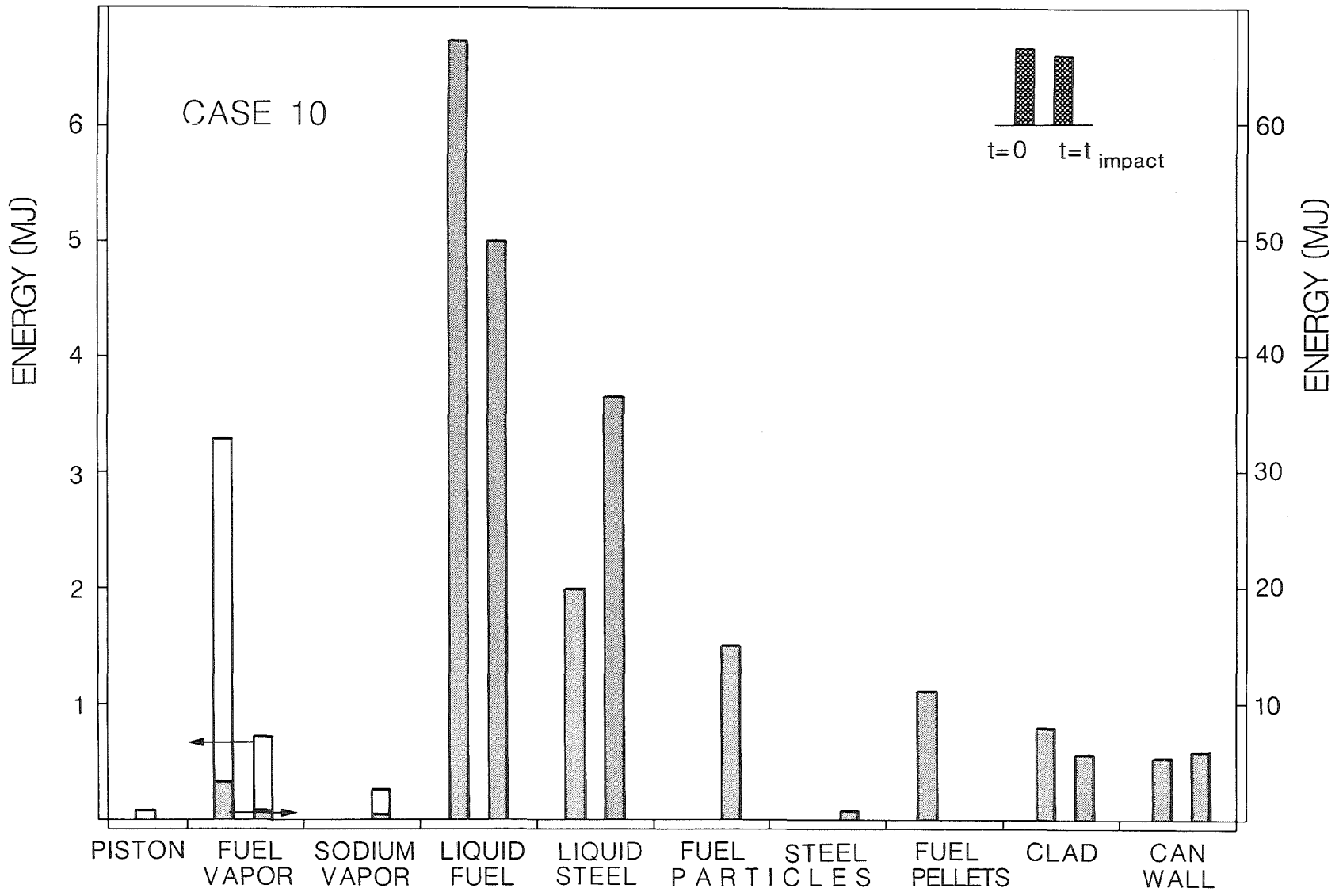

Fig. 26. Total energy summations at two times for Case 10.